Computational Investigation of Microstrip Antennas and Couplers



Thesis submitted to the University of Nottingham for the degree of Master of Research (MRes)

Electrical and Electronic Engineering

by

Chen Ye

Supervised by

Angela Nothofer

Steve Greedy

George Green Institute for Electromagnetics Research- GGIEMR

Department of Electrical and Electronic Engineering

The University of Nottingham, University Park, UK

September 12, 2016

Abstract

With the development of wireless local-area network, more and more applications relies on this frequency band, the 5.5 GHz. Antennas are essential elements of the communication system to provide the transmission and receive of the signal. Due to the Miniaturization and low profile, the microstrip antenna is widely employed in the wireless communication with small dimensions. Whereas the hybrid coupler is applied in the microwave system to provide the power division. It also can realized by microstrip line for small dimension comparing to those made of waveguide.

The aim of this thesis is to design microstrip antennas and couplers at 5.5 GHz for wireless local-area network and investigate to connect these two kinds of devices. Due to the high flexibility in modelling, CST MICROWAVE STUDIO is employed during the whole process of design and simulation.

Two antennas are designed at the resonant frequency of 5.5 GHz, the rectangular microstrip antenna possesses high directivity, whilst the copper coin shape antenna owns broad bandwidth. While two kinds of hybrid couplers are designed in different structure, the quadrature hybrid coupler and rat race ring. Finally the rectangular microstrip antenna is chosen to connect with the quadrature coupler with better division performance.

Key words: WLAN, 5.5 GHz, Microstrip antenna, Hybrid coupler

Declaration

I confirm that this work is carried out by myself under the supervision of Dr. Angela Nothofer and Dr. Steve Greedy at Department of Electrical and Electronic Engineering, the University of Nottingham. Any material used from other sources has been clearly identified and properly referenced.

Acknowledgement

I am highly thankful to my supervisors Dr. Angela Nothofer and Dr. Steve Greedy for the guidance from the beginning of confirming my research project to the final thesis. They guide me not only on the basic theory of the antenna and coupler but also the use of the simulation software. I am also thankful to Mohamed Ismaeel Maricar for discussions of the antenna, from the mechanism to different performance parameters of antenna as well as couplers, which impress me and help me a lot during the design procedure. Also I want to thank the GGIEMR to provide opportunities of different workshop on software using and lately development of our area, which inspires me on my design. In addition, thanks to the CELE of the University of Nottingham the performance of my language both on oral and writing has been improved during this period.

Finally, I shall remain thankful to the University of Nottingham and NJUST, my collage in China, for giving me this opportunity to spend one year living in UK. The cooperative training programme between these two universities gives me new ideas not only on my research but also a different living style from my home country, China.

Table of contents

Abstract i

Declaration ii

Acknowledgement iii

Table of contents iv

List of Figures vii

List of Tables ix

Abbreviation x

Chapter 1 Background 1

1.1 Antenna spectrum 1

1.2 Antenna for WLAN 2

1.3 Aim and objectives 2

1.4 Outline of the thesis 2

1.5 Summary 3

Chapter 2 Literature review 4

2.1 Basic antenna parameters 4

2.1.1 Impedance matching 4

2.1.2 Return loss and VSWR 5

2.1.3 Frequency bandwidth 6

2.1.4 Radiation pattern 6

2.1.5 Directivity 8

2.1.6 Efficiency 9

2.1.7 Gain 9

2.1.8 Polarization 9

2.2 Introduction of transmission lines 12

2.3 Introduction of microstrip antenna 12

2.3.1 Advantages and disadvantages 14

2.3.2 Application 14

2.3.3 History and development of microstrip antenna 15

2.4 The feeding method of microstrip antenna 15

2.4.1 Edge-fed 16

2.4.2 Probe-fed 17
2.4.3 Proximity coupled-fed 17
2.4.4 Aperture coupled-fed 18
2.4.5 Coplanar waveguide (CPW)-fed 20
2.5 Computational electromagnetics (CEM) 21
2.5.1 Method of moments (MoM) 22
2.5.2 Finite element method (FEM) 22
2.5.3 Finite-difference time-domain (FDTD) 23
2.5.4 Finite integration technique (FIT) 23
2.6 Summary 25
Chapter 3 Methodology 26
3.1 Microstrip line 26
3.2 Coplanar waveguide 28
3.3 Rectangular patch antenna 29
3.3.1 Radiation mechanism 30
3.3.2 Design formulas 31
3.3.3 Quarter wavelength transmission line 32
3.4 Summary 33
Chapter 4 Design of microstrip antenna 35
4.1 CST design procedure 35
4.2 Requirements of antennas 36
4.3 Rectangular microstrip antenna 37
4.3.1 Specific parameters and geometry 37
4.3.2 Simulation results 38
4.3.3 Influential parameters 42
4.4 Copper coin shape antenna 48
4.4.1 Specific parameters and geometry 49
4.4.2 Simulation results 50
4.4.3 Influential parameters 54
4.5 Comparison between rectangular MSA and copper coin shape antenna 59
4.6 Summary 61

Chapter 5 Design of coupler 62
5.1 Four-port Networks 62
5.2 Quadrature hybrid coupler 64
5.2.1 Introduction of the quadrature hybrid coupler 64
5.2.2 Even-odd mode analysis of quadrature hybrid coupler..... 65
5.3 Rat race ring 69
5.3.1 Introduction of rat race ring..... 69
5.3.2 Even-odd mode analysis of rat race ring..... 70
5.4 Design of quadrature hybrid coupler in CST 72
5.4.1 Parameters and structure 72
5.4.2 Simulation results..... 74
5.5 Design of the rat race ring in CST..... 77
5.5.1 Parameters and structure 77
5.5.2 Simulation results..... 78
5.6 Comparison between two couplers..... 82
5.7 The microstrip antenna connected to coupler 83
5.7.1 Structure of MSA with coupler..... 83
5.7.2 Simulation results..... 84
5.8 Comparison with the single MSA without the coupler..... 87
5.9 Summary 88
Chapter 6 Conclusion and future work 89
6.1 conclusion 89
6.2 Future work..... 89
6.2.1 Unsolved problem 89
6.2.2 Manufacture..... 90
6.2.3 Application on the antenna with coupler 90
Reference.....91

List of Figures

Figure 2. 1 Antenna input impedance model 4
Figure 2. 2 Donuts shape 3D radiation pattern[5] 6
Figure 2. 3 E-plane and H-plane of donuts shape radiation pattern [6] 7
Figure 2. 4 Polar radiation pattern [7] 8
Figure 2. 5 Rectangular radiation pattern [7] 8
Figure 2. 6 Vertical polarization and horizontal polarization 10
Figure 2. 7 Circular polarization 11
Figure 2. 8 Elliptically polarization 11
Figure 2. 9 Different transmission lines [9] 12
Figure 2. 10 Structure of microstrip antenna 13
Figure 2. 11 Different shapes of patch 13
Figure 2. 12 Different feedline [10] 14
Figure 2. 13 Edge-fed microstrip antenna 16
Figure 2. 14 Probe-fed microstrip antenna 17
Figure 2. 15 Proximity-fed microstrip antenna 18
Figure 2. 16 Aperture coupled-fed microstrip antenna 19
Figure 2. 17 Coplanar waveguide 20
Figure 2. 18 CPW-fed microstrip antenna 21
Figure 2. 19 Classification of CEM [5] 22

Figure 3. 1 Microstrip line 26
Figure 3. 2 Electric and magnetic field of microstrip line 27
Figure 3. 3 Coplanar waveguide 28
Figure 3. 4 Rectangular patch antenna 30
Figure 3. 6 Theory of transmission line 33
Figure 3. 7 $\lambda/4$ transmission line feed microstrip antenna 33

Figure 4. 1 Design procedures in CST 35
Figure 4. 2 Antenna structure in CST 38
Figure 4. 3 S11 parameter of MSA 38
Figure 4. 4 Efficiency of MSA 39
Figure 4. 5 Gain of MSA 40
Figure 4. 6 Surface current of MSA 40
Figure 4. 7 Radiation patterns of MSA 41
Figure 4. 8 Adjustment of the length of patch 42
Figure 4. 9 Adjustment of the width of patch 43
Figure 4. 10 Adjustment of the width of feedline 44
Figure 4. 11 Different feed positions 45
Figure 4. 12 Adjustment of the feed position 45

Figure 4. 13 Adjustment of the thickness of substrate 46
Figure 4. 14 Different GND dimensions 47
Figure 4. 15 Adjustment of the dimension of GND 48
Figure 4. 16 Geometry of the copper coin shape antenna in CST 50
Figure 4. 17 $S11$ parameter of copper coin shape antenna 50
Figure 4. 18 Efficiency of copper coin shape antenna 51
Figure 4. 19 Gain of copper coin shape antenna 52
Figure 4. 20 Surface current of copper coin shape antenna 52
Figure 4. 21 Radiation patterns of copper coin shape antenna 54
Figure 4. 22 Adjustment of the radius of patch 55
Figure 4. 23 Adjustment of the width of inner slot 56
Figure 4. 24 Gap between central feedline and GND 57
Figure 4. 25 Adjustment of the gap between central feedline 57
Figure 4. 26 Distance between patch and GND 58
Figure 4. 27 Adjustment of the distance between patch 59

Figure 5. 1 Four-port coupler 63
Figure 5. 2 Basic structure of hybrid coupler 64
Figure 5. 3 Circuit model of hybrid coupler 65
Figure 5. 4 Analysis of hybrid coupler [9] 66
Figure 5. 5 Network with ABCD matrix 67
Figure 5. 6 Useful ABCD matrices [8] 67
Figure 5. 7 Structure of rat race ring 70
Figure 5. 8 Analysis of rat race ring [57] 71
Figure 5. 9 Structure of hybrid coupler in CST 73
Figure 5. 10 S parameters of the quadrature hybrid coupler 74
Figure 5. 11 Surface current of hybrid coupler 75
Figure 5. 12 E-field of hybrid coupler 76
Figure 5. 13 H-field of hybrid coupler 76
Figure 5. 14 Power flow of hybrid coupler 77
Figure 5. 15 Geometry of rat race ring in CST 78
Figure 5. 16 S parameters of rat race ring 79
Figure 5. 17 Surface current of rat race ring 80
Figure 5. 18 E-field of rat race ring 81
Figure 5. 19 H-field of rat race ring 81
Figure 5. 20 Power flow of rat race ring 82
Figure 5. 21 Structure of MSA connected to the coupler 84
Figure 5. 22 S11 of MSA connected to the coupler 84
Figure 5. 23 Efficiency of MSA connected to the coupler 85
Figure 5. 24 Gain of MSA connected to the coupler 86
Figure 5. 25 Radiation pattern of MSA connected to the coupler 87

List of Tables

Table 1.1 Common spectrum of antenna 1

Table 2. 1 Comparison among four principle feeding methods 20
Table 2. 2 Comparison of different simulation methods 24

Table 4. 1 Design specification of the antenna 37
Table 4. 2 Parameters of MSA 37
Table 4. 3 Parameters of copper coin shape antenna 49
Table 4. 4 Comparison between two antennas 60

Abbreviation

ELF	Extremely Low Frequency
SLF	Super Low Frequency
ULF	Ultra-low Frequency
VLF	Very Low Frequency
LF	Low Frequency
MF	Medium Frequency
HF	High Frequency
VHF	Very High Frequency
UHF	Ultra-high Frequency
SHF	Super High Frequency
EHF	Extremely High Frequency
WLAN	Wireless Local-area Network
CST	Computer Simulation Technology
CST MVS	Computer Simulation Technology Microwave Studio
VSWR	Voltage Standing Wave Ratio
BW	Bandwidth
RF	Radio Frequency
CAD	Computer-aided Drafting
CEM	Computational Electromagnetics
MoM	Method of Moments
FEM	Finite Element Method
FDTD	Finite-difference Time-domain
FIT	Finite Integration Technique
MSA	Microstrip Antenna
GND	Ground Plane

CPW	Coplanar Waveguide
MIMO	Multi-in Multi-out
WiMAX	Worldwide Interoperability for Microwave Access
LTE	Long Term Evolution

Chapter 1 Background

1.1 Antenna spectrum

Nowadays different kinds of antenna are employed in various systems for transferring and receiving signals. And different applications are operated in specific frequency band, which is the spectrum of antenna shown in table 1.1.

Name	Frequency range	Wavelength	Application
Extremely low frequency (ELF)	3-30Hz	10000-100000 km	Underwater communication
Super low frequency (SLF)	30-300Hz	1000-10000 km	AC power(through not a transmission wave)
Ultra-low frequency (ULF)	300-3000Hz	100-1000 km	
Very low frequency (VLF)	3-30KHz	10-100 km	Navigational beacons
Low frequency (LF)	30-300KHz	1-10 km	AM radio
Medium frequency (MF)	300-3000KHz	100-1000 m	Aviation and AM radio
High frequency (HF)	3-30MHz	10-100 m	Shortwave radio
Very high frequency (VHF)	30-300MHz	1-10 m	FM radio
Ultra-high frequency (UHF)	300-3000MHz	10-100 cm	TV, mobile phones, GPS
Super high frequency (SHF)	3-30GHz	1-10 cm	Satellite links, wireless communication
Extremely high frequency (EHF)	30-300GHz	1-10 mm	Astronomy, remote sensing

Table 1.1 Common spectrum of antenna

In this thesis, all devices are designed at 5.5 GHz for wireless communication.

1.2 Antenna for WLAN

Wireless local-area network (WLAN), which provides stable and fast connections between PCs and laptops and other equipments like tablet PC under the local condition [1], has now supplemented or even replaced the wired communication in business, home and campuses [2]. And some new applications like smart home have been brought out to provide much more opportunities for wireless communication. Thus modern technique at 5.5GHz for WLAN witnesses a rapid development. For the sake of convenient carrying, much more interests have been devoted into research for small size systems.

And the Antenna, as a crucial element in the system, consequently requires the same research. Therefore devices built on microstrip line like antenna and coupler, with the low profile and light weight, attracts more attention for such systems. Also due to its easy fabricated, it is convenient to integrate in different systems. Therefore, microstrip antennas and couplers are chosen for research in this thesis.

1.3 Aim and objectives

The project starts from designing the microstrip antenna and couplers. Both of them are then simulated using the CST MICROWAVE STUDIO (CST MVS). It aims to design and simulate microstrip antennas as well as couplers at 5.5GHz for wireless communication. And these two elements are connected as an investigation to compare the results.

The following objectives have been set in order to achieve the aim:

- Literature review on basic antenna theory and important parameters
- Familiar with using CST software for simulation
- Methodology of microstrip line, microstrip antenna design
- Analysis even-odd mode for coupler working principle

1.4 Outline of the thesis

The outline of the thesis is showed below

Chapter 1: It introduces the basic theory and development of microstrip antenna, simulation software (CST MVS), objectives and scope of the project.

Chapter 2: It covers the literature review on basic antenna theory and microstrip antenna in particularly. Besides, different simulation methods and feeding methods are also discussed in this section.

Chapter 3: It introduces the methodology in design for microstrip line, rectangular patch and coplanar waveguide. Also it explains the radiation mechanism of microstrip antenna.

Chapter 4: It deals with the design and simulation of two microstrip antennas and analysis of the influential parameter of the antennas to obtain better performance.

Chapter 5: It gives the basic theory, design and simulation of the four port coupler and then connects the antenna with the coupler to analyse the result of the simulation.

Chapter 6: It provides the conclusion of the whole project and the future work.

1.5 Summary

This chapter introduces the whole projects, followed by a brief introduction about antenna spectrum, wireless communication as well as the reason why we choose the microstrip antenna and coupler. In addition, the aims, objectives, scope of the project are discussed. Finally it indicates the outlines of each chapter in the thesis.

Chapter 2 Literature review

2.1 Basic antenna parameters

When designing and analysing an antenna, several basic parameters are required to determine the performance of the antenna. Therefore it is essential to know these basic parameters before designing. They are showed below.

- Impedance matching
- Return loss and VSWR
- Frequency bandwidth
- Radiation pattern
- Directivity
- Efficiency
- Gain
- Polarization

As the antenna can be seen as a transmission device between transmission line and microwave field, the parameters can be grouped into these two views. Specifically, the first three parameters are related to transmission lines, whereas the others are related to microwave field.

2.1.1 Impedance matching

From the view of transmission lines, the antenna can be seen as a load to a transmission line so impedance matching becomes an important parameter [3]. The definition of the input impedance of an antenna is expressed by its terminal as a relation between voltage and current. The mathematical expression and model of input impedance are showed below.

$$Z_a = \frac{V_{in}}{I_{in}} \tag{2.1}$$

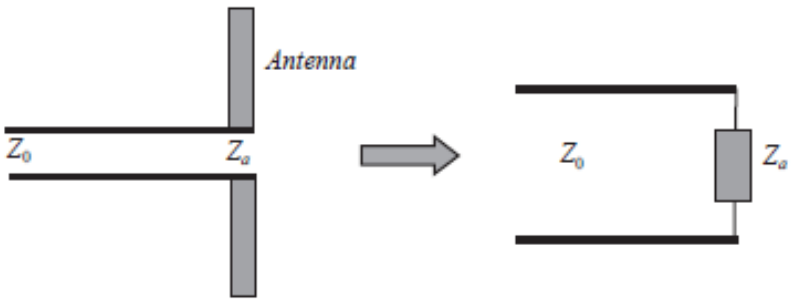


Figure 2. 1 Antenna input impedance model

Where $Z_a$is the input impedance of the antenna, and $V_{in}$and I_{in} refer to the voltage and current of the terminal separately.

In practical, the input impedance of the antenna requires to be 50 Ω or 75 Ω to match with the standard transmission line [4]. If it does not match well less power will delivered to the antenna because part of the energy is reflected back to the generator .Therefore it is important to match the impedance of the antenna.

2.1.2 Return loss and VSWR

The reflection coefficient is used to determine how well the antenna is matched to the transmission line. The representation is shown in (2.2)

$$\Gamma = \frac{Z_a - Z_0}{Z_a + Z_0} \tag{2.2}$$

Where $Z_a$is the input impedance of the antenna, and Z_0 is the characteristic impedance. And r=0 implies the perfect match of antenna.

Return loss is the power which reflects to the generator instead of transferring to load. It is expressed in dB and defined as

$$L_{RT} = -20\log_{10}(|\Gamma|) = -20\log_{10}\left|\frac{Z_a - Z_0}{Z_{a+Z_0}}\right| \tag{2.3}$$

In practical analysis, the antenna can be regarded as a 1-port network both in simulation as well as manufactured measurement. Thus the S_{11} parameter acts as the return loss to test the performance of an antenna.

Another parameter, voltage standing wave radio (VSWR), is also used commonly to measure the impedance mismatch. Its expression is given in (2.4).

$$VSWR = \frac{1+|\Gamma|}{1-|\Gamma|} \tag{2.4}$$

It is obvious through the equation that VSWR is a ratio between 1 and infinity. And VSWR=1 implies a perfect match load to the system. Higher VSWR refers to more power loss due to impedance mismatch.

In general, it is required that an antenna should have the VSWR < 2 or r> 10 dB to work properly in the system.

2.1.3 Frequency bandwidth

Bandwidth is a basic but important parameter from the view of transmission lines. Here the frequency bandwidth refers to the bandwidth related to impedance match. It is defined where the frequency range meets VSWR < 2 or r> 10 dB. In general the frequency bandwidth is often expressed as the difference between upper and lower frequency, or a percentage number related to the ratio of the frequency difference to resonant frequency.

$$BW = f_{upper} - f_{lower}$$

$$= \frac{f_{upper} - f_{lower}}{f_r} \ (\%)$$

For example, if an antenna resonates at 5.5GHz and the bandwidth is from 5.4GHz to 5.6GHz. It can be obtained that the bandwidth of this antenna is 0.2 GHz or 3.6%.

Most antenna systems prefer broad bandwidth hence researches to widen the bandwidth is meaningful for practical application.

2.1.4 Radiation pattern

The radiation pattern is one of the most important parameters of the antenna. It can be regarded as a plot that describes the relation between radiated power and direction away from the antenna. In general, there are three different types of radiation pattern: 3D plot, polar plot and rectangular plot. Figure 2.2 shows a typical donuts shape radiation pattern which belongs to the short current element. Obviously it illustrates the overview of the relation between radiated power and different angle in space.

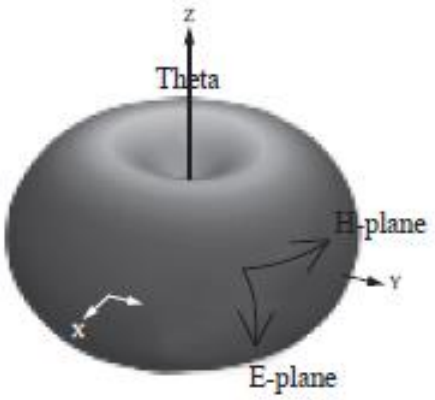


Figure 2. 2 Donuts shape 3D radiation pattern[5]

What's more, it also can be seen as a combination of two planes: the E-plane and the H-plane, as shown in figure 2.3. The E-plane defines the plane where

the E-field located while the H-field illustrates the plane that the magnetic field lies on. How to determine and distinguish these two planes depends on how you put your antenna in space. More specifically, it is related to the current distribution on the antenna. E-plane is the plane which includes the direction of electric current as well as the maximum radiated direction. And the H-plane is perpendicular to the E-plane.

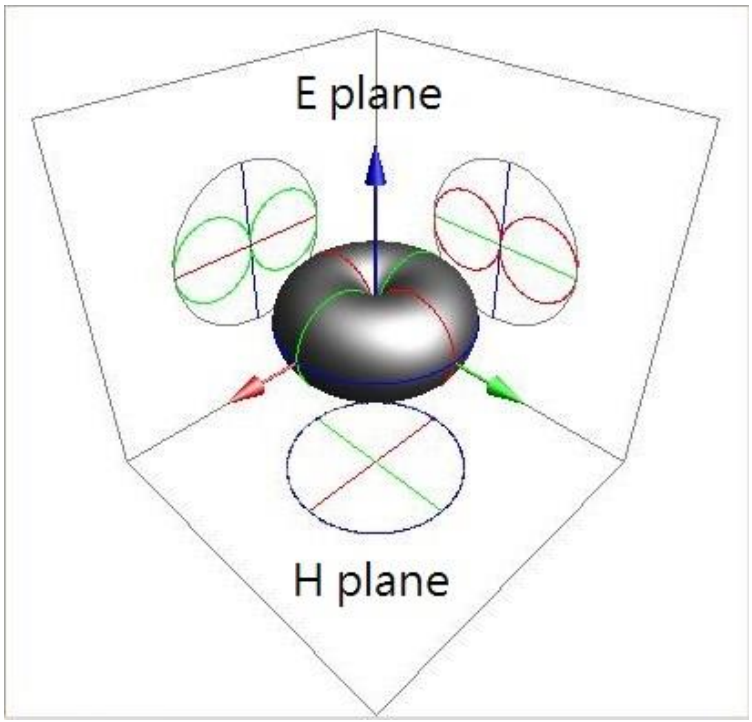


Figure 2. 3 E-plane and H-plane of donuts shape radiation pattern [6]

Polar plot and rectangular plot usually contain more information than 3D plot. They are shown in figure 2.4 and figure 2.5 respectively with different presentation. The polar radiation pattern is plotted with the angle and measured in dB with different circles. As for rectangular plot, the horizontal axis refers to rotation angle and the vertical axis is plotted with the radiated power. Both of these patterns contain one main lobe and several side lobes in the plot. More specifically, the main lobe indicates the maximum radiated power among the space. And the side lobes are used to describe the sharpness and width of the main lobe. Besides, the first side lobe level and the front to back ratio tell the radiation property of side lobe and the relation between main lobe and back lobe separately, which are also important characteristics related to the directivity of the antenna.

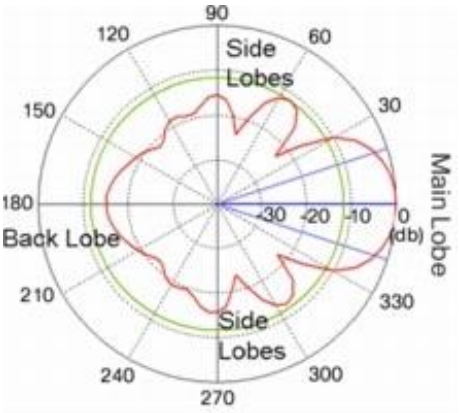


Figure 2. 4 Polar radiation pattern [7]

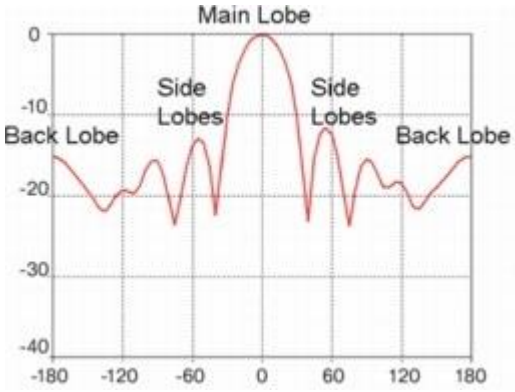


Figure 2. 5 Rectangular radiation pattern [7]

It can be noticed that dB is well used as the unit of measurement in plot, which is because same shape or trend can be easily obtained through logarithmic scale (dB plot). Compared to linear scale, $10\log\frac{P}{P_{max}}$ has the same shape as $20\log\frac{E}{E_{max}}$ when plot. Thus it is more popular to measure radiation pattern in dB.

2.1.5 Directivity

The directivity of the antenna is defined as a ratio of intensity of radiated power in the particular direction to the whole space, as shown in (2.5).

$$D = \frac{U(\theta,\phi)}{U(\theta,\phi)_{av}} \tag{2.5}$$

It can be described using two different units, dBi and dBd, which refer to the comparison of isotropic antenna and dipole antenna separately. Where isotropic antenna refers to the antenna without specific direction or in other word the antenna radiates at all direction. For instance, if the directivity of an antenna is 1.3dBi, it means that it radiates 1.3dB more at the maximum

direction comparing to isotropic antenna under the same situation of radiated power.

2.1.6 Efficiency

There are two kinds of efficiency that can be used to analyse antenna performance: radiation efficiency and total efficiency. The first one refers to the relation between input power and radiated power of the antenna, which is given in (2.6).

$$\eta_e = \frac{P_t}{P_{in}} \tag{2.6}$$

The total efficiency takes impedance mismatch into consideration. In another word, it contains the antenna loss while connecting to a transmission line, as shown in (2.7).

$$\eta_t = M_L \eta_e \tag{2.7}$$

Where M_L is the antenna loss due to mismatch which varies from 0 to 1.

$$M_L = (1 - |\Gamma|^2) \tag{2.8}$$

It can be clearly seen from (2.8) that a perfect match with Γ=0 leads to the largest M_L and total efficiency of the antenna.

2.1.7 Gain

With the concept of directivity and efficiency, it is easy to understand the antenna gain. It illustrates the ratio of radiated power at given direction and power inputted to the antenna. Combining these two parameters, antenna gain describes the power character transformed from input port to output radiation. Thus it is widely employed to judge the performance of an antenna while simulating.

$$G = \eta_e D = \frac{P_t}{P_{in}} D \tag{2.9}$$

2.1.8 Polarization

As a transmitter or receiver in ratio system, the polarization of an antenna refers to the polarization of the waves radiated by the antenna. There are three different types of polarization of radio wave, linear polarization, circular polarization and elliptically polarization. It is an important parameter for EM wave analysis because it describes the travel route of E vector along with

changing time. At first, we assume that the wave propagates along z direction according to the expression below.

$$\boldsymbol{E} = \hat{x}A\cos(\omega t - \beta z) + \hat{y}\,B\sin(\omega t - \beta z) \qquad (2.10)$$

It consists of two components at x and y direction with the amplitudes of A and B separately. If A or B =0, the E vector only has one component which leads to a linear polarization shown in figure 2.6. It shows that the route of E vector moves along one axis just like a line.

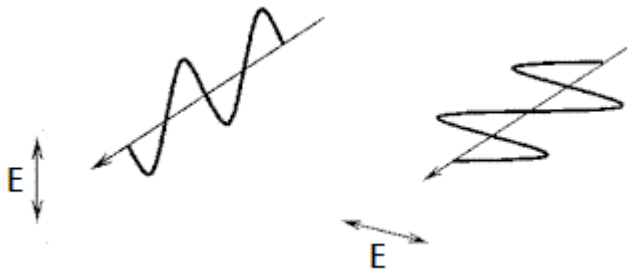
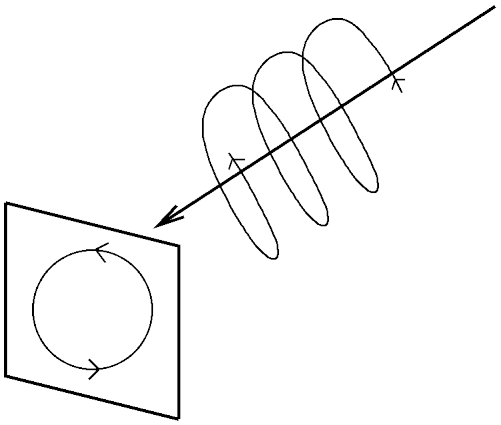
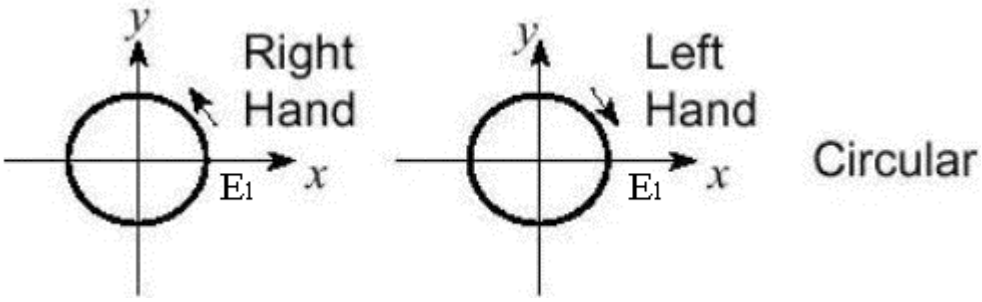


Figure 2. 6 Vertical polarization and horizontal polarization

When A=B, the two components have the same amplitudes and it describes a circular polarization with a circular route shown in figure 2.7(a). Comparing linear polarization and circular polarization, it is not difficult to notice that a circular polarization can be divided to two vertical linear polarization. Thus we have two kinds of circular polarization, right hand circular polarization (RCP) and left hand circular polarization (LCP), due to different order of the two linear polarizations (ahead or behind 90 degree). Right/left hand rule is employed to determine whether a circular polarization is RCP or LCP. As shown in figure 2.7(b), when right thumb directs at the transfer direction at +z axis out the paper, if the route of E vector agrees the right hand along with time passes, it is a RHP and vice versa.



(a) Circuit view



(b) RCP and LCP

Figure 2. 7 Circular polarization

The last situation, elliptically polarization, occurs when$A \neq B \neq 0$ which is shown in figure 2.8.

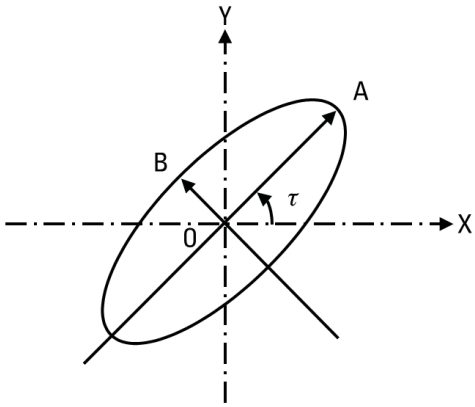


Figure 2. 8 Elliptically polarization

Axial ratio, which defines the relation between these two components of E vector, is introduced to analyse the polarization of EM wave.

$$AR = \frac{A}{B} \tag{2.11}$$

Where $AR = 0\ or\ +\infty$: linear polarization

$AR = 1$: circular polarization

$0 \leq AR \leq +\infty$: elliptically polarization

It is important to match the polarization of transmitting and receiving antenna because a mismatch will cause losses. As circular polarization is friendly to match itself and linear polarization (although 3dB loss), it is widely employed in satellite systems like GPS which requires good characteristic for matching.

2.2 Introduction of transmission lines

The development of transmission lines for low-loss in power at high frequency can be seen as a milestone in microwave engineering. It is used to connect microwave components with circuit elements. Therefore a well-defined characteristics transmission line is required in microwave systems. Many transmission lines have been proposed and used in RF system as shown in the figure 2.9. Waveguides have high power-handling capability and low loss whereas expensive to fabricate [8]. Two-wire lines are inexpensive but lack shielding. Coaxial lines have shields but are difficult to fabricate in complex microwave components. Planar transmission lines, which include microtrip line, stripline, and coplanar waveguides, etc., are widely used in microwave integrated circuits. They are compact, low in cost, and capable of being integrated therefore widely used in microstrip antenna design.

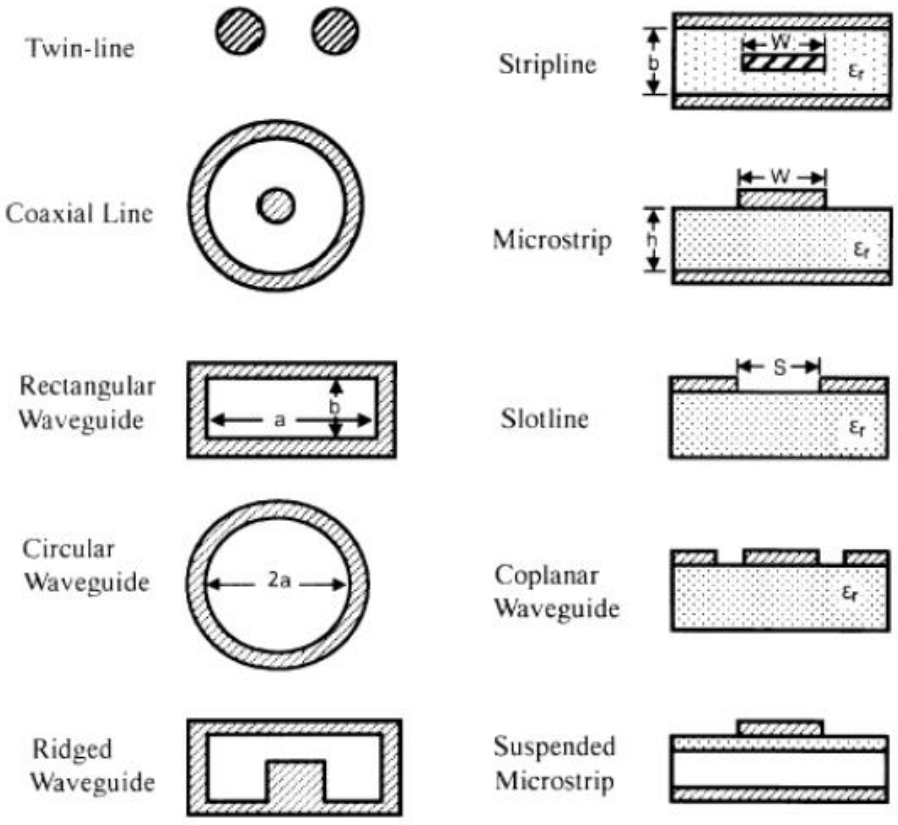


Figure 2. 9 Different transmission lines [9]

2.3 Introduction of microstrip antenna

The microstrip antenna, also known as the patch antenna, has been one of the most popular antennas so far. It consists of a metal patch on the top, a

dielectical substrate in the middle and a ground plane at the bottom[5]. Figure 2.10 shows the structure of a rectangular patch antenna.

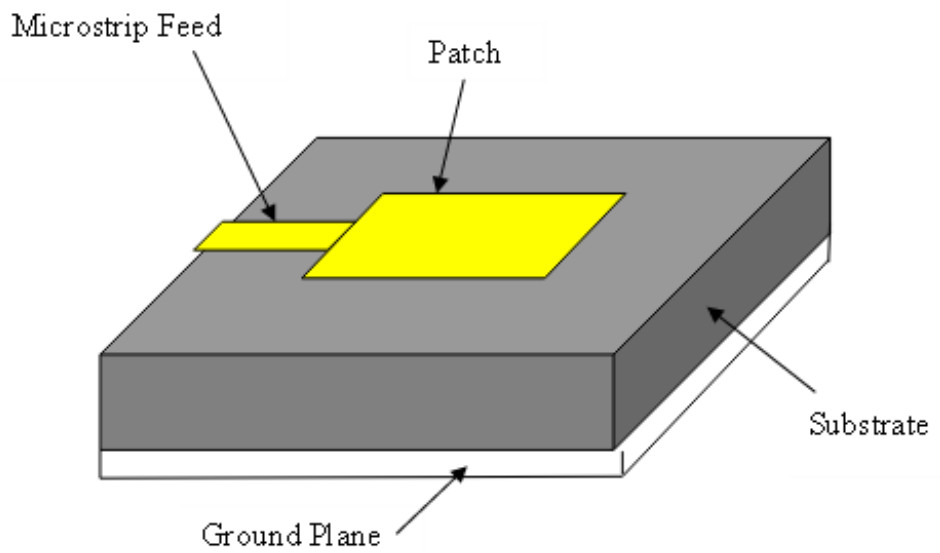


Figure 2. 10 Structure of microstrip antenna

In practical, the patch can have different shapes to fit different design requirements, like rectangular, circular, triangle and circular ring, etc., as shown in figure 2.11.

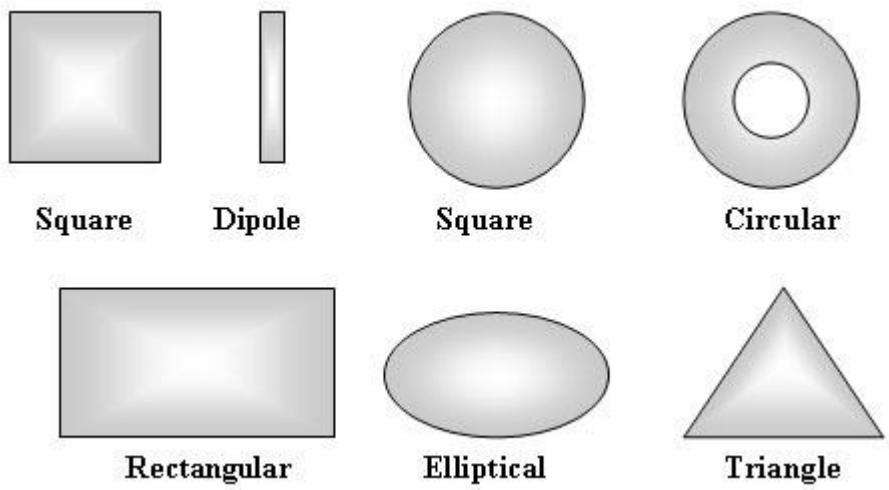


Figure 2. 11 Different shapes of patch

Among them, the square one are most popular due to easy fabricated. While the antenna with the shape like circle, elliptical and circular can reach the same performance with smaller metal size than rectangular ones. Therefore they are well employed in the system which requires small size. However, the rectangular ones possesses the highest gain to meet the relevant requirement. The microstrip antenna with a triangle metal on the top is

usually used for special application like dual-feed or polarization study. And their characteristics like cross-polar radiation can improve the performance of antenna.

Also, the feed methods are various including microtrip line feed, coaxial feed and coplanar waveguide feed (CPW), etc., shown in figure 2.12. They will be further described in section 2.4.

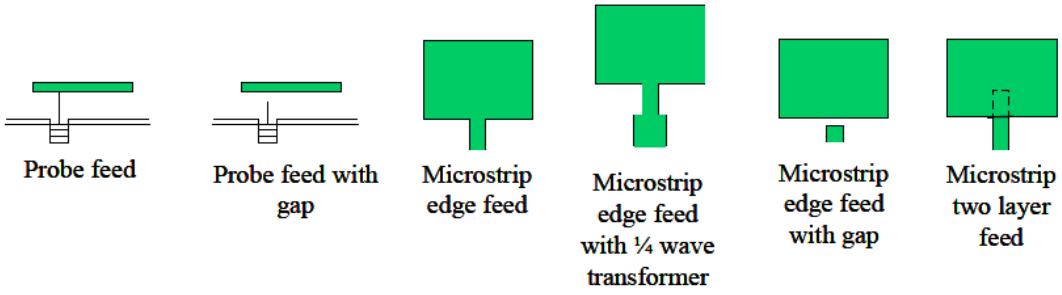


Figure 2. 12 Different feedline [10]

2.3.1 Advantages and disadvantages

There are numerous salient features of the microstrip antenna. First of all, it has small size with light weight which is easy to fabricate through printed technology [11]. Secondly, it is low profile and friendly to planar surfaces. Thirdly, due to its compatible with MMIC (monolithic microwave integrated circuit), it is also convenient to connect the microstrip antenna with other electric elements [12]. What's more, it can be operated in linear polarization as well as circular polarization and even dual resonant frequency. In general, the microstrip antenna can provide good performance with low cost and robust design.

However, besides narrow bandwidth, there are major disadvantages of the microstrip antenna: low efficiency, poor polarization purity and low power capability cannot be ignored[11]. Therefore more and more research has been done to improve its performance. For example, different feed method like coplanar waveguide feed (CPW) is employed to broaden the frequency bandwidth [13] [14].

2.3.2 Application

Due to the advantages mentioned before, there are numerous applications of the microstrip antenna like medical application [15], satellites [16], and radar system [17]. At the beginning, it is used in telecommunication which required minisize antenna which is friendly to the system. Nowadays, it is more

employed in mobile communication system (usually operate at 2.45GHz) and wireless communication equipment (often operate at 5.5GHz) because of its low profile and light weight.

2.3.3 History and development of microstrip antenna

Research and development on the topic of microstrip antennas has been undertaken for the past 40 years with the contribution of different company, government organizations and universities all over the world [18].

Deschamps was the first one who came up with the concept of microstrip antenna in 1953 [19], whereas the practical one was developed by Munson [20] in the mid-1970s. It was a significant advancement because two feeding methods were introduced: the edge-fed and the probe-fed. Both of them are widely used in all patches. In order to improve inherent issues of the microstrip like the narrow impedance bandwidth, some important findings were developed in 1980s. Based on the new means of feeding, two new methods were introduced: the aperture-coupled fed [21] and the proximity coupled fed [22].The bandwidth enhancement was achievable for the aperture-coupled fed method whereas the second one has the similar performance of probe-fed. In addition, using patches in arrays were further investigated and analysed. The 1990s witnessed the development of microstrip antenna into commercial system, like mobile communication base station terminals. Based upon finite difference time domin(FDTD) and finite element method(FEM) methods, accurate computational tools are introduced to achieve results of the antenna. In 2000s, besides bandwidth enhancements, high gain solutions had been achieved to reduce the loss of feed network. For example, utilizing photonic bandgap (PBG) structures to enhance the efficiency and improve the overall radiation performance of microstrip antenna had been explored [23].By the turn of 2010s, the design of microstrip antennas were more driven by the commercial application. Another interesting thing is the combination of patch antenna and other classical antennas for better performance. For instance, the printed dipoles could provide good radiation pattern [24].

2.4 The feeding method of microstrip antenna

The feeding method refers to the way the antenna is excited with signal and power which will influence the impedance bandwidth, radiated field and even the efficiency, etc. What's more, it is also related to the ease of manufacturing in practice. Therefore it is an essential element that cannot be ignored while

designing. There are four foundational methods to excite a microstrip antenna, edge-fed, probe-fed, aperture coupled-fed and proximity-fed. They can be divided into two main classes: direct and non-contact methods [25]. Besides these four methods, the coplanar waveguide-fed attracts more attention recently because of its good performance at wide bandwidth and will also be introduced in this chapter.

2.4.1 Edge-fed

Edge-fed, also well known as microstrip-line fed [20], is a basic method to excite a patch antenna. Figure 2.13 gives the structural diagram of this feeding method, a microstrip line contacts the rectangular patch and the excitation source which is located on the end of the microstrip line. Thus it falls under the classification of direct methods.

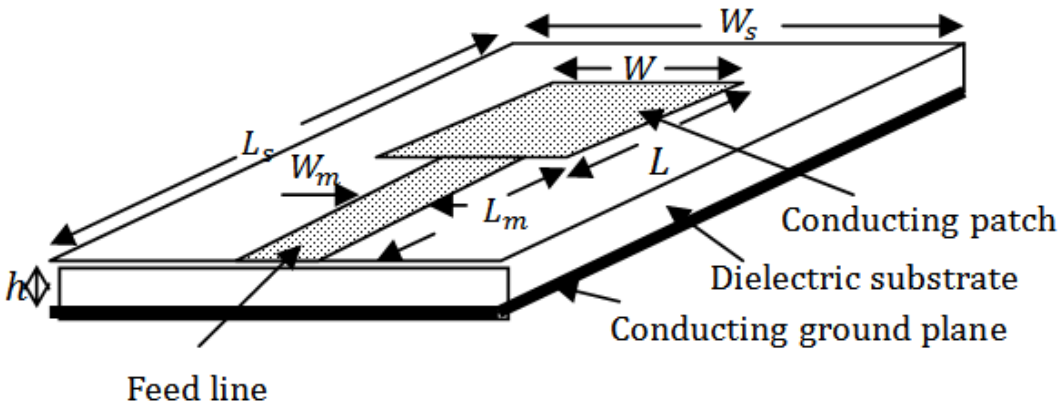


Figure 2. 13 Edge-fed microstrip antenna

The key merit of edge-fed technique is that it is really easy to manufacture. Since it is a section of microstrip line connecting with the patch directly on the same substrate and ground plane, printed CAD technique is convenient for its production. This is also the reason why the edge-fed technique is employed in the application of large plane array design [25]. In addition, it is easy to adjust the input impedance under this feeding method. Just controlling the insert location of the feedline can change the input impedance from very high hundred ohms down to only several ohms [26]. The closer it locates at the center of the patch, the lower impedance it provides. While in simulation we notice that not only the location but also the width of feedline can also influence the impedance performance, which will be discussed in the following chapter.

2.4.2 Probe-fed

Probe-fed, can be seen as the coaxial feed, was introduced in the mid-1970s [20]. It consists of three coaxial elements: an inner pin connected to the metal patch, a dielectrical cylinder and an outer conductor. Figure 2.14 gives the structure of this feeding method. It is also a direct feeding technique because the inner pin connects the patch and the input port.

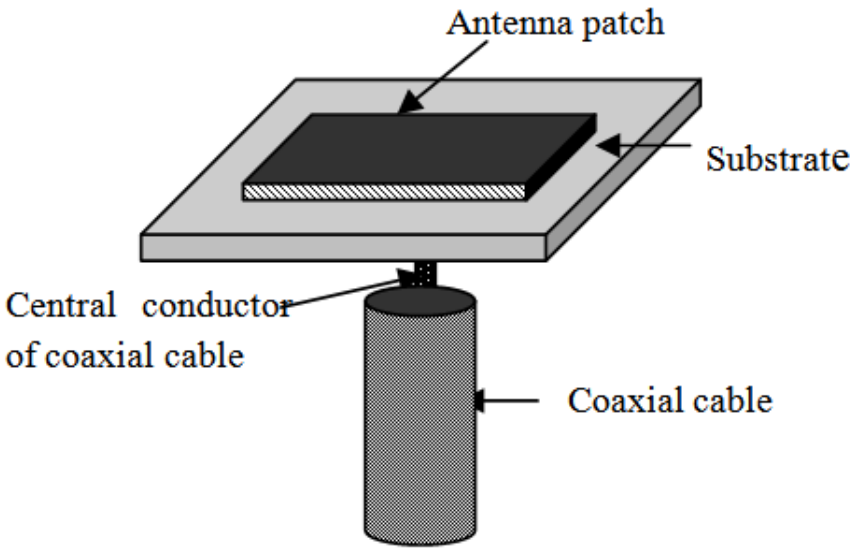


Figure 2. 14 Probe-fed microstrip antenna

From the structure given in the figure we can see that the coaxial feed is isolated from the radiating metal patch through the ground plane. It is the main advantage of this excitation technique because it reduces the unwanted radiation. Therefore probe-fed provides the highest efficiency among these feeding methods because it is direct connecting and independent from patch [27]. Comparing with the edge-fed, the location of the coaxial feed is the only element to control the input impedance, which is easy to operate. However, because the feed is no longer a single layer structure the fabrication could be more complicated.

2.4.3 Proximity coupled-fed

Although direct feeding methods above have several advantages like high efficient and easy to control input impedance, they also have shortcomings in common: the narrow bandwidth and detrimental effect of surface waves. Therefore the non-connect technique was introduced to improve these factors. [21]

Proximity-fed was presented with by Pozar in 1987 [22] with the schematic shown in figure 2.15. The antenna consists of two substrate planes where the

metal patch and the microstrip feedline lie on respectively. The upper substrate layer for patch does not attach by a ground plane on the bottom so that the power is coupled electromagnetically from the feedline. That is the reason why the proximity-fed is also known as electromagnetically coupled.

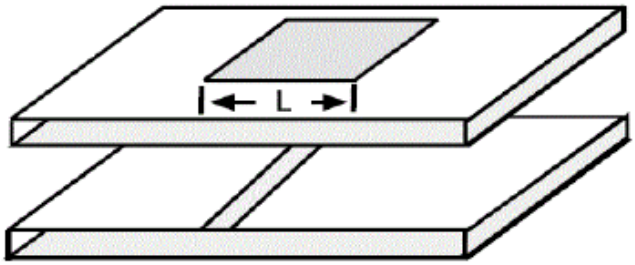


Figure 2. 15 Proximity-fed microstrip antenna

The structure of proximity-fed allows different operation on different substrate layers due to the independence of them in some extent. However, due to not fully isolated electromagnetic coupling, unwanted radiation still exists. Therefore essential adjustment is required for good efficiency performance. Also thicker material is often employed to enhance the frequency bandwidth in practice.

2.4.4 Aperture coupled-fed

Aperture coupled-fed is another principle non-connect feeding method [21]and its geometry is shown in figure 2.16. Multiple layers are used in this technique for operation. More specifically, the metal patch and microstrip feedline purchase different substrate layers of their own, which are separated by the ground plane in the middle with an aperture on it. And the aperture is usually located at the center of the patch to provide coupling feed through the microstrip feedline.

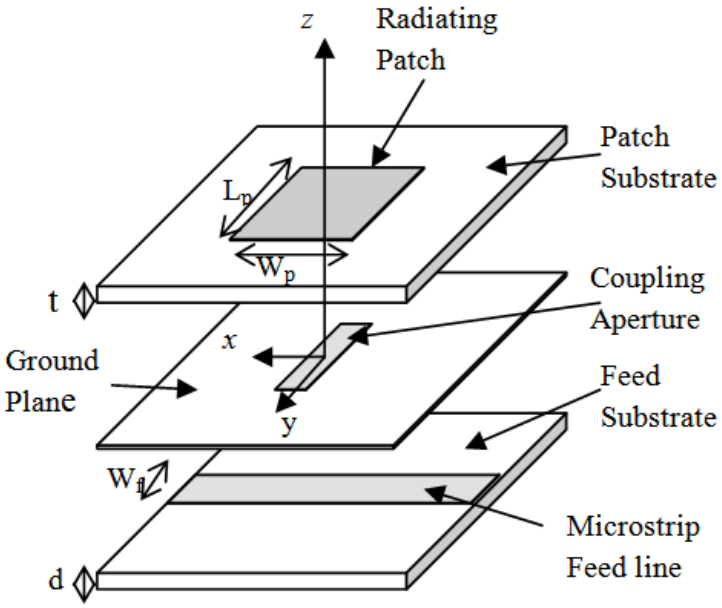


Figure 2. 16 Aperture coupled-fed microstrip antenna

In contrast with proximity-fed, this excitation mechanism stands out in fully independent optimization of two substrate layers, which belong to metal patch and feedline respectively [28]. Because of this feature, it is convenient to integrate the patch antenna with other active devices. Compared to the probe-fed, the manufacture process will be much easier for aperture coupled-fed without the requirement of vertical interconnects. It can be easily achieved by printed CAD technique. However, some weaknesses also appear due to the dispersion of multi layers. For example, the gap between layers plays a significant role in controlling input impedance. Also the material requires to be not lossy for efficiency consideration.

Table 2.1 shows the comparison among these four basic feeding methods in several aspects.

Characteristics	Edge-fed	Probe-fed	Proximity coupled-fed	Aperture coupled-fed
Spurious feed radiation	More	More	Less	Minimum
Reliability	Better	Poor due to soldering	Good	Good
Ease of manufacture	Easy	Soldering and drilling required	Alignment required	Alignment required
Impedance matching	Easy	Easy	Easy	Easy

Frequency bandwidth	2-5%	2-5%	2-5%	13%

Table 2. 1 Comparison among four principle feeding methods

From the table it can be easily seen that the edge-fed by microstrip line is the simplest one for fabrication with enough stability, but power maybe lost through unwanted radiation. And aperture coupled-fed can provide the widest bandwidth and the least spurious radiation among these four technique, however more attention needs to be paid on the adjusting while manufacture. Similarly, proximity coupled-fed also needs alignment in practice. Probe-fed has the worst behavior both in stability and fabrication due to its complicated construction.

2.4.5 Coplanar waveguide (CPW)-fed

Coplanar waveguide-fed, as the name implies, is an excitation mechanism realized by coplanar waveguide. Figure 2.17 gives the geometry of this kind of transmission line. It consists of a central conductor together with two ground planes located on the side. All these three metal lines are located on the same side of the dielectric substrate. And on the other side there is not an additional ground plane on the bottom, which is the biggest difference between CPW-fed and other feeding methods.

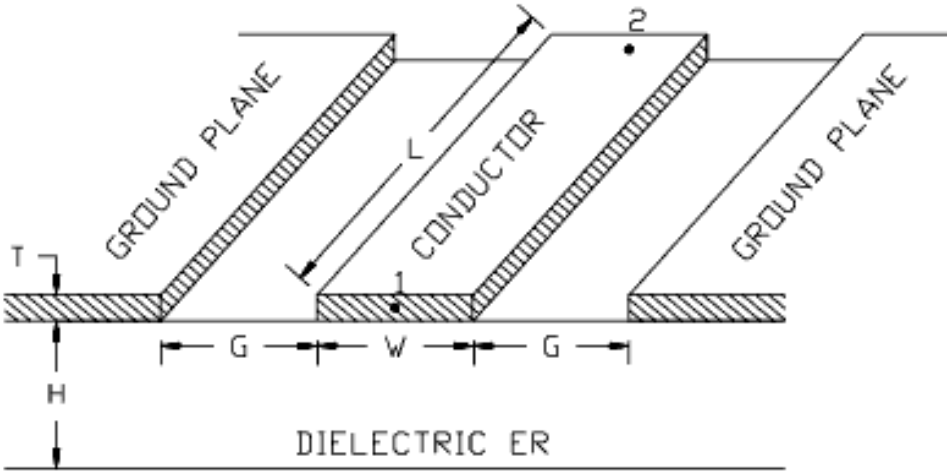


Figure 2. 17 Coplanar waveguide

The main merit of CPW-fed is its ease to fabricate and integrate. Due to the metal patch, transmission line and ground plane sit on the same side, it is even easier than microstrip line while manufacturing using printed circuit technique. Besides this, it also performs well at high frequency operation and circuit isolation [14] [29], which meets the requirement of microwave system. What's more, the impedance match can be easily realized by adjusting the width of the central conductor. Figure 2.18 shows a microstrip antenna using CPW-fed simulated using CST software. Because the shape of the patch looks

like traditional Chinese copper coin, it is named copper coin shape antenna in the following chapters.

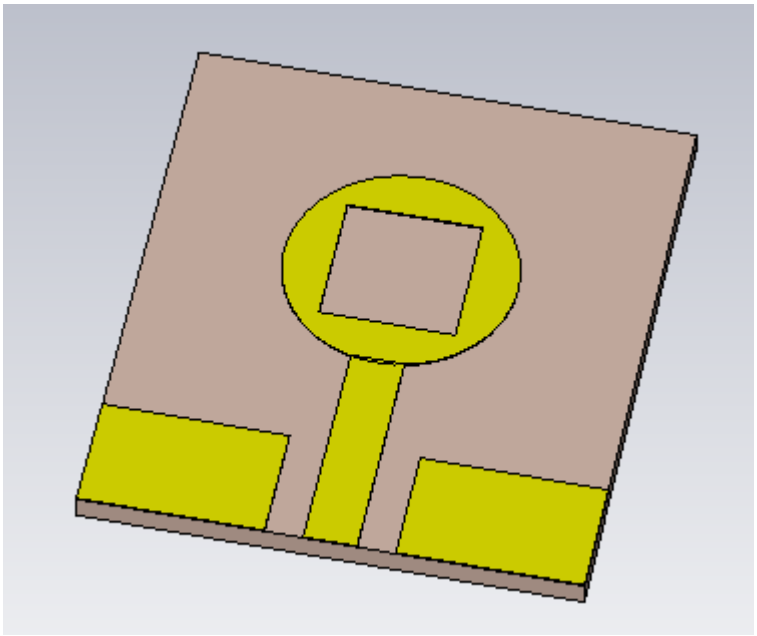


Figure 2. 18 CPW-fed microstrip antenna

As the design formulas are pretty complicated for CPW, we will pay more attention on its influential parameters in the following chapter.

2.5 Computational electromagnetics (CEM)

With the increasing requirement of antenna in terms of different frequency bands and operation environments, simulation plays an important role in design to ensure the antenna meets the specification. At the same time, not only design problems but also the influence of antenna could be obtained easier in simulation software at an early stage. Different computational electromagnetics are employed by different software packages.

Computational electromagnetics is an important subject for electromagnetics research [30] because it deals with modelling the effect and response of electromagnetic field under specific environment. It is widely employed to calculate antenna performance, radar wave propagation and also power direction of the system, etc. It includes many methods in application which can be divided into two main classes, the numerical methods and high frequency methods[5]. More specifically, numerical methods are suitable for elements with small dimensions whereas high frequency methods fit large structures. Figure 2.19 gives a flow chart of the classification of CEM.

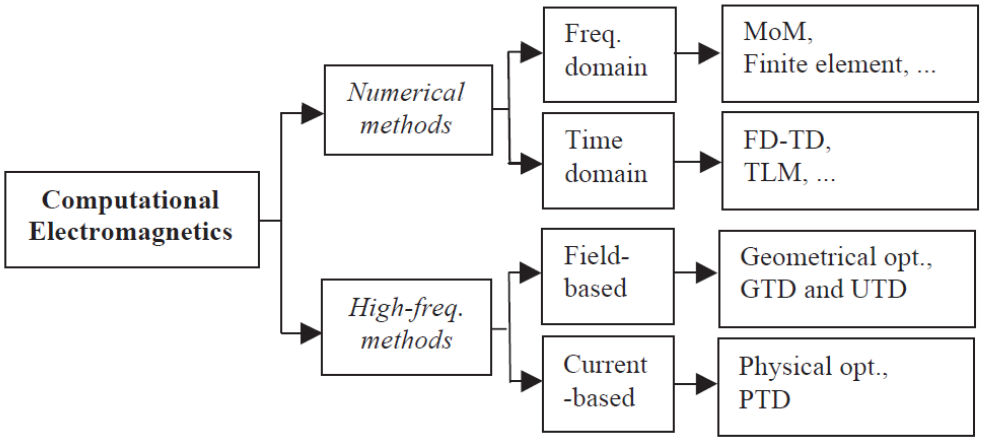


Figure 2. 19 Classification of CEM [5]

The right computation method is essential since the wrong choice will lead to incorrect results or long calculating time. As for the microstrip antenna, numerical methods are more popular depending on its small size. Thus several related methods are introduced as follow.

2.5.1 Method of moments (MoM)

The method of moments [31] solves linear equations which were transformed from integral or differential equations. The basis equation is crucial because it influences the computation time as well as accuracy in some extent. As it only calculates the boundary values instead of values of the whole field, it is more efficient on small size structure with low ratio of surface to volume [32]. It builds ‘’mesh’’ on the surface of the model before simulation and then solves the problem according to its calculating. Thus the simulation time tends to change according to the size of model and problem.

For antenna application, MoM method is widely employed in wire-type antenna simulation, like dipole antenna. And the commercial simulation software based on MoM method includes EZNEC.

2.5.2 Finite element method (FEM)

The finite element method [33], which is based on energy principle, aims to find the approximate solution of partial difference and integral equation. Also the main task of this method is to find and establish the approximate equation for solving. It subdivides the large problem into small parts which called finite element and the simulation would be taken on each element. Assembled these separate analyses on the whole system an approximately

solution with high precision would be got. Thus it has been one of the most popular and established techniques in commercial application[34] due to its accuracy . However, the shortcome is that it takes long time for simulation and requires large computer memory while simulating.

FEM is well used in large structure analysis like the reflector antenna. HFSS is a kind of software which based on FEM and it gives a good comprehension of physics structure when modelling.

2.5.3 Finite-difference time-domain (FDTD)

Finite-difference time-domain [35]method is the most popular computational method so far. Unlike those two methods mentioned before, this method is based on time domain thus it can cover wide frequency band. It divides the simulation domain into several cells and simulates through time steps according to the Maxwell's equation in partial difference form [36], which needs more work than MoM and FEM. The equation is solved in electric field at given time step and then turn to magnetic field at same time step, and repeat the process [37]. It analysis E-field and H-field directly to provide animated displays of the electromagnetic movement, which is useful in simulation. Therefore the accuracy of solution depends on two elements, the cell size and time steps. What's more, the material property, like ε, μ and σ, can also be taken into consideration into FDTD just like the way they are in the Maxwell's equation.

Nowadays, over thirty kinds of commercial and developing software are based on FDTD method, EMPIRE is one of them.

2.5.4 Finite integration technique (FIT)

The finite integration technique was introduced by Thomas Weiland in 1977 [38] and has been developed during the following years. It is very similar to the FDTD method which approximately describes Maxwell's equations on a grid space and can be written in time domain as well as in frequency domain. Also it is not restricted to a certain grid type [39]. The time domain solver, which only requires linear scale with mesh nodes, reduces the problem size effectivity. Therefore it is widely used in large radiate structures and even complete arrays to get a quick solution, whereas the high accuracy related to long solution time. Besides, it allows specific material at all points during the simulation domain but the domain itself must be infinite to provide effective residence.

A comparison table among these four methods is given in table 2.2, which gives a clear explanation of these four popular computational electromagnetic methods and relevant commercial software.

	MoM	FEM	FDTD	FIT
Meshing elements	Line or surface	Tetrahedron volumes	Cuboid volumes	Cuboid volumes
Discretization	Objects, only	Complete space	Complete space	Complete space
Boundaries	None	Absorbing BC	Absorbing BC	Absorbing BC
Simulation domain	Frequency domain	Frequency domain	Time domain	Time domain Frequency domain
Solver	Full matrix linear equation	Sparse matrix linear equation	Iterative solution small time steps	Iterative solution small time steps
Advdantages	Good at large problem Easily combined with other method	Fast at single frequency	Good at small size and broadband solution Material properties	High flexibility in modelling Broadband solution Material properties
Disadvantages	Mesh only on surface Inhomogeneous material	Large computer memory and long simulation time	Stair casing	Dilution of accuracy on large structure
Software	EZNEC	HFSS	EMPIRE	CST

Table 2. 2 Comparison of different simulation methods

CST MICROWAVE STUDIO ® (CST MWS) is based on the Finite Integration Technique (FIT) [40]which possesses powerful modelling ability as well as the flexibility of operation. Although its accuracy diluted while the size increasing, it still suits different principles for antennas and couplers especially for those purchases small dimension.

In conclusion, CST MWS offers a single design environment which fulfils almost all requirements of antenna and friendly operation for simulating on different character. Thus it is employed in microstrip antenna and coupler design in this project.

2.6 Summary

This chapter discusses the basic theory of antennas including some important parameters like S11, VSWR, BW, efficiency, gain and directivity. In addition, the general knowledge about microstrip antennas like the characteristic and development are also discussed based on the transmission line theory. Besides this, it also covers the four popular feeding methods applied in the design of microstrip antenna. This includes microstrip-line fed and CPW-fed, which are employed in this project. Finally it deals with various simulation methods and CST software with FIT technique is chosen for the following simulation.

Chapter 3 Methodology

Before creating models in simulation software, the theoretical methodology plays an important role in designing a microstrip antenna. According to the mathematical estimation, the dimension of a transmission line or patch antenna can be determined approximately. Based on this information, it will be much easier to build and adjust the model of the device using software.

3.1 Microstrip line

Microstrip line is widely employed in radio system to connect different devices since it is easily manufactured and integrated. The geometry of it is given in figure 3.1. It consists of a conductor with width w printed on a substrate layer with the permittivity ε_r and the height h, and the metal ground plane is on the bottom.

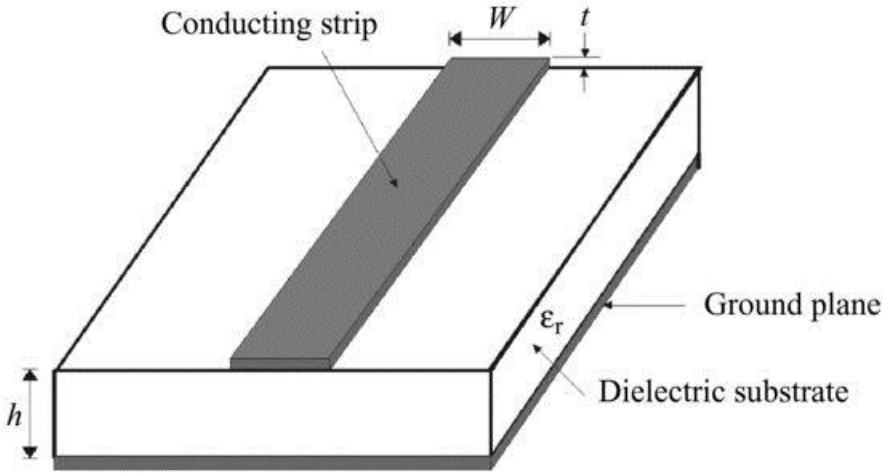


Figure 3. 1 Microstrip line

To analyse the methodology of it we also need the distribution of electric and magnetic field in the near space of microstrip line, as shown in figure 3.2. As some of the field lines are in air instead of the dielectric area, ε_e is introduced as the effective dielectric constant for discussion, which range from 1 to ε_r .

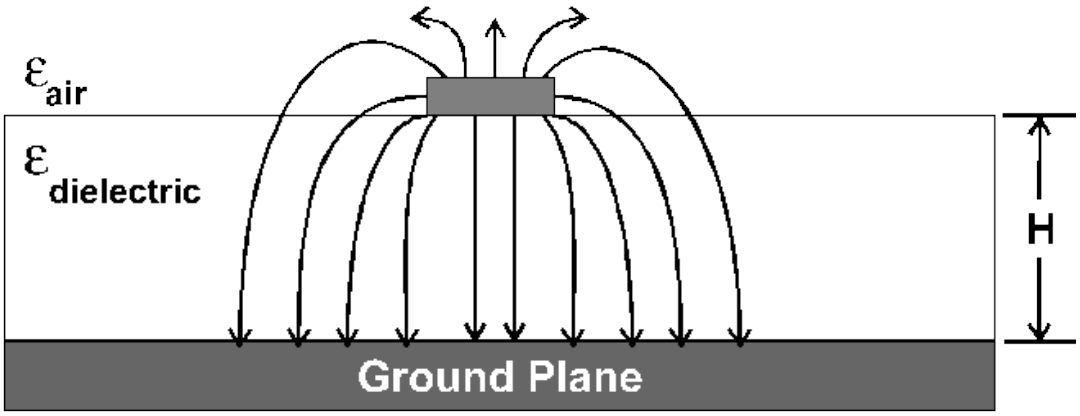


Figure 3. 2 Electric and magnetic field of microstrip line

More accurately, ε_e depends on several elements like substrate thickness and strip line width. And the approximate expression of it is given below [41, 42].

$$\varepsilon_e = \frac{\varepsilon_r+1}{2} + \frac{\varepsilon_r-1}{2}\frac{1}{\sqrt{1+\frac{12h}{w}}} \tag{3.1}$$

Where *h* refers to the height of substrate layer and *w* is the width of strip line. It is obvious that the larger the ratio $\frac{W}{h}$, the smaller the ε_e.

Next step is to determine the characteristic impedance of the transmission line under given dimension [43].

$$Z_0 = \begin{cases} \frac{60}{\sqrt{\varepsilon_e}} \ln\left(\frac{8h}{W} + \frac{W}{4h}\right) & for\ \frac{W}{h} \le 1 \\ \frac{120\pi}{\sqrt{\varepsilon_e}\left[\frac{W}{h}+1.393+0.667\ln\left(\frac{W}{h}+1.444\right)\right]} & for\ \frac{W}{h} \ge 1 \end{cases} \tag{3.2}$$

On the contrary, if the dielectric constant ε_r and characteristic impedance are set, then the dimension can be found through the ratio of *W* to *h* [41].

$$\frac{W}{h} = \begin{cases} \frac{8e^A}{e^{2A}-2} & for\ \frac{W}{h} < 2 \\ \frac{2}{\pi}\left[B - 1 - \ln(2B-1) + \frac{\varepsilon_r - 1}{2\varepsilon_r}\left\{\ln(B-1) + 0.39 - \frac{0.61}{\varepsilon_r}\right\}\right] & for\ \frac{W}{h} > 2 \end{cases} \tag{3.3}$$

Where

$$A = \frac{Z_0}{60}\sqrt{\frac{\varepsilon_r+1}{2}} + \frac{\varepsilon_r - 1}{\varepsilon_r + 1}\left(0.23 + \frac{0.11}{\varepsilon_r}\right)$$

$$B = \frac{377\pi}{2Z_0\sqrt{\varepsilon_r}}.$$

From (3.2) and (3.3), we can obtain that besides the property of substrate, the impedance of a microstrip line is only related to its width and substrate height. That is to say, the length of the transmission line can be ignored in some extent when designing.

In practical, the impedance of 50 Ω is always employed to connect between electric devices. Thus we assume $Z_0 = 50\ \Omega$ as a certain condition for the following calculation. Then we guess that $\frac{W}{h} < 2$ in (3.3) to see if the result agrees with our assumption. If they are consistent with each other then the ratio $\frac{W}{h}$ is determined. If not matched, we just need to try the other situation assuming $\frac{W}{h} > 2$, and calculating relevant result using the equation above.

As a basic transmission line, the microstrip line is required not only in patch antenna design but also coupler design to connect specific elements with power sources. Therefore it is an indispensable component in this project. Basic theory and design of couplers will be discussed in chapter 5 in detail.

3.2 Coplanar waveguide

The coplanar waveguide is applied in recent antenna designs due to its ease of fabrication and good performance at high frequencies [44]. However the design formulas of CPW are complicated [45]because of multiple influential elements in its geometry. They are width *W* and thickness *t* of central conductor, substrate heigth *h* and gap *G* between ground plane and central conductor, as shown in 3.3.

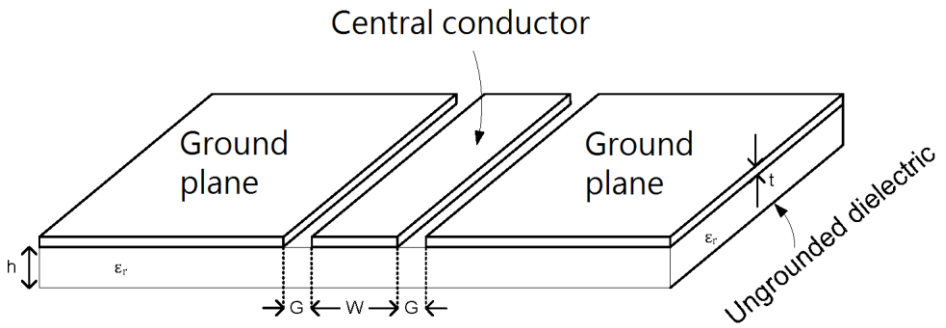


Figure 3. 3 Coplanar waveguide

Because of too many influential factors, it is not possible to give accurate mathematical formulas like for the microstrip line. Some approximations have been made in formulas [5, 8] ignoring the thickness t of central conductor.

$$\varepsilon_e = \frac{\varepsilon_r + 1}{2}\left\{\tanh\left[0.775 \ln\frac{h}{G} + 1.75\right] + \frac{kG}{h}[0.04 - 0.7k + 0.01(1 - 0.1\varepsilon_r)(0.25 + k)]\right\} \tag{3.4}$$

Where

$$k = \frac{W}{W+2G} \tag{3.5}$$

And the characteristic impedance is

$$Z_0 = \frac{30\pi}{\sqrt{\varepsilon_e}}\frac{K'(k)}{K(k)} \tag{3.6}$$

Where $K(k)$ refers to the elliptical function, that

$$k' = \sqrt{1 - k^2}$$
$$K'(k) = K(k') \tag{3.7}$$

And

$$\frac{K'(k)}{K(k)} = \begin{cases} \left[\frac{1}{\pi}\ln\left(2\frac{1+\sqrt{k'}}{1-\sqrt{k'}}\right)\right] & if\ 0 < k < 0.707 \\ \left[\frac{1}{\pi}\ln\left(2\frac{1+\sqrt{k}}{1-\sqrt{k}}\right)\right]^{-1} & if\ 0.707 < k < 1 \end{cases} \tag{3.8}$$

Similarly, the practical value for Z_0 is $50\ \Omega$ in design. The equations above are quite complex for an approximate result. Therefore in the following section we will focus more on how the relevant factors of CPW influence the performance of the patch antenna.

3.3 Rectangular patch antenna

The rectangular patch antenna is the most popular microstrip antenna due to its easy fabrication and design. Based on the knowledge mentioned before about microstrip line, the rectangular patch antenna is introduced as presented in the following section. Figure 3.4 gives the dimension of a patch antenna.

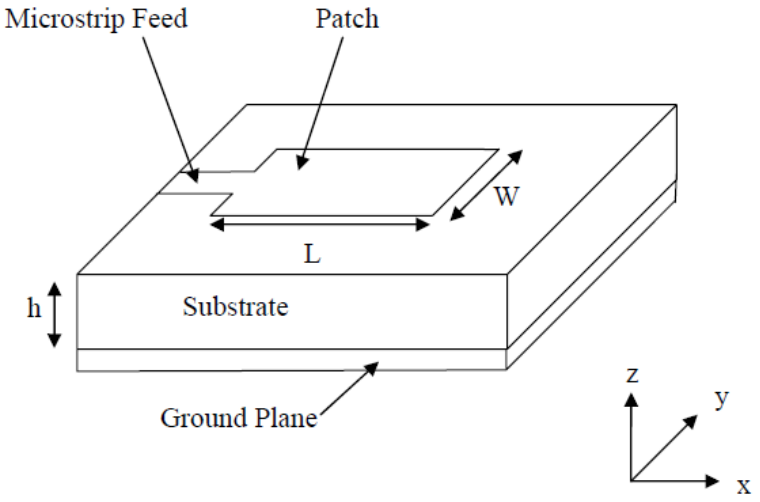


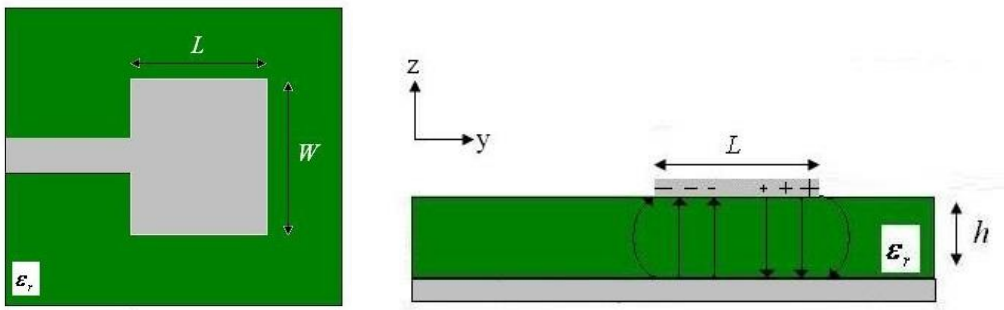
Figure 3. 4 Rectangular patch antenna

Generally, the length *L* is about $\frac{\lambda_0}{2}$, and the width *W* is shorter than λ_0. However, if the width *W* is too small it will become a microstrip line instead of a radiating antenna.

3.3.1 Radiation mechanism

Understanding the principle why the antenna is radiating is helpful for designing. It is known that radiation is caused by accelerating charges which produces changing electric field. And the magnetic field would also be changed through the Maxwell's equations. Hence we have electromagnetic radiation.

From the side view of the patch antenna in figure 3.5, the patch can be considered as an open circuited transmission line ($L = \frac{\lambda_0}{2}$) with two fringes at two sides.



(a) Top view (b) Side view

Figure 3. 5 Structure of the patch antenna [46]

According to the theory of transmission line, the start and the end of the open circuited line are the voltage antinodes, like figure 3.6 shows. As the figure 3.5(b) shows, it has the maximum voltage at the end(+V) and minimum voltage at the start(-V) Based on the transfer characteristic of half-wavelength line, the current on the two sides of the patch are current nodes. Therefore the E-fields between the patch and the ground plane have different directions. However, they have the same propagation direction(+y) at the two fringes, which adds up the current in phase.

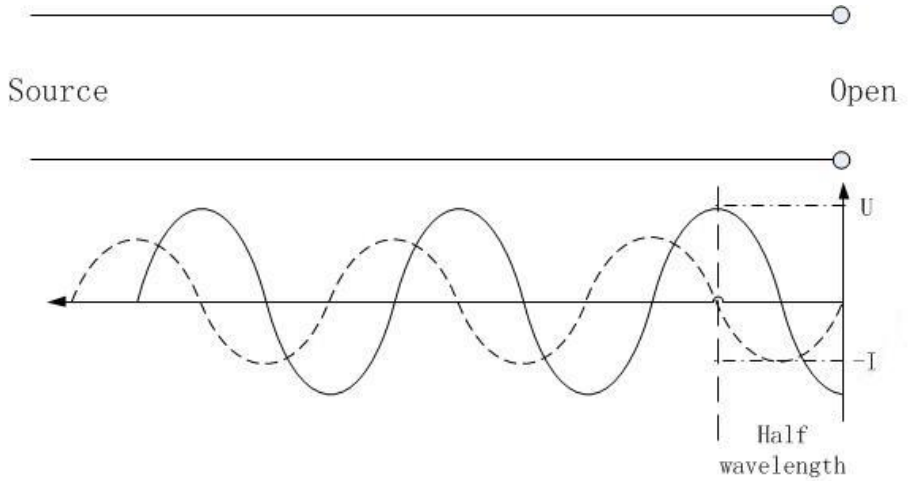


Figure 3. 6 Theory of transmission line

The E-field changes with the current propagation and leads to the changing H-field. According to the radiation theory mentioned before, the two fringes therefore leads to the radiation of the microstrip antenna [47]. More specifically, it is the two fringing fields adding in phase that give the radiation of the antenna.

3.3.2 Design formulas

For rectangular patch antenna the main design is to determine the dimension of the rectangular patch. Due to the fringing effect, the electrical size of the patch is a little bit bigger than its physical size. The extension on the length *L* is given by [48].

$$\Delta L = \frac{0.412d(\varepsilon_e+0.3)\left(\frac{W}{h}+0.264\right)}{(\varepsilon_e-0.258)\left(\frac{W}{h}+0.8\right)} \tag{3.9}$$

Where ε_e is the effective dielectric constant and has been given in (3.1), which is related to the ratio $\frac{W}{h}$.

So the effect length of the rectangular patch is

$$L_{eff} = L + 2\Delta L \tag{3.10}$$

And the resonant frequency of the wave prorogated through the patch is

$$f_r = \frac{1}{2L_{eff}\sqrt{\varepsilon_e}\sqrt{\varepsilon_0\mu_0}} \tag{3.11}$$

Where ε_0 and μ_0 refer to the electric constant and magnetic constant respectively in free space.

$$c_0 = \frac{1}{\sqrt{\varepsilon_0\mu_0}} \tag{3.12}$$

Here c_0 is the light speed in free space which equals to $3\times10^8\ m/s$, thus (3.11) can be writen in a simpler way.

$$f_r = \frac{3\times10^8}{2(L_{eff})\sqrt{\varepsilon_e}} \tag{3.13}$$

Correspondingly, the effective length L_{eff} of the patch can be calculated easily.

$$L_{eff} = \frac{3\times10^8}{2f_r\sqrt{\varepsilon_e}} \tag{3.14}$$

Finally the width of the radiating patch is

$$W = \frac{3\times10^8}{2f_r}\sqrt{\frac{2}{\varepsilon_r}} \tag{3.15}$$

Based on these equations the size of the rectangular patch can be determined under the given addition of substrate (ε_r, h) and resonant frequency (f_r) following these steps.

- Determine W through formula (3.15)
- Calculating effective constant ε_e using (3.1)
- Obtain the enlargement part ΔL of L by (3.9)
- Finally computing the realistic length of the patch from (3.14)

3.3.3 Quarter wavelength transmission line

Apart from the basic type, there is another typical type popular used in practical application. It is fed by a quarter-wavelength transmission line and a standard transmission line, which shown in top view in figure 3.6.

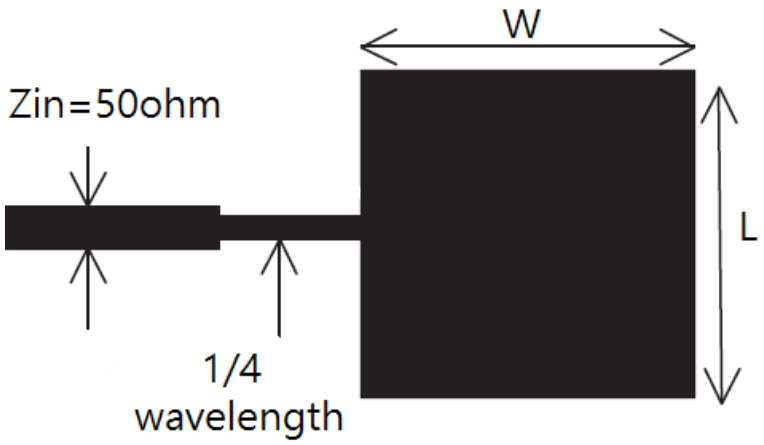


Figure 3. 7 λ/4 transmission line feed microstrip antenna

Here the quarter-wavelength line is employed as a transformer to provide the match of impedance between the patch and the 50 Ω standard transmission line.

The input impedance at the edge of the rectangular patch is similar to the following equation.

$$Z_L \approx 90 \frac{{\varepsilon_r}^2}{\varepsilon_r - 1} \left(\frac{L}{W}\right)^2 \tag{3.16}$$

And the transform characteristic of quarter-wavelength transmission line is

$$Z_{in} = \frac{{Z_0}^2}{Z_L} \tag{3.17}$$

Where Z_{in} refers to the 50 Ω of the standard transmission line. And Z_0 is the characteristic impedance of $\frac{\lambda}{4}$ transmission line.

Then we can use (3.2) to determine the width of the $\frac{\lambda}{4}$ transform line as well as the standard transmission line.

3.4 Summary

This chapter explains the radiation mechanism of microstrip antenna. Also the principle methodologies are included for microstrip line, coplanar waveguide and rectangular patch antenna respectively. It gives the calculation formulas for the dimensions determined under specific conditions of resonant frequency and substrate status. The mathematical estimation is the first step

before others and is important for understanding the working principle of the devices. Therefore it plays an indispensable role in the whole design procedure.

Chapter 4 Design of microstrip antenna

4.1 CST design procedure

When employing CST software in designing an electrical device, it can be divided into several steps. Figure 4.1 gives the flowchart of the design procedures in CST.

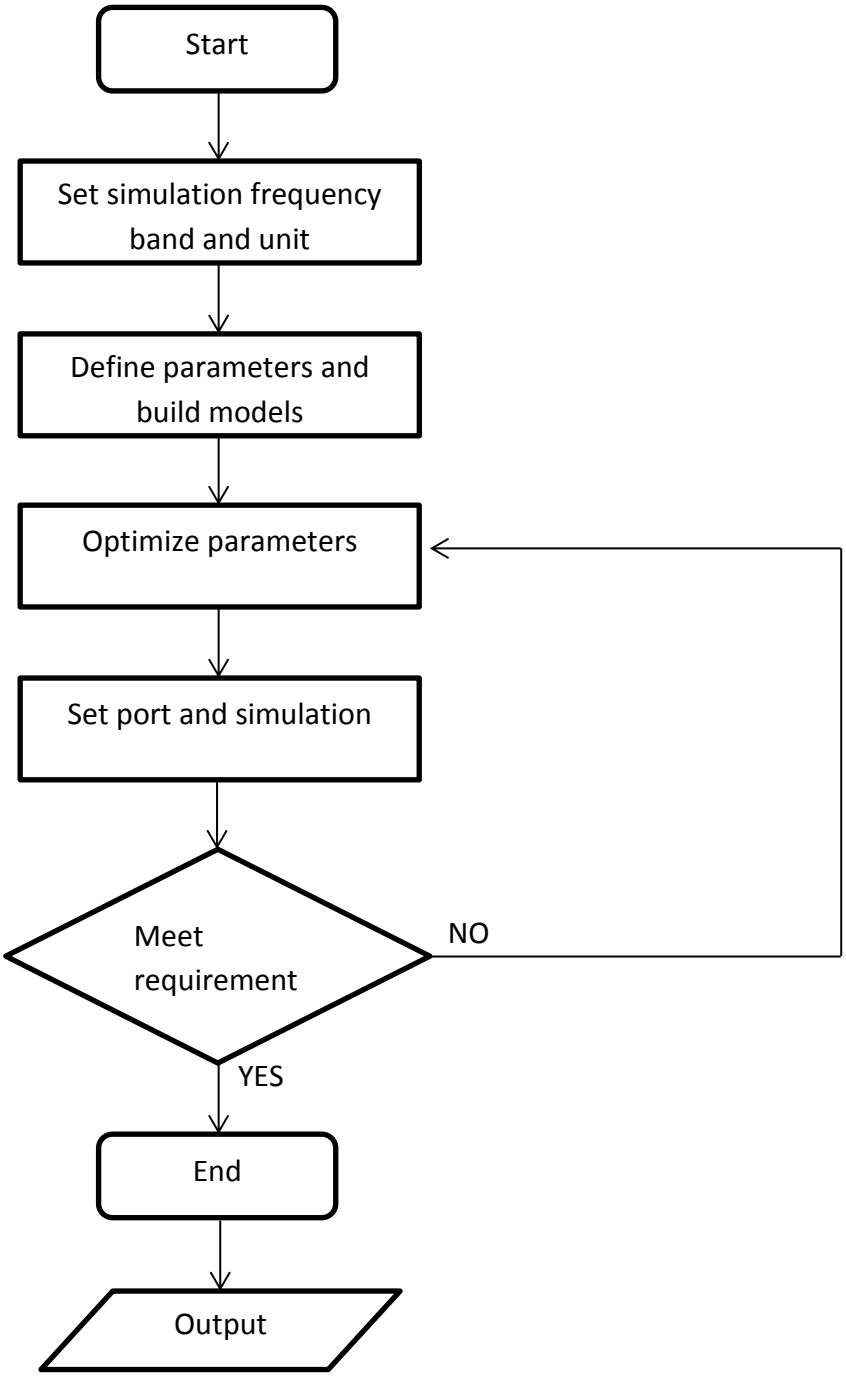


Figure 4. 1 Design procedures in CST

It starts from choosing the suitable module. Here the option of planar antenna in MWS is employed because it meets the character of the patch antenna. And then we set the simulation frequency band and unit of variable. In this thesis, the simulation frequency band is set from 4 GHz to 7 GHz with the central frequency of 5.5 GHz and the unit of dimension is millimeter (mm).

Then the model is built according to the calculation result from chapter 3. Compare to other softwares like HFSS, CST is easy-operated in building models due to its working coordinate system could be aligned with the selected points or surface. That is to say, it is very convenient to move the model or insert a parameter to change it, which is friendly in the later optimize process. Also the mesh controls the accuracy of the simulation results which also increase the simulation time. Hence it should be well chosen.

Based on the theory, the parameters still need to be adjusted slightly to meet the requirements that the antenna radiates well at resonant frequency 5.5 GHz. Instead of using 'Optimizer' in the software directly, the 'Par.sweep' is well used because it is based on the quick sweep on selected parameter to achieve the goal instead of random operation optimize.

After adjustment the antenna with better performance will be chosen as the output of the simulation. Here we choose the popular ones like S parameter, efficiency, gain and radiation pattern in the result tree. Also the current display could be seen on the model. Besides the history tree gives the clear information of your operation which is useful in simulation as well.

4.2 Requirements of antennas

The table below gives the design specification of the antenna like resonant frequency and dielectric material of substrate. Both the rectangular microstrip antenna and copper coin shape antenna as shown in section 2.4.5 are based on these requirements for design. Then according to the methodology mentioned in chapter 3 and the procedures above, the geometry of these two antennas can be optimized.

Relevant items of antenna	Data
Resonant frequency(f_r)	5.5 GHz
Substrate material	FR-4($\varepsilon_r = 4.3$)
Patch material	Copper
Thickness of substrate	2 mm

Table 4. 1 Design specification of the antenna

4.3 Rectangular microstrip antenna

4.3.1 Specific parameters and geometry

According to table 4.1, the parameters of the antenna can be confirmed using the formulas in chapter 3. For instance, the dimension of the patch and the width of transmission line are illustrated in table 4.2. It can be noticed that the width of the patch is longer than the length due to the calculation result in section3.3.2. In comparison, the parameters after adjustment are given as well and the adjustment process will be given in section 4.3.3 to discuss how influence on the performance of the antenna.

Parameters	Original value	Adjusted value
Width of patch	16.6 mm	16.6 mm
Length of patch	12.21 mm	11.9 mm
Width of 50 Ω feedline	3.832 mm	1.5 mm
Length of substrate	30 mm	25 mm
Width of substrate	30 mm	22.5 mm
Feed position	Central of the patch edge	Central of the patch edge

Table 4. 2 Parameters of MSA

Finally the model of antenna is built in CST on account of these specific parameters above, like the figure 4.2 shows. It consists of the metal patch on the top, the dielectrical substrate on the metal ground plane and a microstrip line for providing the source.

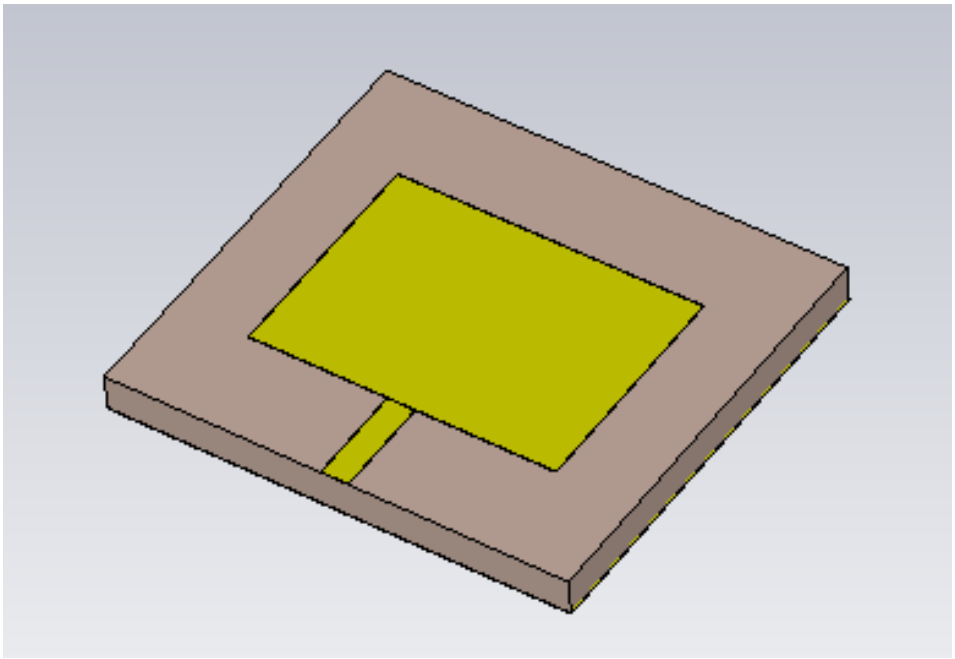


Figure 4. 2 Antenna structure in CST

4.3.2 Simulation results

- S_{11} parameter

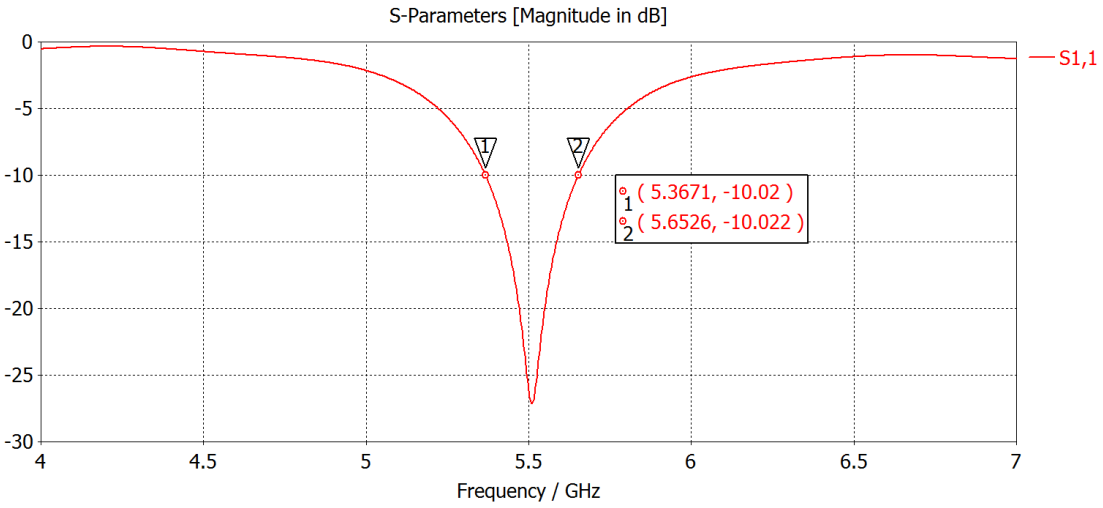


Figure 4. 3 S11 parameter of MSA

We can see from the figure that the curve experiences a slow fluctuation from 4 GHz to 5GHz and also 6 GHz to 7 GHz. However it changes sharply from 5 GHz to 6 GHz and peak at 5.5 GHz with the magnitude of -27 dB, in which located the resonant frequency.

As section 2.1.1 and 2.2.2 illustrate, a better impedance match leads to a small value of VSWR and S_{11} as well. It can be also verified in equation (2.2).

Hence figure 4.3 also illustrates a good match of impedance because the value of the parameter at 5.5 GHz is pretty low. According to section 2.1.2, the frequency bandwidth (for lower than 10 dB) can also be determined.

$$BW = 5.6526\ GHz - 5.3671\ GHz = 0.2855\ GHz = 5.2\%$$

- Efficiency

  According to the theory in section 2.1.6, the radiation efficiency and total efficiency can be obtained from figure 4.4.

$$\eta_e = -2.7797\ dB$$

$$\eta_t = -3.1376\ dB$$

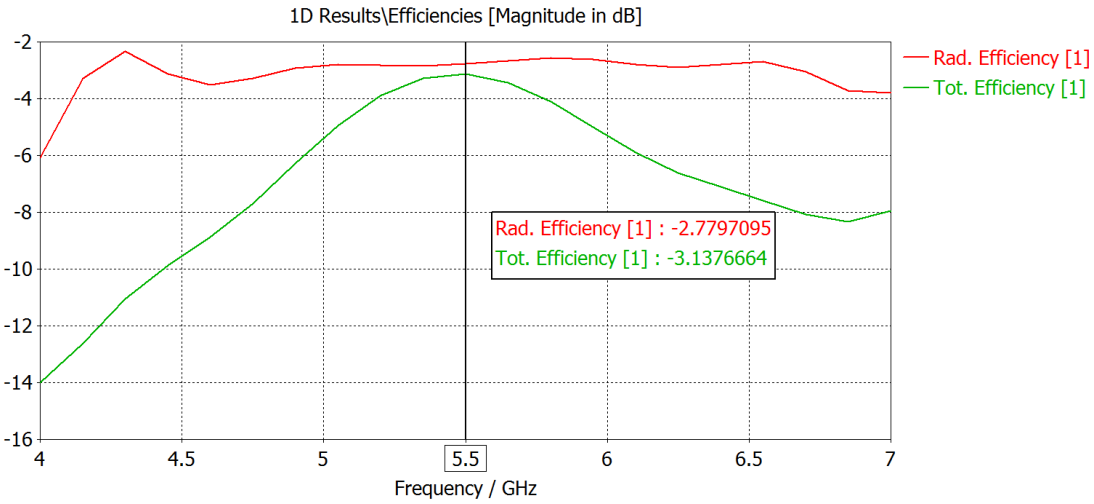


Figure 4. 4 Efficiency of MSA

It can be seen that the curve of radiation efficiency (red line) changes from -6 dB to -2 dB with small fluctuation and gets -2.78 dB at central frequency. Whereas the total efficiency(green line) increases sharply from -14 dB at 4 GHz to -3.14 dB at 5.5 GHz and then drop down to -8 dB at the end. From which we can obtain that highest total efficiency is located at the resonant frequency.

- Gain

  Based on the knowledge in section 2.1.7, the gain of the antenna at resonant frequency is shown in figure 4.5.

$$G = 3.5756\ dB$$

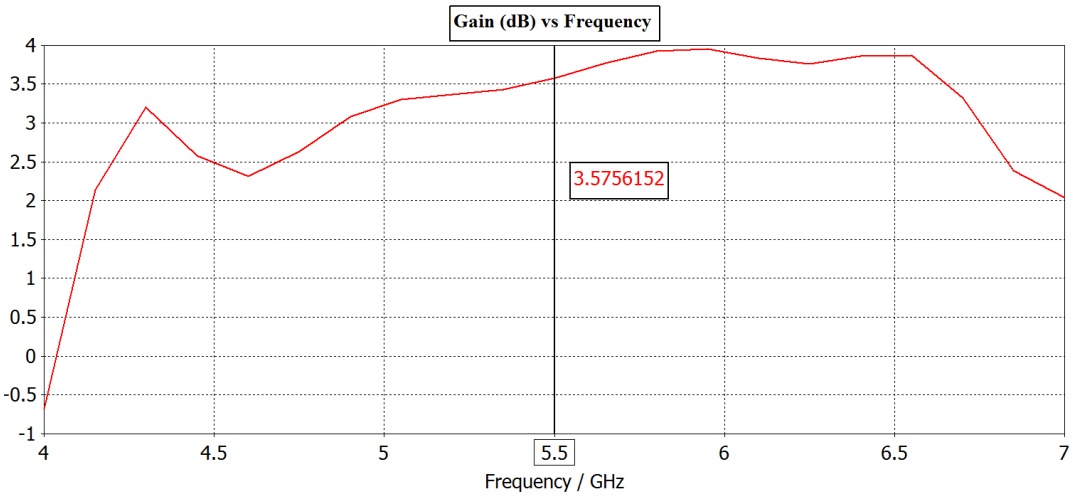


Figure 4. 5 Gain of MSA

The line in this figure waves through the simulation band and reaches 3.58 dB at resonant frequency, which shows the similar trend of the radiation efficiency in figure 4.4. It is due to the relation between radiation efficiency and gain in (2.9).

- Surface current

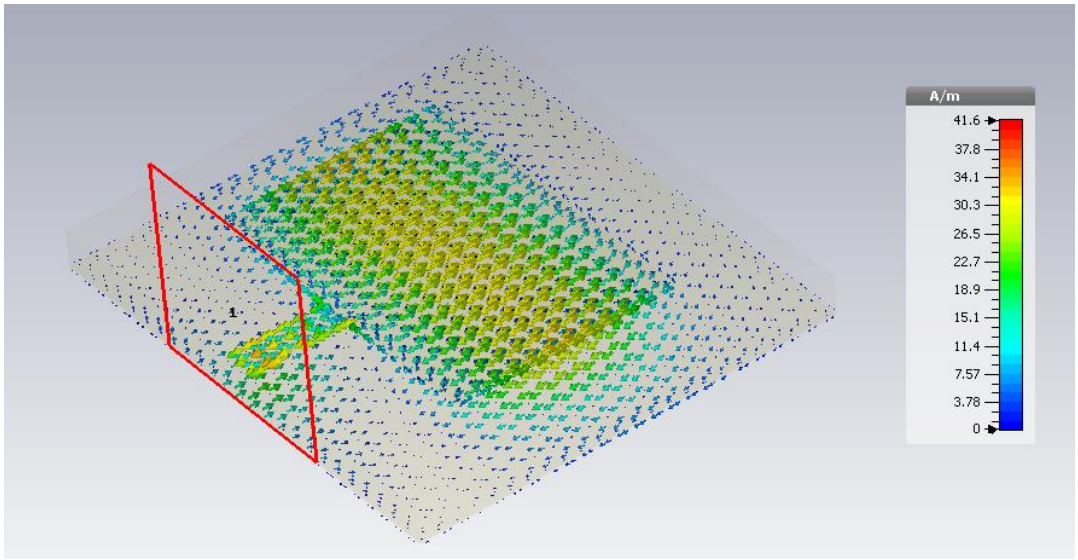


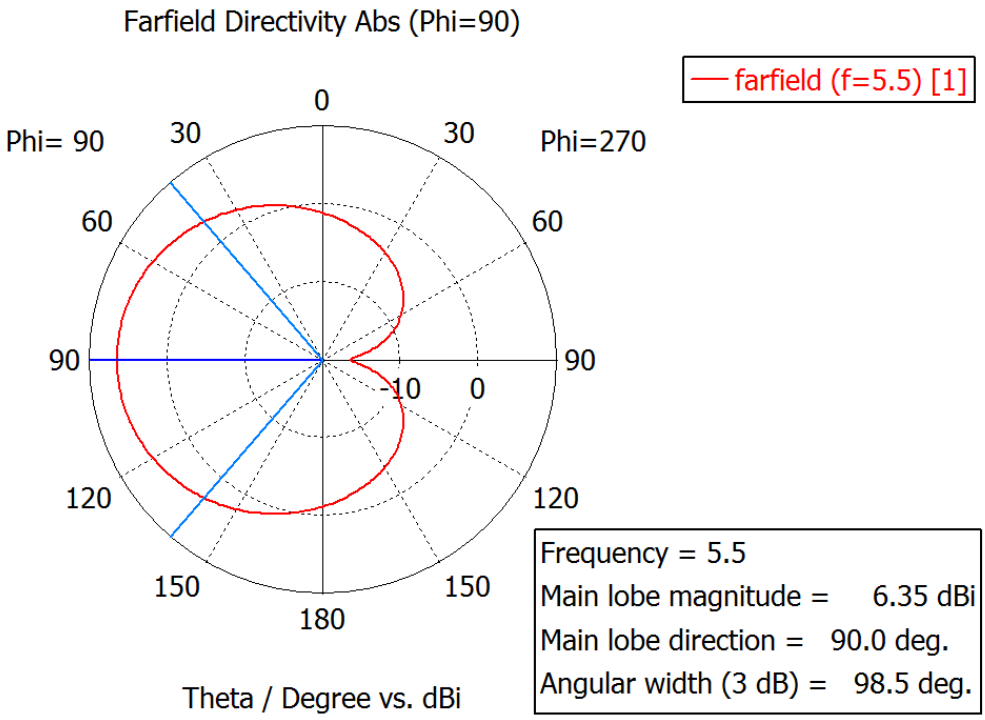
Figure 4. 6 Surface current of MSA

This figure gives the current distribution of the MSA. Obviously most of currents flow to the metal patch, which gives the radiation of the whole antenna.

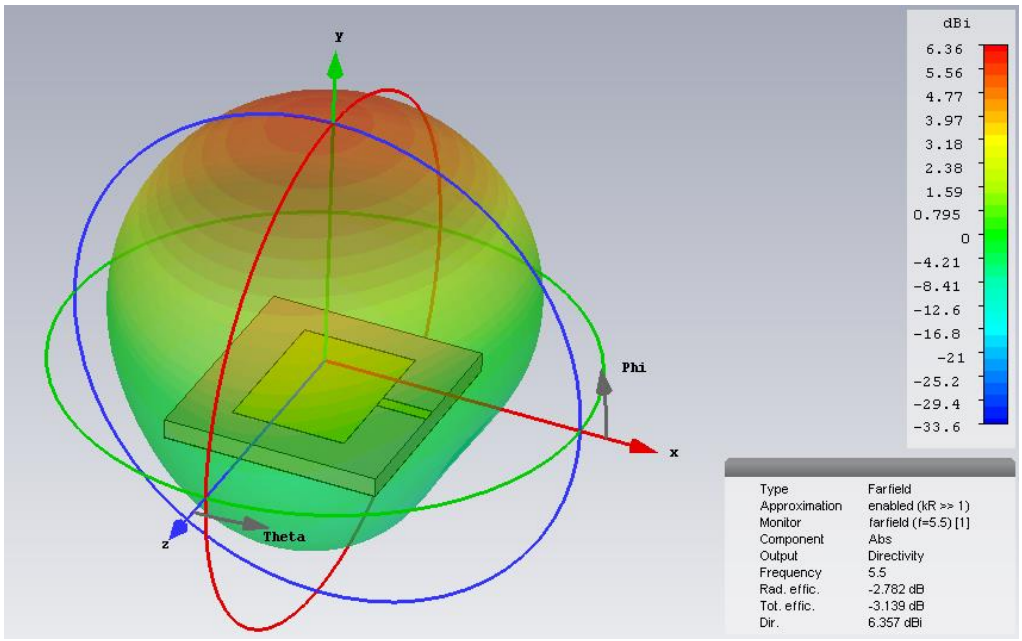
- Radiation patterns

From section 2.1.5, the directivity of the antenna can be obtained from figure 4.7 (b).

$$D = 6.357\ dBi$$



(a) Polar pattern



(b) 3D pattern

Figure 4. 7 Radiation patterns of MSA

From the 2D pattern in figure 4.7(a), we can get the shape of the radiation pattern. It indicated to be directional at $\phi = 90^{\circ}$, which corresponds with the +y axis in figure 4.7 (b), the 3D pattern. The antenna radiates more energy to the upside space. The same figure also shows the directivity of the antenna is 6.357 dBi. Combined with the discussion before, we can also verify (2.9) in simulation.

$$G(dB) = D(dBi) + \eta_e(dB)$$

We have G=3.58 dB, D=6.357 dBi, η_e=-2.78 dB, which satisfies the equation above.

4.3.3 Influential parameters

As mentioned in methodology chapter (chapter 3), there are several elements that will influence the performance of an antenna, both on patch and feedline. They have been determined by formulas in section 3.3, however differences still exist between theory and practical simulation. Thus we need to adjust these parameters to find how they influence the antenna's performance and determine the best value. It is an essential part among simulation process.

- Length of the rectangular patch

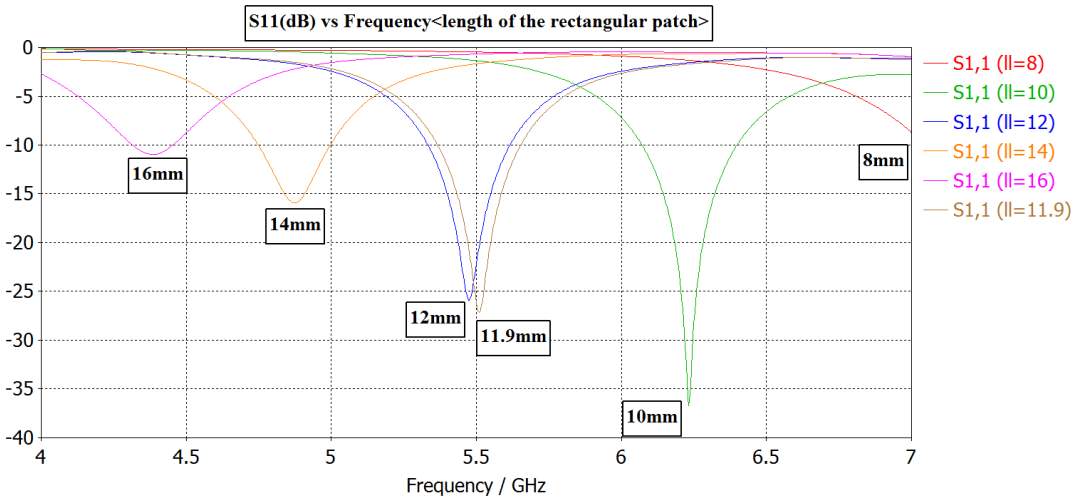


Figure 4. 8 Adjustment of the length of patch

Here the patch length has been varied between 8 mm and 16 mm. Figure 4.8 shows the change of S_{11} when adjusting the length of patch. From which it can be seen that the length of patch influences not only the input impedance but also the resonant frequency. Specifically the antenna gets best match of impedance when the length of patch is 10 mm but not resonant at the target

frequency for wireless communication at 5.5 GHz. As for the resonant frequency, it decreases when the length increases and meets the requirement of 5.5 GHz at 11.9 mm. Also this relation agrees with the theory in chapter 3.3.2, the equation (3.14).

- Width of the rectangular patch

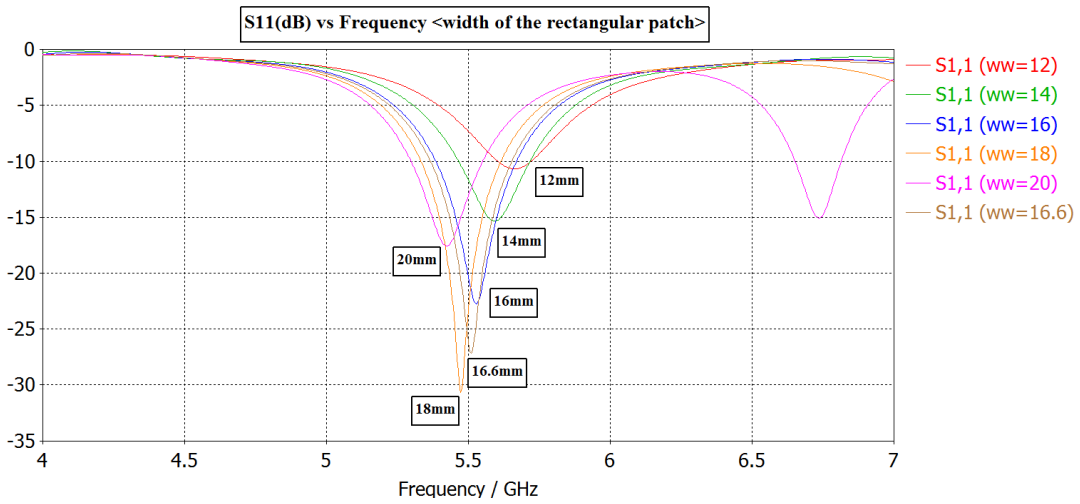


Figure 4. 9 Adjustment of the width of patch

From figure 4.9 it can be seen that the width of patch is operated between 12 mm and 20 mm. Obviously the width of patch mainly determines the impedance match of the antenna. Generally better match is provided by a wider patch from 12 mm to 18 mm and the goal frequency is obtained at 16.6 mm. However, a different behaviour can be seen at 20 mm which has a worse match (-17 dB) than 16 mm (-23dB) and two peaks exist at 5.4 GHz and 6.7 GHz separately.

- Width of feedline

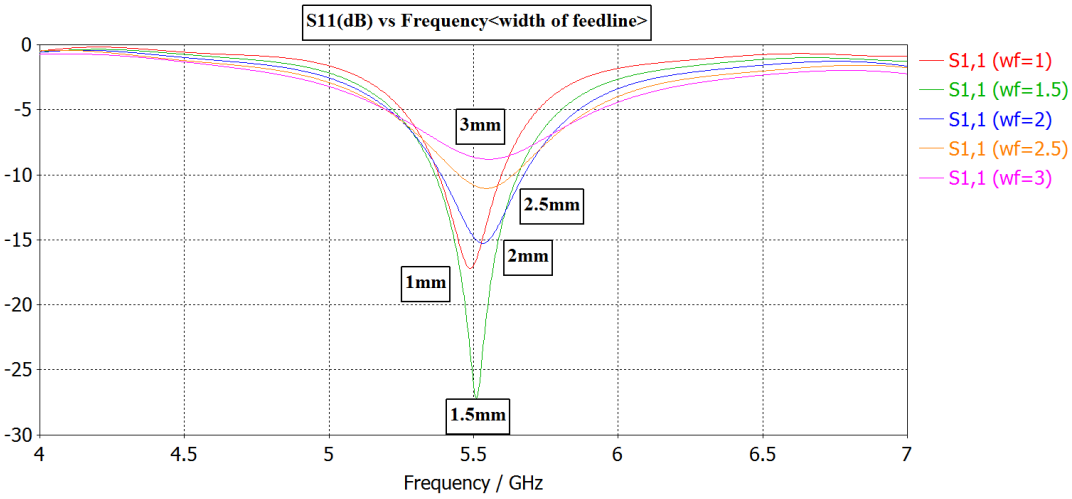
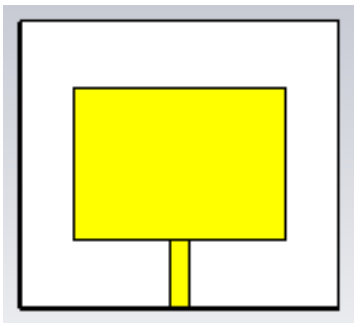


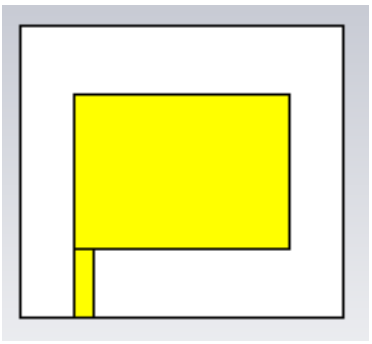
Figure 4. 10 Adjustment of the width of feedline

Apart from the metal patch, another element the feedline is also essential to be studied because it connects the antenna with the signal port during the simulation. First of all, we look at the width of the feedline as the figure 4.10 shows. With the increase of the width of feedline, the input impedance of the feedline varies in some extent. More specifically, the value of S_{11} fluctuates from -17 dB at 1 mm to -7 dB at 3 mm and has the best value of -27 dB at 1.5 mm. It just verifies the relation between impedance and width of microstrip line in chapter 3.1, formula (3.2).

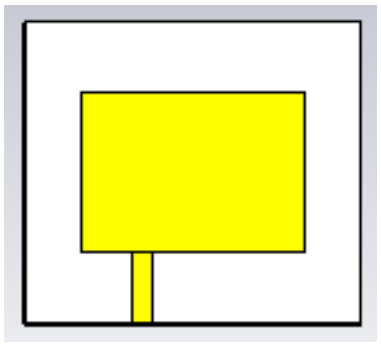
- Feed position



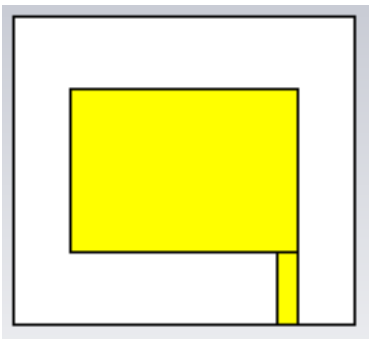
(a) Middle



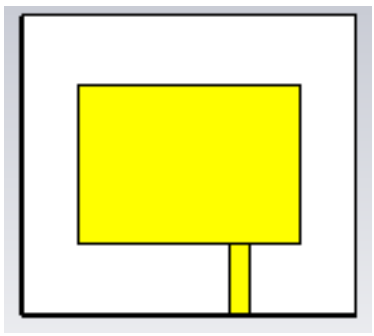
(b) Left side



(c) Left



(d) Right side



(e) Right

Figure 4. 11 Different feed positions

Another important issue of the feedline is the feed position of the antenna. Like figure 4.11 shows, five different positions are investigated.

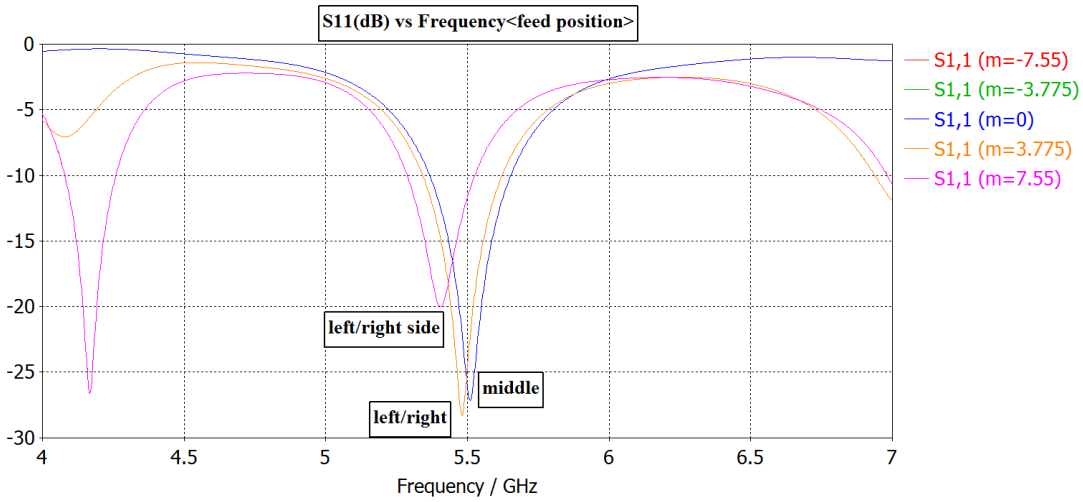


Figure 4. 12 Adjustment of the feed position

Here a variable *m* has been set to change the distance between the feed positon and the middle positon of the patch edge. For example, $m = 0$ illustrates the feed positon is exactly at the middle of the patch edge, like figure 4.11 (c) shows. And $m = 7.55$ states the feed position is located at the

right side of the patch edge like figure 4.11 (e) shows. And the rest can be done in the same manner.

Figure 4.12 shows three different results among five positions. Due to the symmetry of the structure, the right positon has the same result as the corresponding left position. It can be clearly seen that the side feed leads to more than one peak of resonant frequency which should be avoided in our design. Therefore feeding at middle position has been determined for more accurate simulation.

Apart from the elements on the top layer, we also want to study the other layers to find whether they influence the performance of an antenna. They are the substrate layer and the ground plane layer which are discussed as follow.

- Thickness of substrate

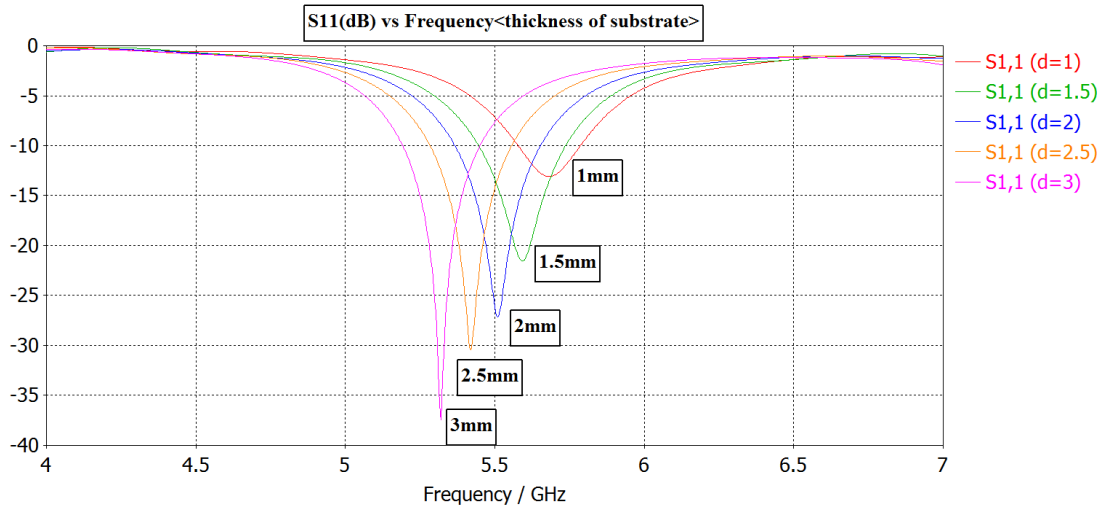
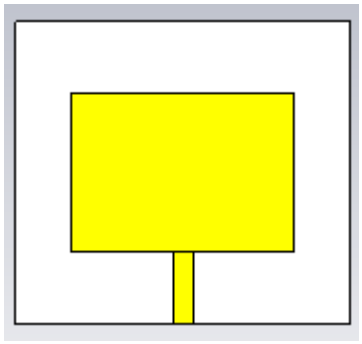


Figure 4. 13 Adjustment of the thickness of substrate

Because the value of substrate thickness is tiny it has been adjusted in a small range from 1 mm to 3 mm. Figure 4.13 shows the variation trend of S_{11} under different situation of thickness. It can be easily seen that the resonant frequency reduces with increasing the substrate thickness. This can be verified from chapter 3.3.2, the equation (3.9), (3.10) and (3.11). The thickness will influence the ΔL in L_{eff}, which will determine the resonant frequency f_r in (3.11).

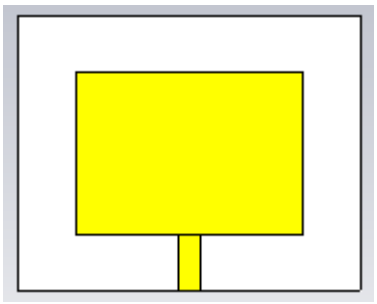
On the other hand, better match of input impedance is obtained with the same trend. This can be explained from the aspect of microstrip line in chapter3.1, formula (3.2). It illustrates that the thickness of substrate determined the characteristic impedance of the element. Therefore the theory has been verified well in simulation results.

- Dimension of ground plane

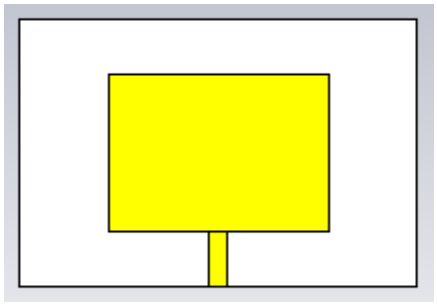


22.5*25

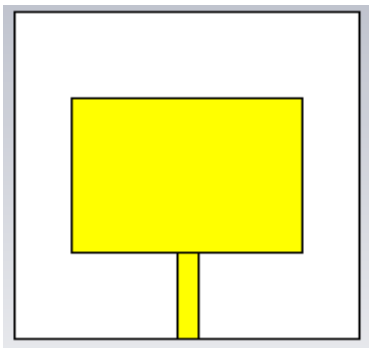
(a) Original dimension



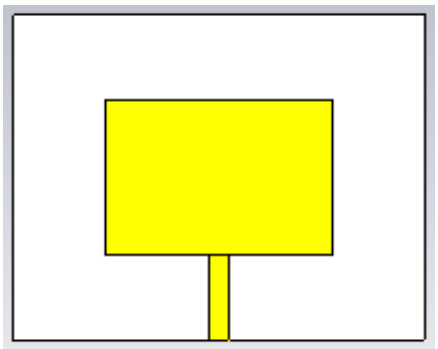
20*25



20*30



25*25



25*30

(b) Different dimensions

Figure 4. 14 Different GND dimensions

Besides the original dimension of ground plane, four different sizes are also taken into consideration. And the size of substrate also changes because it lay on the ground plane. They are expressed as the form of width * length.

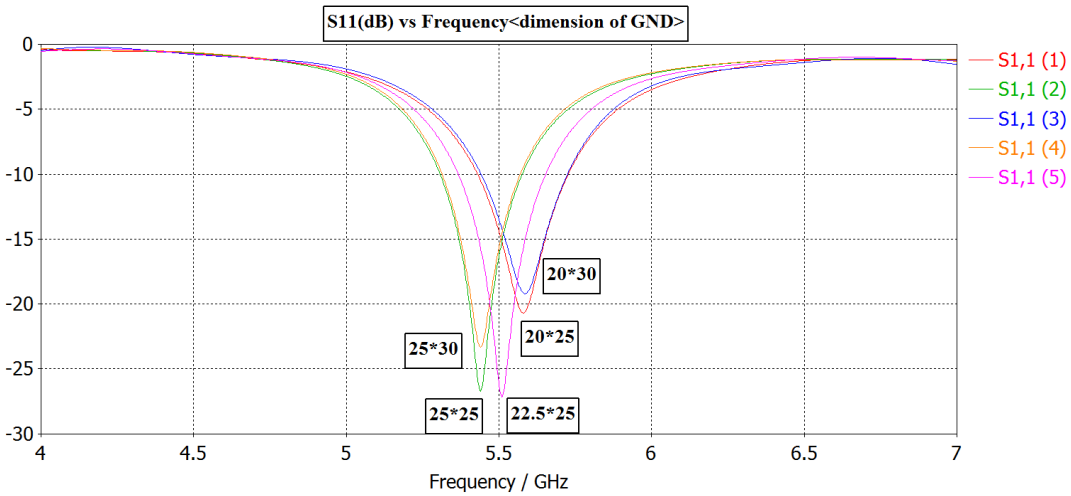


Figure 4. 15 Adjustment of the dimension of GND

Figure 4.15 shows slight difference in S_{11} under different dimension of ground plane. Further it can be seen that the width of ground plane determined the resonant frequency while the length of ground plane controls the impedance.

To explain it accurately we take the two ground planes with the width of 25 mm as examples. They possess the same resonant frequency at about 5.4 GHz while the one with length of 25 mm is sharper than the other. And compare with the planes with width of 20 mm, they are different in central frequency.

Generally the ground plane possesses the same dimension with the substrate when design a microstrip antenna. And from the simulation results above the influence of ground plane is slight comparing with other parameters. So the influence of the ground plane is often ignored while design and analysis.

4.4 Copper coin shape antenna

As the development of the communication, wide bandwidth is required for transferring more information like the video instead of figures and message. Also with the popular of the mobile devices like smartphone and PAD, the requirement of small sizes also has been an essential aim for electrical elements. Hence the antenna with wide bandwidth and small size has been studied a lot. Based on the feeding method of coplanar waveguide in section 2.4.5, this antenna is designed for wide bandwidth [49].

The shape of this antenna is like the traditional Chinese copper coin with a square slot inside the circular patch. Compared to the rectangular patch, the circular patch is slightly smaller and only has one degree of freedom in its conductor shape [50], the radius. Starting from the geometry of a rectangular patch we can roughly determine the size of circular patch and adjust it for better performance using simulation. However, besides the patch shape other elements also affect the antenna performance which are discussed in section 4.4.3.

4.4.1 Specific parameters and geometry

The basic relevant items of this antenna are shown in table 4.1. The material properties are the same as the rectangular microstrip antenna in the last section. As mentioned before the size of circular patch is slightly smaller than the rectangular patch, thus an approximate radius is calculated. And the geometry of coplanar feed is a result of references [13, 14, 29, 49, 51, 52] and simulation because the methodology is complicated as mentioned in section 2.4.5.

Thus the parameters are given in table 4.3.

Parameters	Original value	Adjusted value
Radius of patch	8 mm	7.25 mm
Width of 50 Ω feedline	3.832 mm	1.5 mm
Length of substrate	30 mm	35 mm
Width of substrate	30 mm	31 mm
Length of central feedline	14 mm	14 mm
Width of central feedline	3.832 mm	3.3 mm
Length of ground plane	13 mm	7.25 mm
Width of ground plane	13.35 mm	11.5 mm
Width of square slot	7 mm	8.4 mm

Table 4. 3 Parameters of copper coin shape antenna

The model built in CST software is based on these parameters and given in figure 4.16.

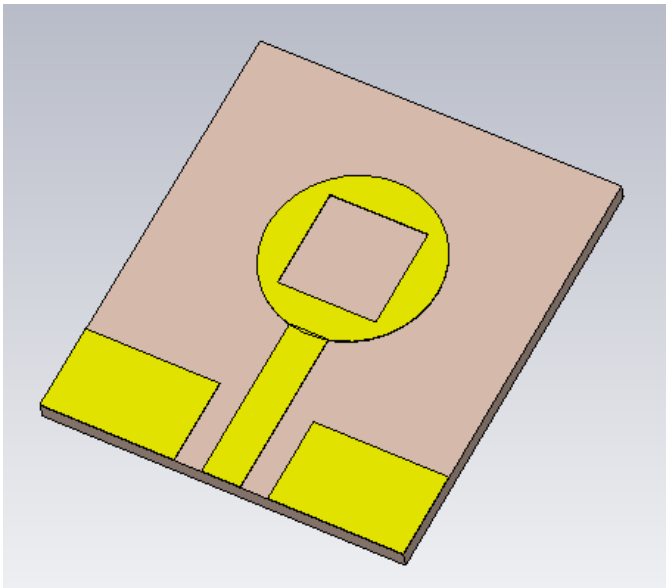


Figure 4. 16 Geometry of the copper coin shape antenna in CST

As the picture shows, this antenna consists of the circular patch with a square slot and the coplanar waveguide which includes a central feedline and two ground plane segments. All these elements are located on the same side of the substrate.

4.4.2 Simulation results

- S_{11} parameter

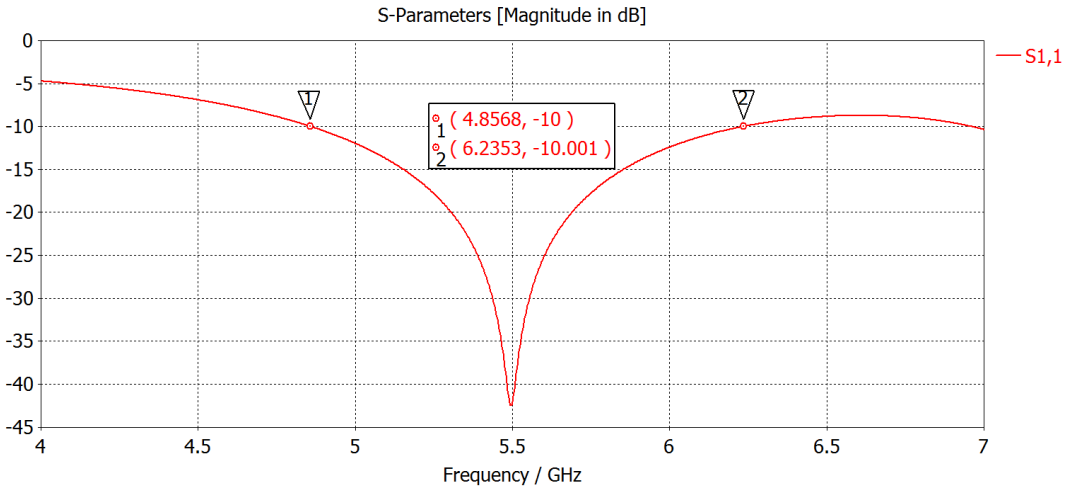


Figure 4. 17 S_{11} parameter of copper coin shape antenna

We can see from the figure that the curve experiences a slow fluctuation from 4 GHz to 4.5GHz and also 6.5 GHz to 7 GHz. However it changes sharply from 4.5 GHz to 6.5 GHz and peak at 5.5 GHz with the magnitude of -42 dB, in which located the resonant frequency. It also illustrates a good match of impedance because the value of the parameter at 5.5 GHz is pretty low.

According to section 2.1.2, the frequency bandwidth (for lower than 10 dB) can also be determined.

$$BW = 6.235\ GHz - 4.857\ GHz = 1.378\ GHz = 25.05\%$$

- Efficiency

  According to the theory in section 2.1.6, the radiation efficiency and total efficiency can be obtained from figure 4.18.

$$\eta_e = -0.3352\ dB$$

$$\eta_t = -0.9681\ dB$$

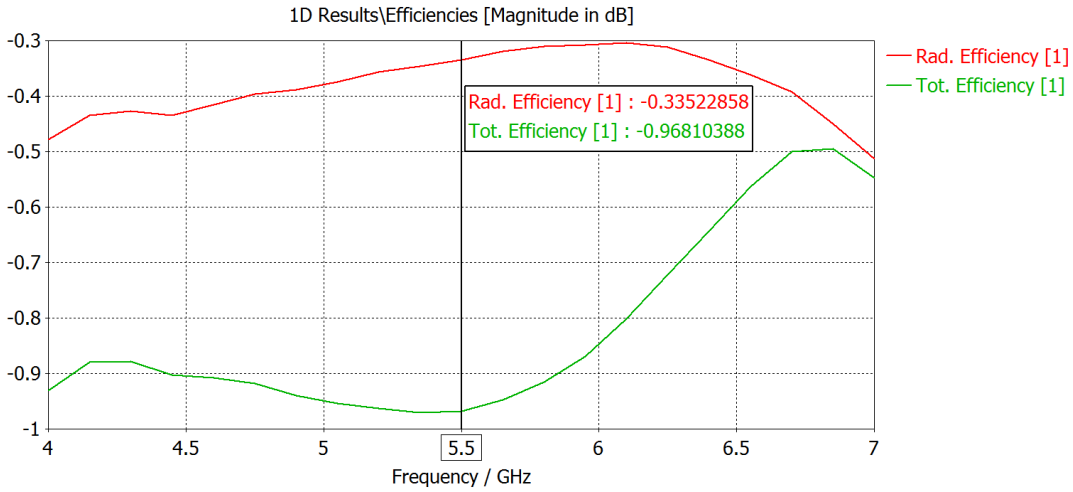


Figure 4. 18 Efficiency of copper coin shape antenna

It can be seen that both of these two curves fluctuate slightly between -1 dB and -0.3 dB. And the radiation efficiency (red line) reaches -0.3352 dB at resonant frequency whereas the total efficiency (green line) is -0.9681 dB. However, the total efficiency peaks at higher frequency instead of the resonant frequency which requires more research in the future work.

- Gain

  Based on the knowledge in section 2.1.7, the gain of the antenna at resonant frequency is shown in figure 4.19.

$$G = 3.2955\ dB$$

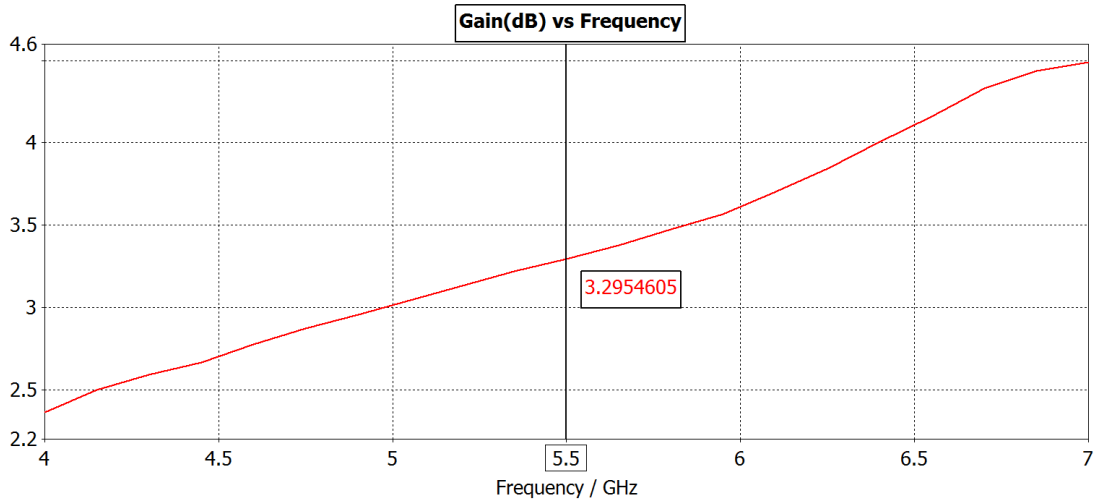


Figure 4. 19 Gain of copper coin shape antenna

The line in this figure experiences an increasing trend through the simulation band and reaches 3.2954 dB at resonant frequency, which shows the similar trend of the radiation efficiency in figure 4.18. It is due to the relation between radiation efficiency and gain in (2.9).

- Surface current

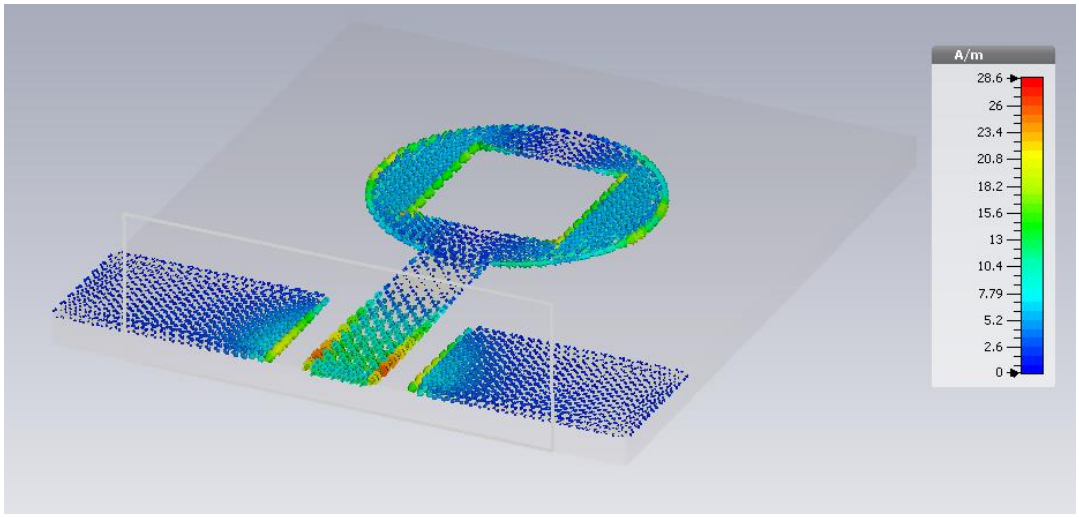


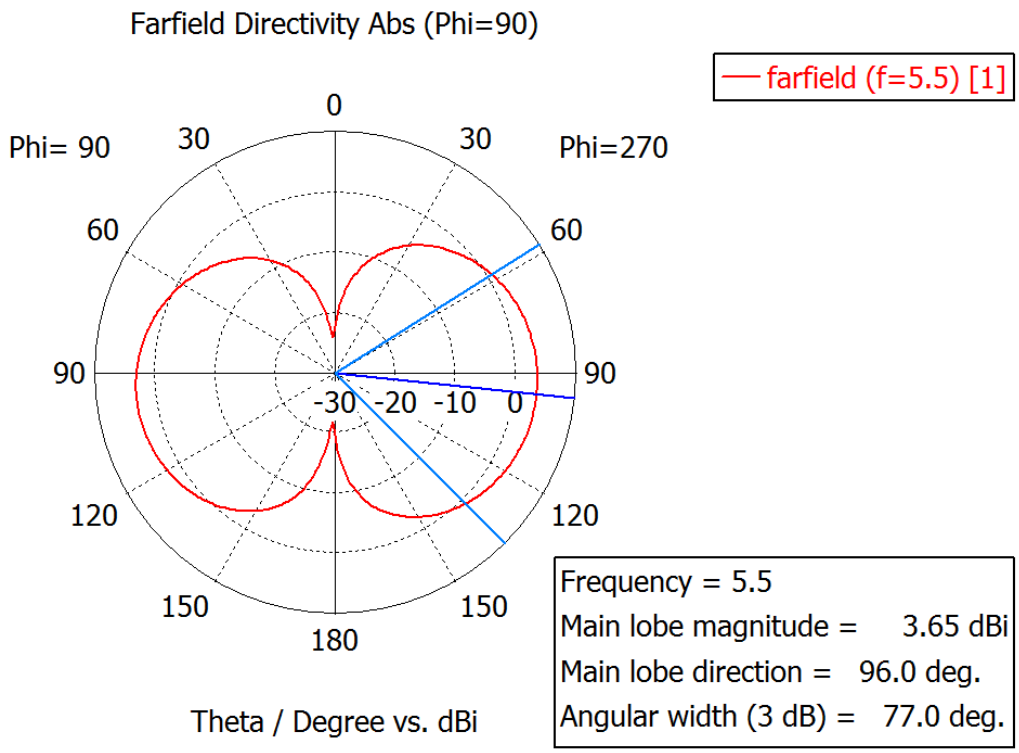
Figure 4. 20 Surface current of copper coin shape antenna

This figure gives the current distribution of the copper coin shape antenna. Obviously most of currents flow through the coplanar waveguide to the metal patch, which gives the radiation of the whole antenna.

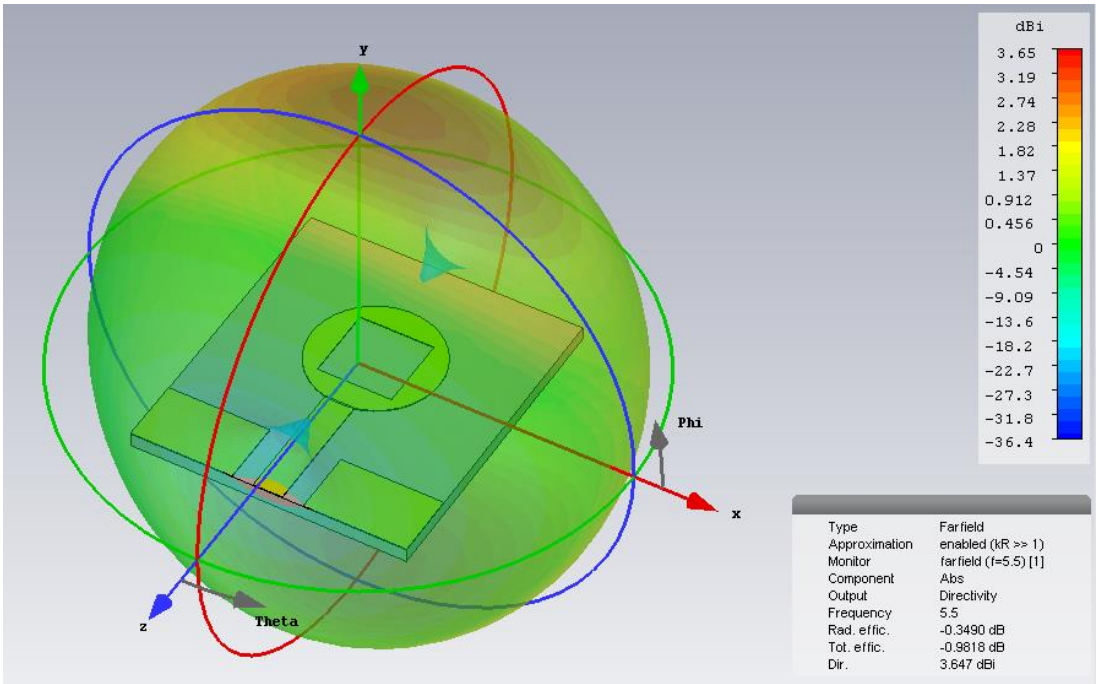
- Radiation patterns

From section 2.1.5, the directivity of the antenna can be obtained from figure 4.21 (b).

D=3.647 dBi



(a) Polar pattern



(b) 3D pattern

Figure 4. 21 Radiation patterns of copper coin shape antenna

From the 2D pattern in figure 4.21(a), we can get the shape of the radiation pattern. It is directional at $\phi = 96^{\circ}$ and $\phi = 270^{\circ}$, which corresponds with the positive and negative y-axis in the 3D pattern in figure 4.21 (b). It may be causes by the two components of ground plane which should be further discussed in the future work. The same figure also shows the directivity of the antenna is 3.647 dBi. Combined with the discussion before, we can also verify (2.9) in simulation.

$$G(dB) = D(dBi) + \eta_e(dB)$$

We have G=3.2955 dB, D=3.647 dBi, η_e=-0.3352 dB, which satisfies the equation above.

4.4.3 Influential parameters

In section 4.3.3, we have investigated the effects of some parameters that will influence the antenna performance. Besides these there are further elements we are interested in under the particular situation. For instance, the radius of the circular patch in the copper coin shape antenna and also the width of the square slot. In addition, some discussions about the structure of the coplanar waveguide are also given in this section. As mentioned before in chapter 3, we focus on the influential parameters rather than the methodology of CPW, as the latter would be beyond the scope of this project.

- radius of the circular patch

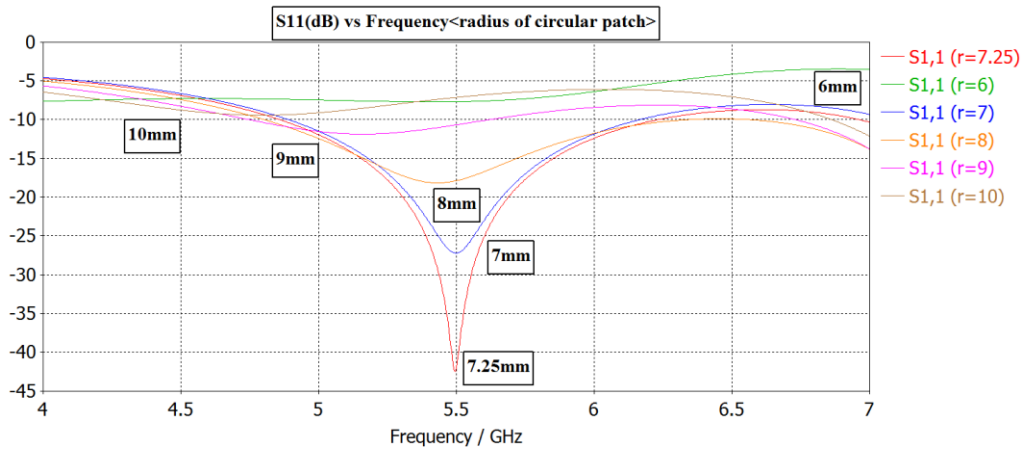


Figure 4. 22 Adjustment of the radius of patch

Unlike the rectangular shape of patch, the circular patch only has one degree of freedom to operate—— the radius. Hence it is been adjusted between 6 mm and 10 mm. From figure 4.22 it can be clearly seen that the radius affects both the resonant frequency and the impedance match. More specifically, the antenna with the radius of 6mm and 10mm don't seem to have a resonauc at the frequency range from 4GHz to 7GHz because their curves look flat in the frequency band. The one design with the radius of 9mm has a gentle curve resonating at about 5GHz with poor impedance match as the S_{11} is -12 dB.

The trend can be obtained from the remaining three data sets. As the radius increases from 7mm to 8mm the resonant frequency decreases from 5.5 GHz to 5.4 GHz and gets the best impedance match at 7.25 mm.

- Width of slot

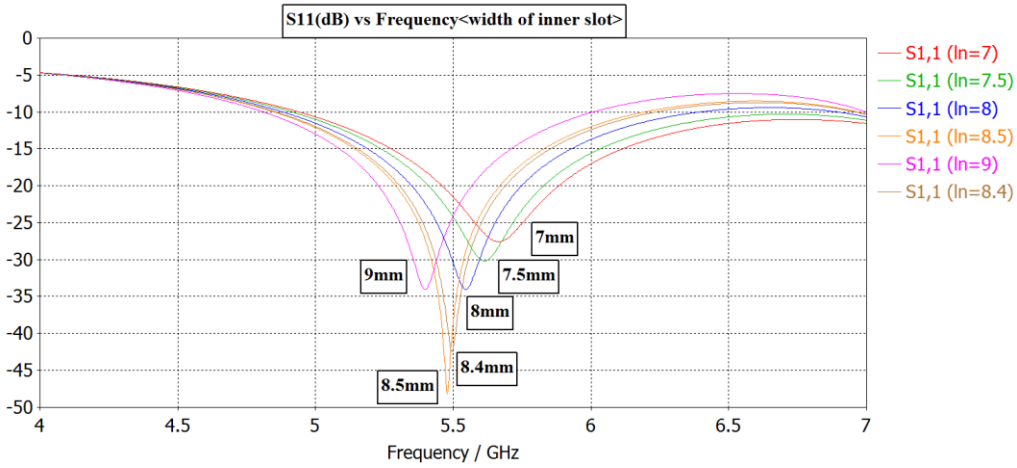


Figure 4. 23 Adjustment of the width of inner slot

Another point of this copper coin shape antenna is the square slot inside the circular patch, which would not only reduce the size of the patch but also affect the performance of the antenna.

From the figure 4.23 it is clearly seen that the width of the square slot affect the impedance match as well as the resonant frequency. More specifically, the resonant frequency decreases while the width of slot increases from 5.7 GHz at 7 mm to 5.4 GHz at 9 mm. On the contrary, with the increase of the width initially, better impedance match is obtained with the best one at 8.5 mm. But it reduces with the continued increase of width. However, the width of 8.4 mm is chosen considering of both the resonant frequency and impedance match.

- Gap between central feedline and ground plane

As the coplanar waveguide is employed in this antenna to provide feed, it will also affect the performance of the antenna. According to section 3.2, the gap between central feedline and ground plane is taken into account according to the design formula (3.4). Hence it is discussed in this section. It changes by adjusting the width of the ground plane.

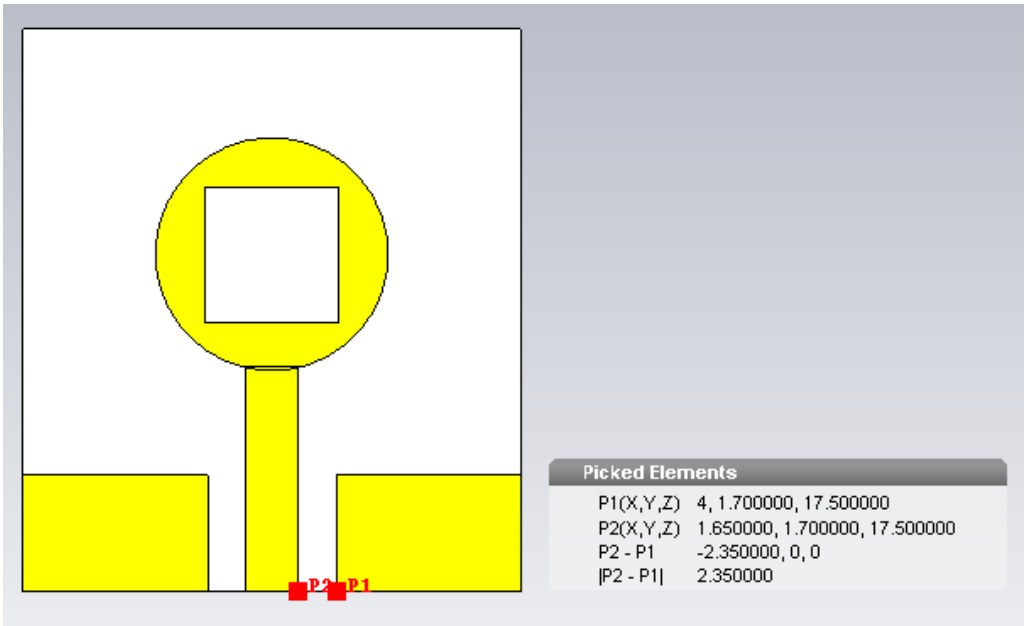


Figure 4. 24 Gap between central feedline and GND

As figure 4.24 shows, two points are chosen for analysis. It is easily seen that the distance between P1 and P2 is the gap between central feedline and ground plane. Therefore it is operated by adjusting the width of the ground plane during the following discussion in this section.

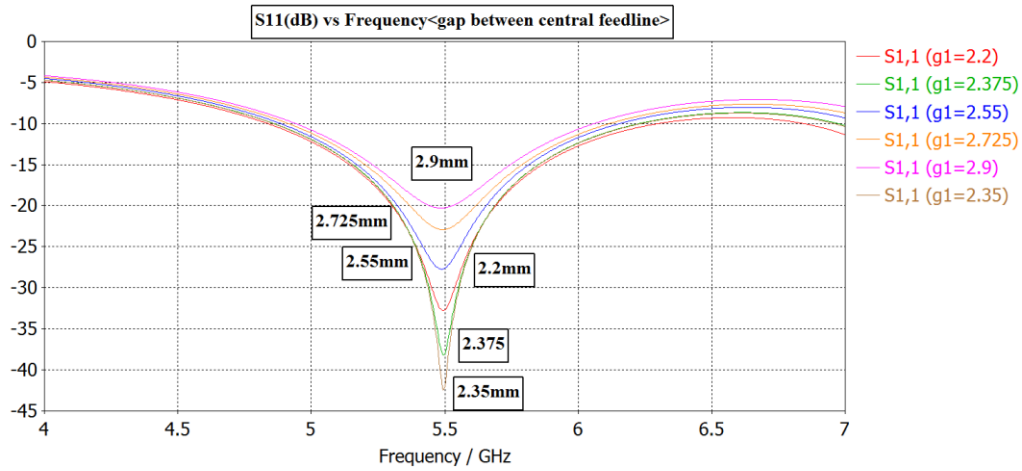


Figure 4. 25 Adjustment of the gap between central feedline

Here the gap is adjusted between 2.2mm and 2.9mm. The figure above illustrates the trend of how it influences the impedance match of the antenna. With the increase of the gap from 2.2mm to 2.35mm, the antenna obtains better match of impedance. However, a contrary trend appears after between 2.35mm and 2.9mm. Obviously the antenna obtains the best impedance match at 2.35mm of the gap.

That is to say that a particular value exits for the gap to get the best impedance match of the antenna. It is convenient and simple to adjust the simulation model in the software for a better match.

- Distance between patch and ground plane

Apart from the gap between central feedline and ground plane, the distance between patch and ground plane also attracts our attention. It is relied on adjusting the length of the ground plane to change the distance.

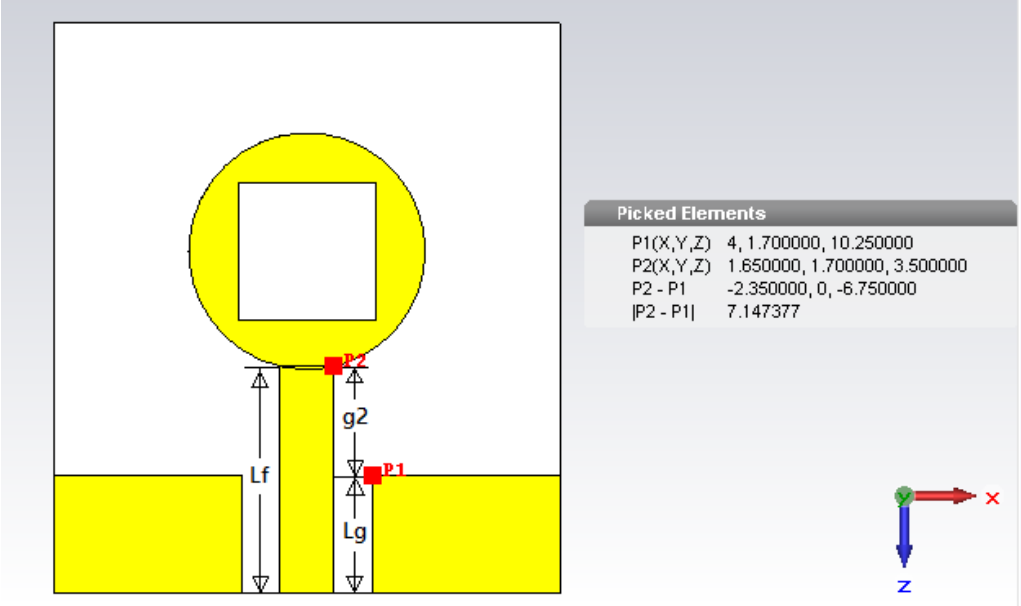


Figure 4. 26 Distance between patch and GND

As figure 4.26 shows, two points are also picked and the distance between them is measured by the software. It is easily to see that the relation between the three marks in this figure is

$$L_f = g_2 + L_g$$

Where g_2 is what we are looking for and refers to the vertical distance between P1 and P2. L_g is the length of the ground plane that will be operated to change the distance. And L_f refers to the length of feedline which remains constant.

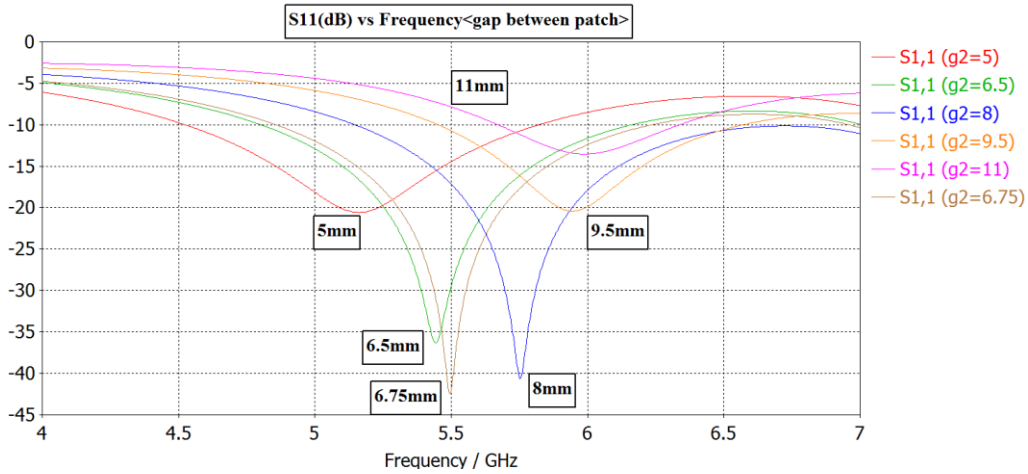


Figure 4. 27 Adjustment of the distance between patch

Figure 4.27 describes the variation trend of the S_{11} parameter while the distance between patch and ground plane changing. Obviously it will influence the resonant frequency as well as the impedance match. More specifically, as the distance increases the resonant frequency of the antenna also increases from 5.1 GHz at 5mm to 5.9 GHz at 9.5mm. On the contrary, the effect on impedance match is not that simple. Better impedance match is obtained whilst increasing of the distance is 6.75mm with the best match of -43dB of S_{11}. After that the match becomes worse with larger distance.

4.5 Comparison between rectangular MSA and copper coin shape antenna

According to the simulation results in previous section, a comparison table of the performance between these two antennas is given below for further discussion.

Characteristic		Rectangular MSA	Copper coin shape antenna
Dimension		11.9 mm*16.6 mm	31 mm*35 mm
Ground plane		On plane below	On the same plane
S_{11} at 5.5 GHz		-26 dB	-42 dB
BW		0.2855 GHz (5.2%)	1.378 GHz (25.05%)
Radiation efficiency		-2.7797 dB	-0.3352 dB
Total efficiency		-3.1376 dB	-0.9681 dB
Gain		3.5756 dB	3.2955 dB
Directivity		6.357 dBi	3.647 dBi
Radiation pattern	**Shape**	Rounded on one side	Rounded on two sides
	Main lobe magnitude	6.35 dBi	3.3 dBi
	Angular width (3 dB)	98.5 deg.	77 deg.

Table 4. 4 Comparison between two antennas

Geometrically, both of these two antennas possess small dimensions. However, the size of the rectangular MSA is nearly half of that of the copper coin shape antenna. But there is no additional ground plane on the copper coin antenna due to the coplanar waveguide feed it used. Thus rectangular MSA is a good choice for the miniature system which requires small size element.

As for the performance of antenna, the latter does well at S_{11} parameter and efficiency. Especially, it possesses -42 dB of S_{11} at resonant frequency and pretty wide bandwidth of 25.05% compare to those of -26 dB and 5.2% of the rectangular MSA. Thus it could be employed in wide band system to provide good impedance match. Also it is more efficient than the rectangular one both in radiation efficiency and total efficiency. However, the reason of these improvements still need to be confirmed as it might be caused by the CPW fed, which could be the future work.

Due to the half value of directivity compare to the rectangular one, the copper coin antenna possesses small gain as well. It is also can be seen at the main lobe magnitude of radiation pattern, which is similar to the directivity.

What's more, the shapes of radiation pattern between these two antennas are different, refers to figure 4.7 and figure 4.21. The rectangular one is more directional compare to the copper coin one. From figure 4.7 (a) it can be seen that the rectangular MSA radiates mainly on one side where $\phi = 90^{\circ}$ with the angular width of 98.5 degree. Whereas the copper coin shape antenna

radiates at two sides where $\phi = 90^{\circ}$ and $\phi = 270^{\circ}$ with a small angular width of 77 degree.

In conclusion, the copper coin shape antenna could be employed in wide bandwidth system and provides high efficiency. And the rectangular MSA would act well in the system which only requires radiation at one direction. In addition, due to the ground plane the rectangular MSA is more convenient to connect directly with other device in simulation as well as in highly integrated fabrication.

4.6 Summary

This chapter focuses on the simulation of two different kinds of antenna, the rectangular MSA and copper coin shape antenna separately. Based on the methodology theory, the models are built in the CST software firstly and then adjusted for better performance. Besides these, influential parameters are also discussed to determine how they influence the performance of an antenna. Finally, the comparison between these two antennas is given and then discussed for their application in different systems.

Chapter 5 Design of coupler

A coupler is a microwave component designed to divide the input power into several output ports with less power [53]. The main structure of the coupler possesses three or four ports for signal transmission, which take forms from the T-junction and the directional coupler separately [8]. Power dividers usually provide output with same power division, 3dB or half power with a phase shift of 90 or 180 degree between two output ports. However, unequal arbitrary division is also employed in practice. In this thesis, we will focus on the characteristics of four-port couplers like the quadrature hybrid coupler and rat race ring as well as the design procedure in CST.

5.1 Four-port Networks

The S-parameters of an arbitrary four-port network can be expressed as below:

$$[S] = \begin{bmatrix} S_{11} & S_{12} & S_{13} & S_{14} \\ S_{21} & S_{22} & S_{23} & S_{24} \\ S_{31} & S_{32} & S_{33} & S_{34} \\ S_{41} & S_{42} & S_{43} & S_{44} \end{bmatrix} \tag{5.1}$$

Because of the symmetric structure, we can obtain that $S_{ij} = S_{ji}$. And if the ports are well matched with the load, then we have$S_{ii} = 0$. Thus the S-matrix can be rewrite in a simpler way in (5.2).

$$[S] = \begin{bmatrix} 0 & S_{12} & S_{13} & S_{14} \\ S_{12} & 0 & S_{23} & S_{24} \\ S_{13} & S_{23} & 0 & S_{34} \\ S_{14} & S_{24} & S_{34} & 0 \end{bmatrix} \tag{5.2}$$

Due to unitarity of the network, also consider the multiplication of row 1, 2 and row 3, 4 respectively:

$$S_{13}^* S_{23} + S_{14}^* S_{24} = 0 \tag{5.3a}$$

$$S_{14}^* S_{13} + S_{24}^* S_{23} = 0 \tag{5.3b}$$

Using S_{24}^* and S_{13}^* to multiply (5.3a) and (5.3b) separately and then subtract, we can obtain

$$S_{14}^*(|S_{13}|^2 - |S_{24}|^2) = 0 \tag{5.4}$$

Similarly analysis on row 1, 3 and row 2, 4 gives

$$S_{23}(|S_{12}|^2 - |S_{34}|^2) = 0 \tag{5.5}$$

For satisfying both (5.4) and (5.5) at the same time, we assume that$S_{14} = S_{23} = 0$, which results in the directional coupler. The S matrix in (5.2) turns to a simpler form

$$[S] = \begin{bmatrix} 0 & S_{12} & S_{13} & 0 \\ S_{12} & 0 & 0 & S_{24} \\ S_{13} & 0 & 0 & S_{34} \\ 0 & S_{24} & S_{34} & 0 \end{bmatrix} \tag{5.6}$$

Then using unitarity rule in each row respectively to obtain that

$$|S_{12}|^2 + |S_{13}|^2 = 1 \tag{5.7a}$$

$$|S_{12}|^2 + |S_{24}|^2 = 1 \tag{5.7b}$$

$$|S_{13}|^2 + |S_{34}|^2 = 1 \tag{5.7c}$$

$$|S_{24}|^2 + |S_{34}|^2 = 1 \tag{5.7d}$$

It is obvious that$|S_{13}| = |S_{24}|$ and$|S_{12}| = |S_{34}|$.

Figure 5.1 shows the basic operation of a four-port coupler. From which we can obtain that the wave incidents in port 1divides power into ports 2 and 3 but not into port 4. Take the analysis beyond into consideration, we can also get that the wave incidents in port 4, the power is coupled into ports 2 and 3 but not into port 1.

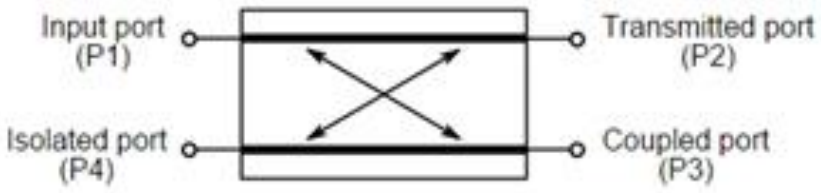


Figure 5. 1 Four-port coupler

All the discussion above is ideal, it is impossible to get total isolation in practice. Thus we have following parameters to judge the performance of a coupler [8].

$$Coupling = C = 10\log\frac{P1}{P3} = -20\log|S_{13}|\,dB \tag{5.8a}$$

$$Directivity = D = 10\log\frac{P3}{P4} = 20\log\frac{|S_{13}|}{|S_{14}|}dB \tag{5.8b}$$

$$Isolation = I = 10\log\frac{P1}{P4} = -20\log|S_{14}|\,dB \tag{5.8c}$$

$$Insertion\ loss = L = 10\log\frac{P1}{P2} = -20\log|S_{12}|\,dB \tag{5.8d}$$

As expressed by these equations, the coupling illustrates the section of input power coupled to the output port. The directivity indicates the ratio of coupled port to isolated port. The isolation measures the unwanted power delivered to uncoupled port. It is easily to find in the expression that the relation between these three factors is

$$I = D + C \tag{5.9}$$

Besides, the insertion loss can be seen as the transmission factor between input port and through port.

5.2 Quadrature hybrid coupler

5.2.1 Introduction of the quadrature hybrid coupler

A quadrature hybrid coupler, also known as branch line coupler, is a 3dB directional coupler with 90 degree phase shift between two output ports [8]. The basic structure of it is shown in figure 5.2.

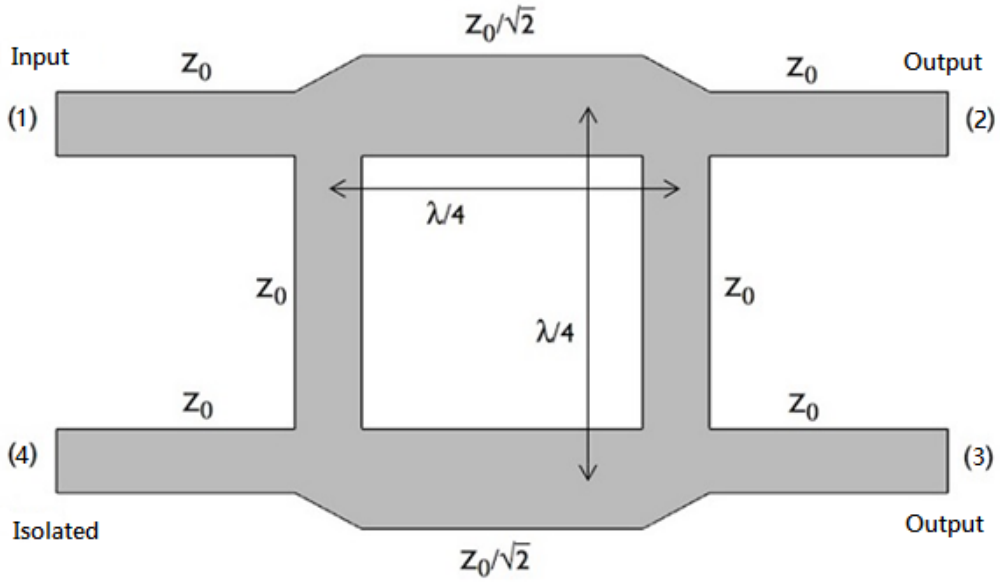


Figure 5. 2 Basic structure of hybrid coupler

In order to analyse the characteristic of this coupler, we should start with the circuit network. If all ports in given figure are well matched, then port 2 and 3 have equal power divided from port 1 while port 4 is isolated. The S – matrix of it is like below:

$$[S] = \frac{1}{\sqrt{2}}\begin{bmatrix} 0 & j & 1 & 0 \\ j & 0 & 0 & 1 \\ 1 & 0 & 0 & j \\ 0 & 1 & j & 0 \end{bmatrix} \tag{5.10}$$

From the expression it is obvious that the branch-line coupler has a symmetrical structure. As the statistic in each row can be seen as a transform from row 1, each port can be seen as the input port while the output and isolated ports will change as well. More specifically, the output ports are located on the opposite side of input port while the isolated port is on the same side.

5.2.2 Even-odd mode analysis of quadrature hybrid coupler

For more accurate analysis of the working principle of quadrature hybrid coupler, the even-odd mode [54] is introduced in this chapter. As shown in the circuit model of the coupler in figure 5.3, we assume that all ports are well matched with unit impedance $Z_0 = 1$, and the impedance of the quarter wavelength arm is $\frac{1}{\sqrt{2}}$. Also, the wave with unit amplitude $A_1 = 1$is incident at port 1.

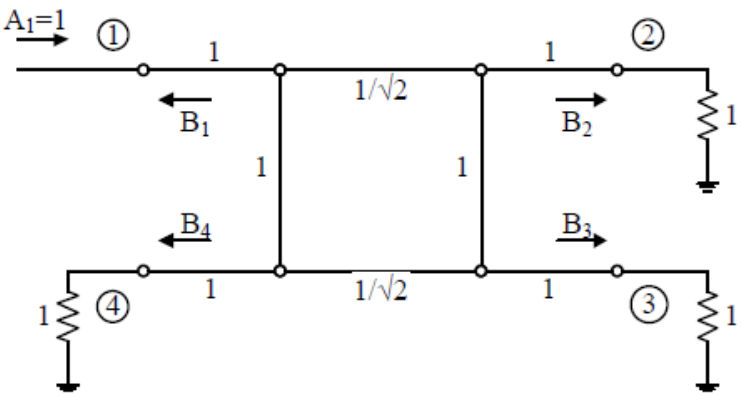
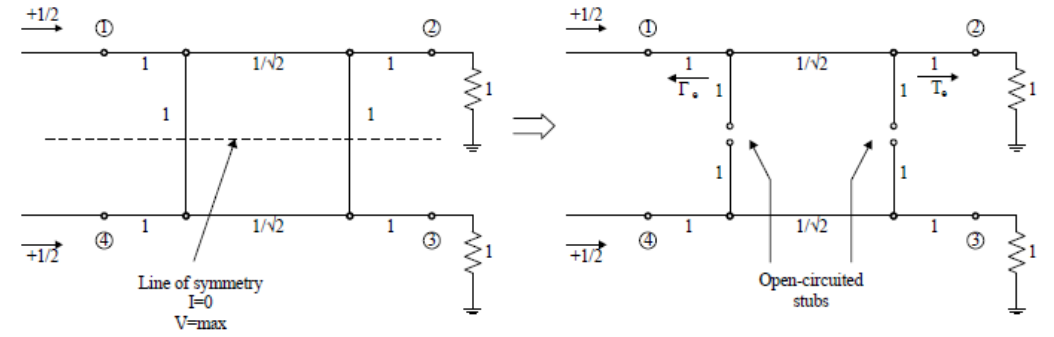
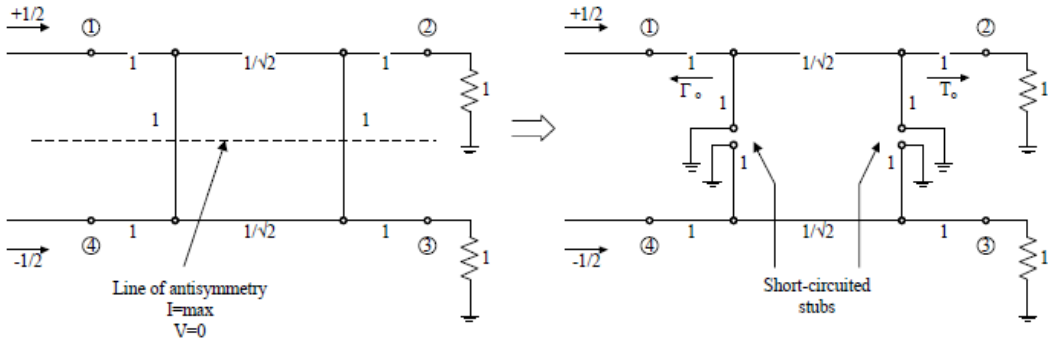


Figure 5. 3 Circuit model of hybrid coupler

The model above can be resolved into even-mode excitation and odd-mode excitation motivated from port 1 and port 4 with half input power, like the figure 5.4(a) and figure 5.4(b). The output of the whole network will be the sum of these two modes. Due to the symmetry and asymmetry of the excitation, the modes can be further developed in detail, which are widely employed in analysis.



(a) Even mode excitation



(b) Odd mode excitation

Figure 5. 4 Analysis of hybrid coupler [9]

As the figure above indicates, the situation of each port can be expressed as follows:

$$B_1 = \frac{1}{2}\Gamma_e + \frac{1}{2}\Gamma_o \quad (5.11a)$$

$$B_2 = \frac{1}{2}T_e + \frac{1}{2}T_o \quad (5.11b)$$

$$B_3 = \frac{1}{2}T_e - \frac{1}{2}T_o \quad (5.11c)$$

$$B_4 = \frac{1}{2}\Gamma_e - \frac{1}{2}\Gamma_o \quad (5.11d)$$

Where Γ_e: reflection coefficient of even mode

Γ_o: reflection coefficient of odd mode

T_e: transmission coefficient of even mode

T_o: transmission coefficient of odd mode

To further analyse the even mode network, it is divided into three networks with two ports separately, where ABCD matrices [3]are employed to analyse

the transfer characteristics conveniently. The sketch of a basic ABCD matrix is shown in figure 5.5 and the expression is also given in (5.12).

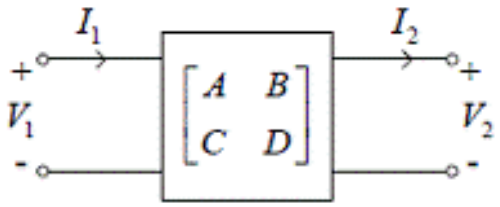


Figure 5. 5 Network with ABCD matrix

$$V_1 = AV_2 + BI_2 \tag{5.12a}$$

$$I_1 = CV_2 + DI_2 \tag{5.12b}$$

$$\begin{bmatrix} V_1 \\ I_1 \end{bmatrix} = \begin{bmatrix} A & B \\ C & D \end{bmatrix} \begin{bmatrix} V_2 \\ I_2 \end{bmatrix} \tag{5.12c}$$

$$\begin{bmatrix} V_1 \\ I_1 \end{bmatrix} = \begin{bmatrix} A_1 & B_1 \\ C_1 & D_1 \end{bmatrix} \begin{bmatrix} A_2 & B_2 \\ C_2 & D_2 \end{bmatrix} \begin{bmatrix} V_2 \\ I_2 \end{bmatrix} \tag{5.12d}$$

Due to the ABCD matrix of the cascade connection network can be easily obtained by multiplying the individual one, it is widely employed in analysis. And the ABCD matrices for shunt and transmission line are showed in figure 5.6, in which we can easily get the expression of these two networks.

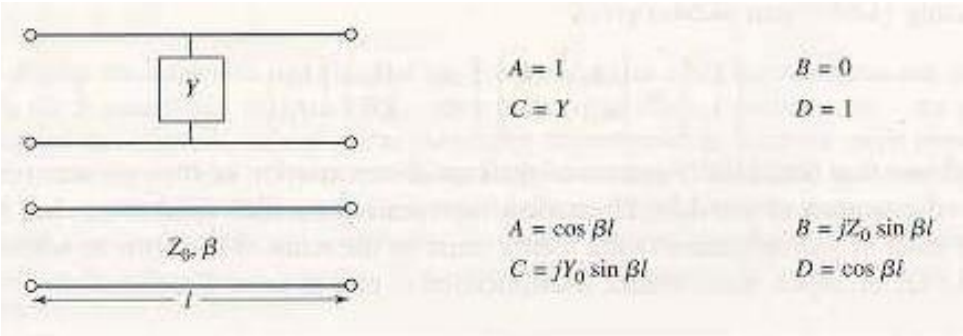


Figure 5. 6 Useful ABCD matrices [8]

Take the even mode in figure 5.4 (a) as an example: as mentioned before, the even mode can be divided into three networks. Taking the above ABCD matrices into consideration, we can get the expression of these three connection network in (5.13).

$$\begin{bmatrix} A & B \\ C & D \end{bmatrix} = \begin{bmatrix} 1 & 0 \\ \frac{1}{Z_0} j \tan \beta l & 1 \end{bmatrix} \begin{bmatrix} \cos \beta l & jZ_0 \sin \beta l \\ j \frac{1}{Z_0} \sin \beta l & \cos \beta l \end{bmatrix} \begin{bmatrix} 1 & 0 \\ \frac{1}{Z_0} j \tan \beta l & 1 \end{bmatrix} \tag{5.13}$$

More specifically, the first and the third network can be seen as $l = \frac{\lambda}{8}$ shunt network with admittance $Y_1 = Y_2 = \frac{1}{Z_0} j \tan \beta l = 1$. And the middle one refers to the network of a $\frac{\lambda}{4}$ transmission line. $Z_0 = 1$ is applied in all networks. Using the models above the ABCD matrices, we can easily get the expression of it below.

$$\begin{bmatrix} A & B \\ C & D \end{bmatrix}_e = \begin{bmatrix} 1 & 0 \\ j & 1 \end{bmatrix} \begin{bmatrix} 0 & \frac{j}{2} \\ j\sqrt{2} & 0 \end{bmatrix} \begin{bmatrix} 1 & 0 \\ j & 1 \end{bmatrix}$$

$$= \frac{1}{\sqrt{2}} \begin{bmatrix} -1 & j \\ j & -1 \end{bmatrix} \tag{5.14}$$

To obtain the output signal in (5.11), we need reflection and transmission coefficient which can be acquired by converting ABCD parameters to S parameters below.

$$S_{11} = \frac{A + \frac{B}{Z_0} - CZ_0 - D}{A + \frac{B}{Z_0} + CZ_0 + D} \tag{5.15a}$$

$$S_{12} = \frac{2(AD - BC)}{A + \frac{B}{Z_0} + CZ_0 + D} \tag{5.15b}$$

Where S_{11} refers to reflection coefficient, S_{12} refers to transmission coefficient. Thus Γ_e and T_e are calculated in (5.16)

$$\Gamma_e = \frac{A+B-C-D}{A+B+C+D} = \frac{(-1+j-j+1)/\sqrt{2}}{(-1+j+j-1)/\sqrt{2}} = 0 \tag{5.16a}$$

$$T_e = \frac{2}{A+B+C+D} = \frac{2}{(-1+j+j-1)/\sqrt{2}} = \frac{-1}{\sqrt{2}}(1+j) \tag{5.16b}$$

Similar analysis based on odd mode excitation is given below:

$$\begin{bmatrix} A & B \\ C & D \end{bmatrix}_o = \begin{bmatrix} 1 & 0 \\ -j & 1 \end{bmatrix} \begin{bmatrix} 0 & \frac{j}{2} \\ j\sqrt{2} & 0 \end{bmatrix} \begin{bmatrix} 1 & 0 \\ -j & 1 \end{bmatrix}$$

$$= \frac{1}{\sqrt{2}} \begin{bmatrix} 1 & j \\ j & 1 \end{bmatrix} \tag{5.17}$$

Thus the coefficients of the odd mode are

$$\Gamma_o = \frac{A+B-C-D}{A+B+C+D} = \frac{(1+j-j-1)/\sqrt{2}}{(1+j+j+1)/\sqrt{2}} = 0 \tag{5.18a}$$

$$T_o = \frac{2}{A+B+C+D} = \frac{2}{(1+j+j+1)/\sqrt{2}} = \frac{1}{\sqrt{2}}(1-j) \tag{5.18b}$$

Combining (5.16) and (5.18) in (5.11) shows the results below

$$B_1 = 0 \tag{5.19a}$$

$$B_2 = -\frac{j}{\sqrt{2}} \tag{5.19b}$$

$$B_3 = -\frac{1}{\sqrt{2}} \tag{5.19c}$$

$$B_4 = 0 \tag{5.19d}$$

It can be easily seen from the equation above that good matching results in no signal output of port 1. Port 2 possesses half-power signal from the input port 1, as dose port 3. However, there is a 90 degree shift between these two output ports. And port 4 is isolated ideally. Obviously, the analysis result agrees with the characteristic of hybrid coupler shown in the S matrix in (5.10).

5.3 Rat race ring

5.3.1 Introduction of rat race ring

The rat race ring, also knowns as 180 degree ring coupler, is a four port network which provides 180 degree phase shift between two output ports [55]. Figure 4.6 gives the structure of the rat race ring, four ports are located on the ring with the distance of $\frac{3\lambda_g}{4}$ between port 2 and 4 and $\frac{\lambda_g}{4}$ between the other ports. Where λ_g refers to the guide wavelength related to the material. The four ports are well matched with Z_0 and the impedance of the ring is $\sqrt{2}Z_0$ [56].

When seen as a divider, the signal incident in port 1 divides power into port 2 and 3 with the same amplitude as well as phase, whereas port 4 is isolated. Similarly, if port 4 is input port then the port 1 will be isolated and port 2 and 3 are output ports with same power but 180 degree difference in phase.

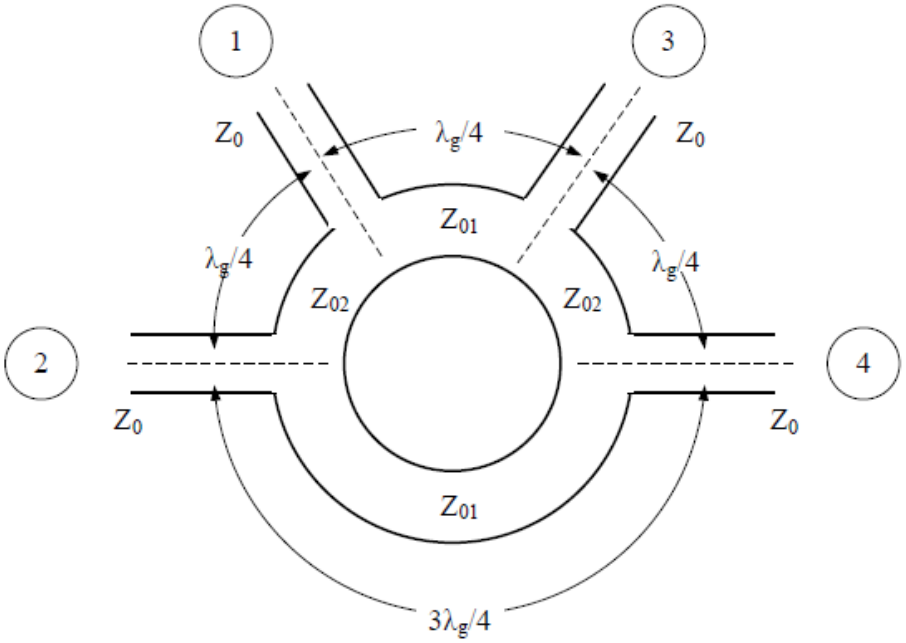


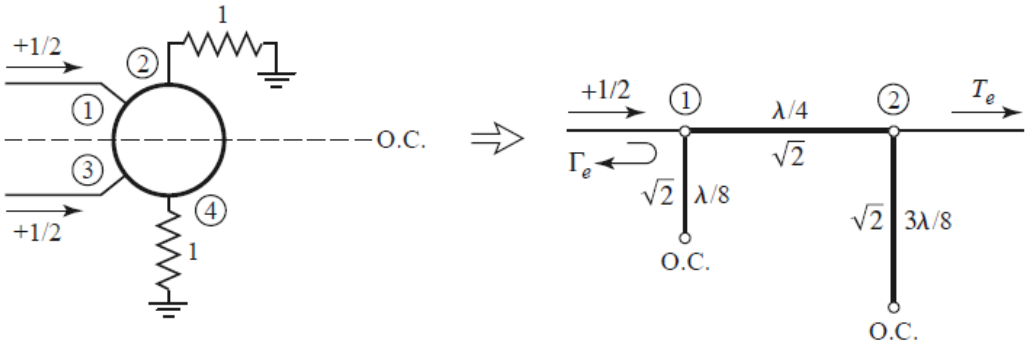
Figure 5. 7 Structure of rat race ring

Another operation of ring coupler is acting as a combiner instead of divider. When signals applied at port 2 and 3 as input, then port 1 will obtain the sum of the input while port 4 will obtain the difference of input. However, this thesis will focus on the divider characteristic of rat race ring so the combiner part will be skipped. The s matrix of rat race ring is shown as follow

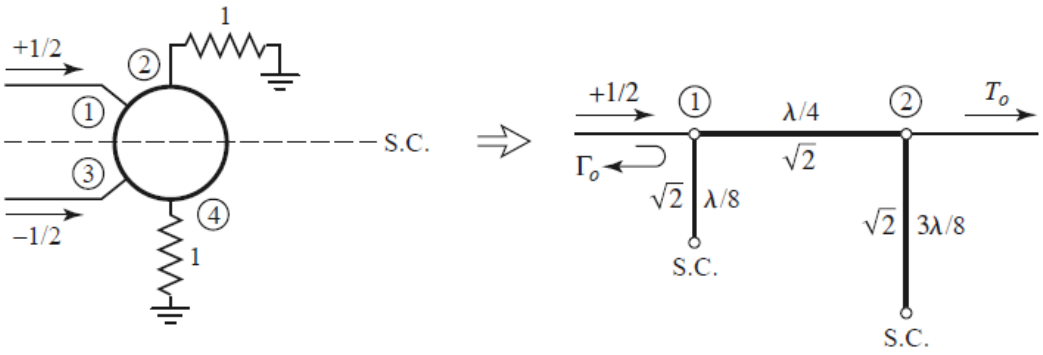
$$[S] = \frac{1}{\sqrt{2}}\begin{bmatrix} 0 & 1 & 1 & 0 \\ 1 & 0 & 0 & -1 \\ 1 & 0 & 0 & 1 \\ 0 & -1 & 1 & 0 \end{bmatrix} \tag{5.20}$$

5.3.2 Even-odd mode analysis of rat race ring

We also employ even-odd mode [54]to analyse the working principle of rat race ring in this chapter. Using the previous knowledge introduced in 5.2.1 we can easily obtain the basic circuit model of this ring coupler in figure 5.8. Here we assume that the signal is applied in port 1.



(a) Even mode excitation



(b) Odd mode excitation

Figure 5. 8 Analysis of rat race ring [57]

The output of each port is indicated below:

$$B_1 = \frac{1}{2}\Gamma_e + \frac{1}{2}\Gamma_o \tag{5.21a}$$

$$B_2 = \frac{1}{2}T_e + \frac{1}{2}T_o \tag{5.21b}$$

$$B_3 = \frac{1}{2}\Gamma_e - \frac{1}{2}\Gamma_o \tag{5.21c}$$

$$B_4 = \frac{1}{2}T_e - \frac{1}{2}T_o \tag{5.21d}$$

Even mode excitation in figure 5.8 (a) is chosen to briefly introduce the working principle of the ring coupler. From the symbol the network consists of three cascade connection network, the $\frac{\lambda}{8}$ shunt, the $\frac{\lambda}{4}$ transmission line and the $\frac{3\lambda}{8}$ shunt. All these networks are equipment with $Z_0 = \sqrt{2}$. Then taking the ABCD matrices model into (5.13), we can obtain that $Y_1 = j\tan\beta l\frac{1}{Z_0} = j\sqrt{2}$, and $Y_2 = j\tan\beta l\frac{1}{Z_0} = -\frac{j}{\sqrt{2}}$. Thus the expression of the whole network is given as follows.

$$\begin{bmatrix} A & B \\ C & D \end{bmatrix}_e = \begin{bmatrix} 1 & 0 \\ j\sqrt{2} & 1 \end{bmatrix} \begin{bmatrix} 0 & j\sqrt{2} \\ \frac{j}{\sqrt{2}} & 0 \end{bmatrix} \begin{bmatrix} 1 & 0 \\ -\frac{j}{\sqrt{2}} & 1 \end{bmatrix}$$

$$= \begin{bmatrix} 1 & j\sqrt{2} \\ j\sqrt{2} & -1 \end{bmatrix} \tag{5.22}$$

Similarly, the expression of odd-mode in figure 5.7(a) is:

$$\begin{bmatrix} A & B \\ C & D \end{bmatrix}_o = \begin{bmatrix} -1 & j\sqrt{2} \\ j\sqrt{2} & 1 \end{bmatrix} \tag{5.23}$$

Taking (5.22) and (5.23) back into (5.15) for coefficients

$$\Gamma_e = \frac{-j}{\sqrt{2}} \tag{5.24a}$$

$$T_e = \frac{-j}{\sqrt{2}} \tag{5.24b}$$

$$\Gamma_o = \frac{j}{\sqrt{2}} \tag{5.24c}$$

$$T_o = \frac{-j}{\sqrt{2}} \tag{5.24d}$$

Using equations in (5.24) into (5.21), we have

$$B_1 = 0 \tag{5.25a}$$

$$B_2 = \frac{-j}{\sqrt{2}} \tag{5.25b}$$

$$B_3 = \frac{-j}{\sqrt{2}} \tag{5.25c}$$

$$B_4 = 0 \tag{5.25d}$$

It illustrates that when the port is well matched, there is no signal reflected back to port 1. And the power is evenly divided into port 2 and 3 in-phase. Port 4 has no output due to isolated ideally. The analysis result agrees with the characteristic of rat race ring in (5.20).

5.4 Design of quadrature hybrid coupler in CST

5.4.1 Parameters and structure

Based on the theory above and the methodology about transmission line in chapter 3, the basic parameters have been calculated as follow in table 5.1.

Here we use 50 Ω as the value of Z_0 and the material of substrate is FR-4 with $\varepsilon_r = 4.3$ and $h = 2\ mm$.

After simulation, we have adjusted the value of these parameters for better performance which is also shown below in the table.

Parameters	Original Value	Adjusted value
Width of 50 Ω transmission line	3.832 mm	1.675 mm
Width of 35.4 Ω transmission line	1.13 mm	2.7 mm
Quarter wavelength	6.5mm	6.5 mm
Length of feedline	6.5mm	6.5 mm
Width of substrate	22.85 mm	30 mm
Length of substrate	22.85 mm	22.85 mm

Table 5. 1 Parameters of hybrid coupler

The differences between same parameters in these two tables could be caused by the influence of the metal ground plane. It will affect the electromagnetic field of the device.

The model has been built in CST using the data above, shown in figure 5.9. To realize by microstrip line the designed coupler also includes substrate and ground plane.

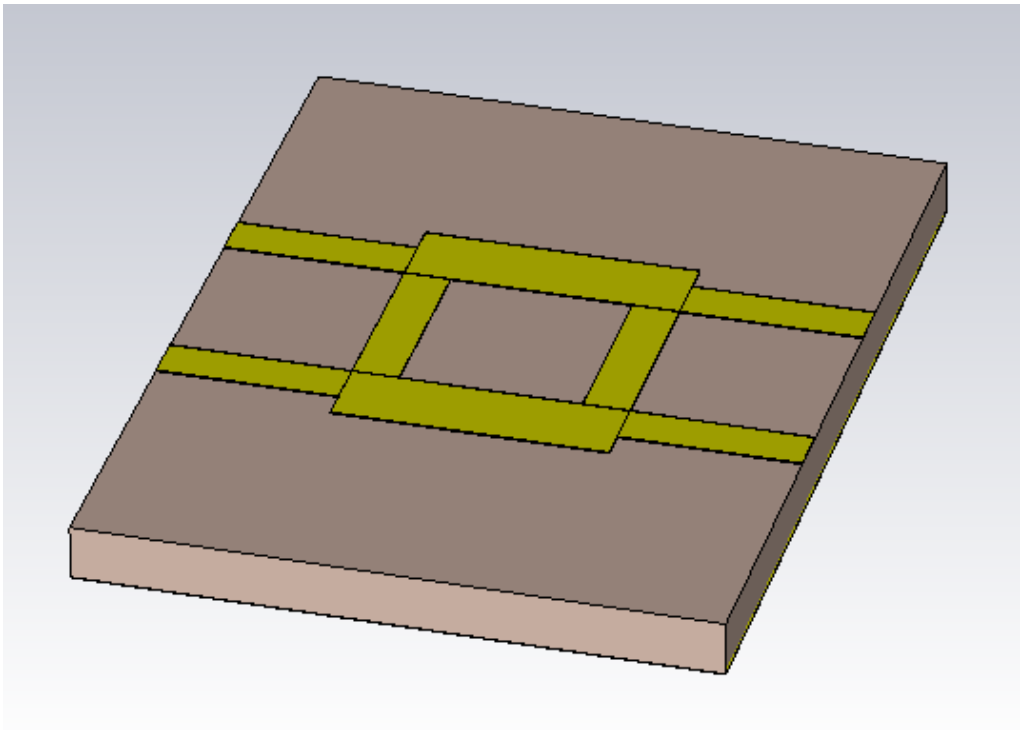
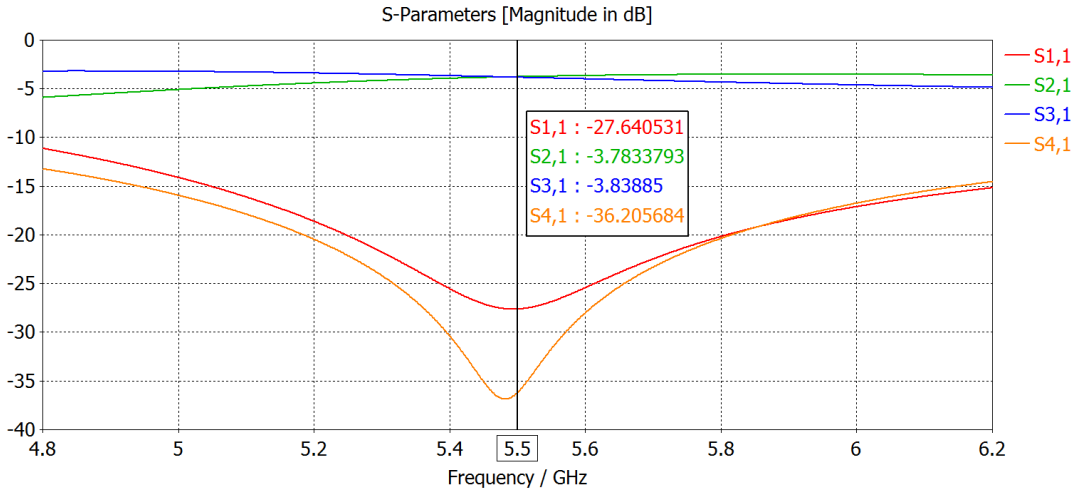


Figure 5. 9 Structure of hybrid coupler in CST

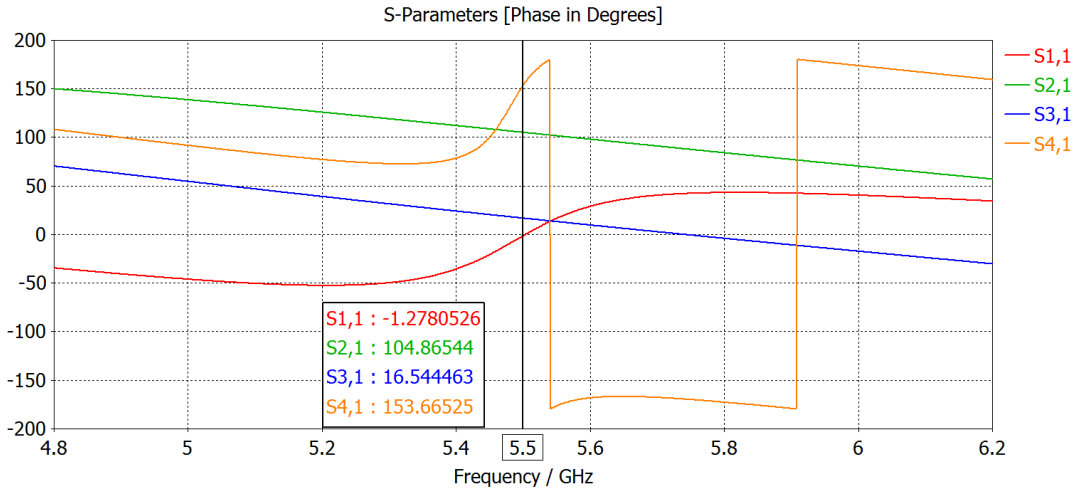
5.4.2 Simulation results

- S parameters

As a hybrid coupler which can provide 3 dB power division, the 2 output ports should have equal energy with a 90 degree phase shift. Figure 5.10 gives the information about S parameters of the coupler.



(a) Magnitude



(b) Phase

Figure 5. 10 S parameters of the quadrature hybrid coupler

It can be clearly seen that at resonant frequency, 5.5GHz, it has $s_{21} = -3.7834, s_{31} = -3.8388$ for the two output ports. It indicates that the power is divided nearly equally to these two ports. Also the s_{11} and s_{41} shows that little power transforms to these two ports due to the small value of -27.6405 dB and -36.2057 dB respectively at central frequency. And figure 5.10 gives

phase information of s_{11} parameter. At central frequency 5.5 GHz, $s_{21} = 104.86°, s_{31} = 16.54°$, the difference between these two ports is approximately 90°. Using the (5.8), we can also obtain the characteristic of this hybrid coupler.

$$Coupling = C = -11.6839\ dB$$

$$Directivity = D = -19.4917\ dB$$

$$Isolation = I = -31.1756\ dB$$

$$Insertion\ loss = L = -11.5576\ dB$$

In order to clearer demonstrate, the behaviours of the coupler several figures are given below.

- Surface current

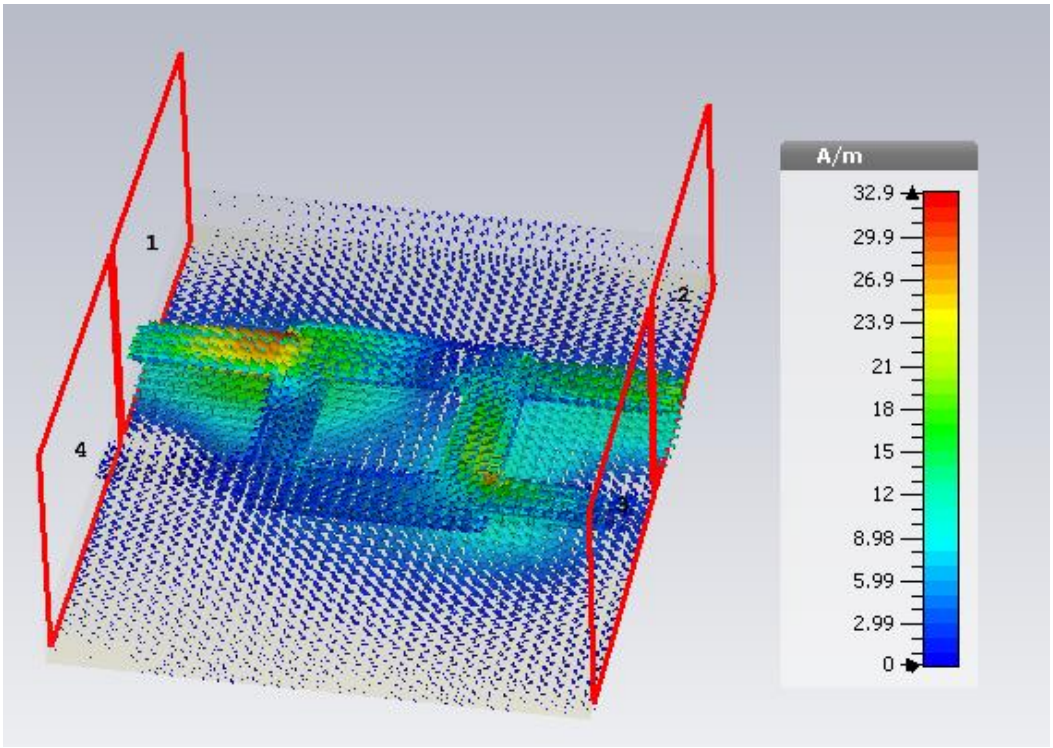


Figure 5. 11 Surface current of hybrid coupler

- E-field

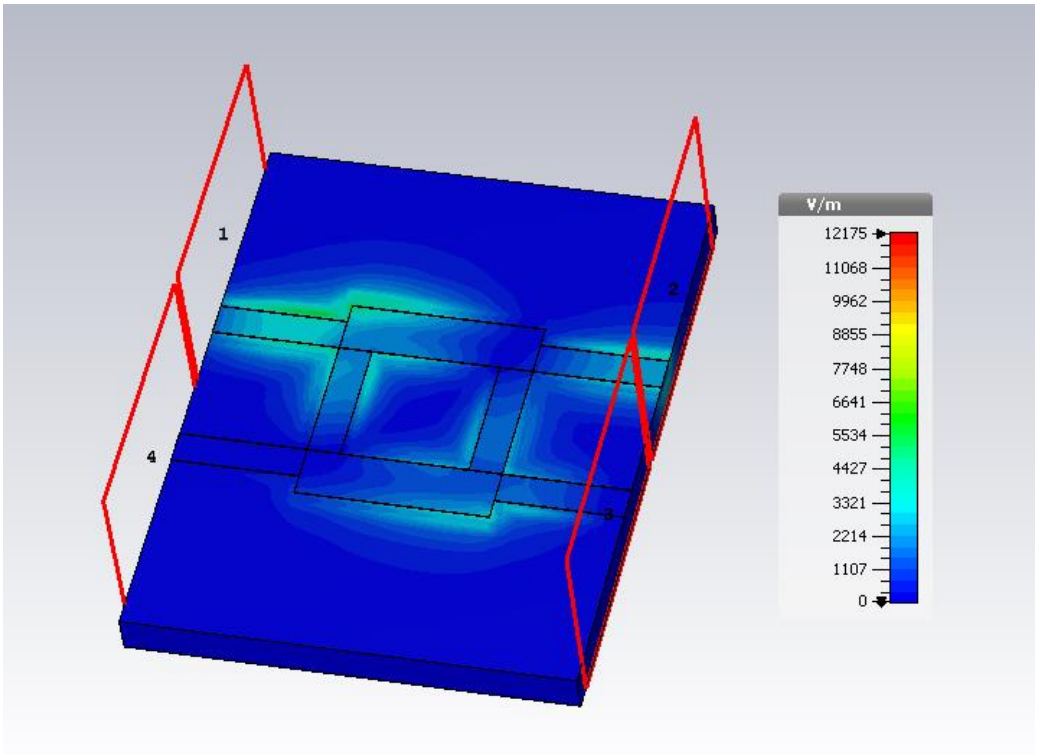


Figure 5. 12 E-field of hybrid coupler

- H-field

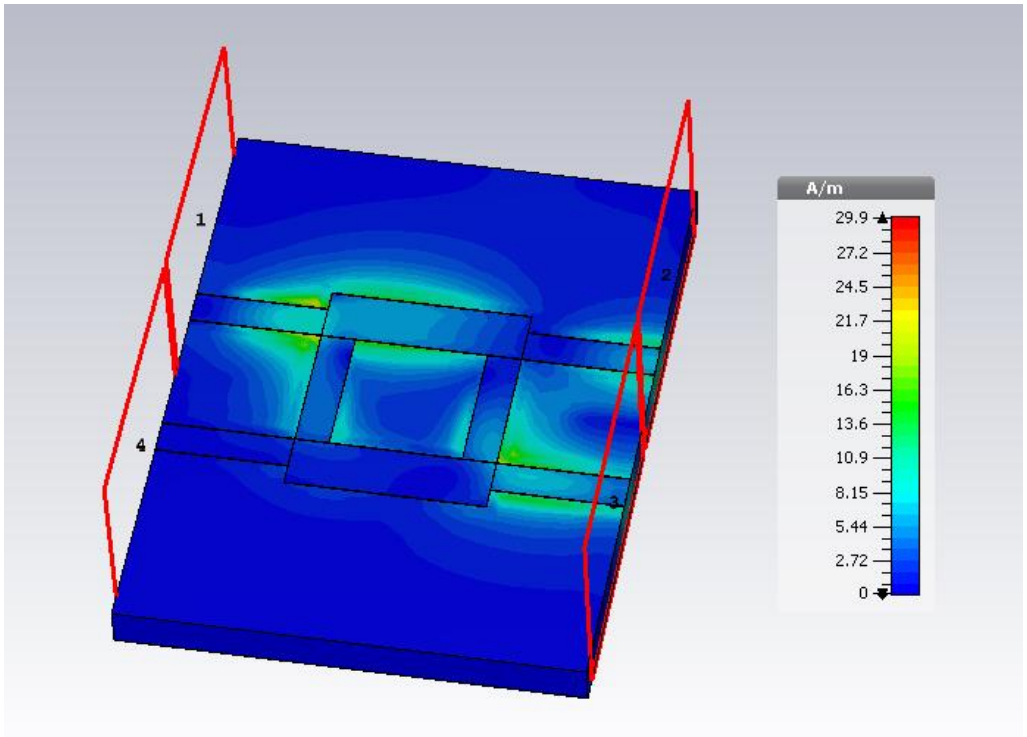


Figure 5. 13 H-field of hybrid coupler

- Power flow

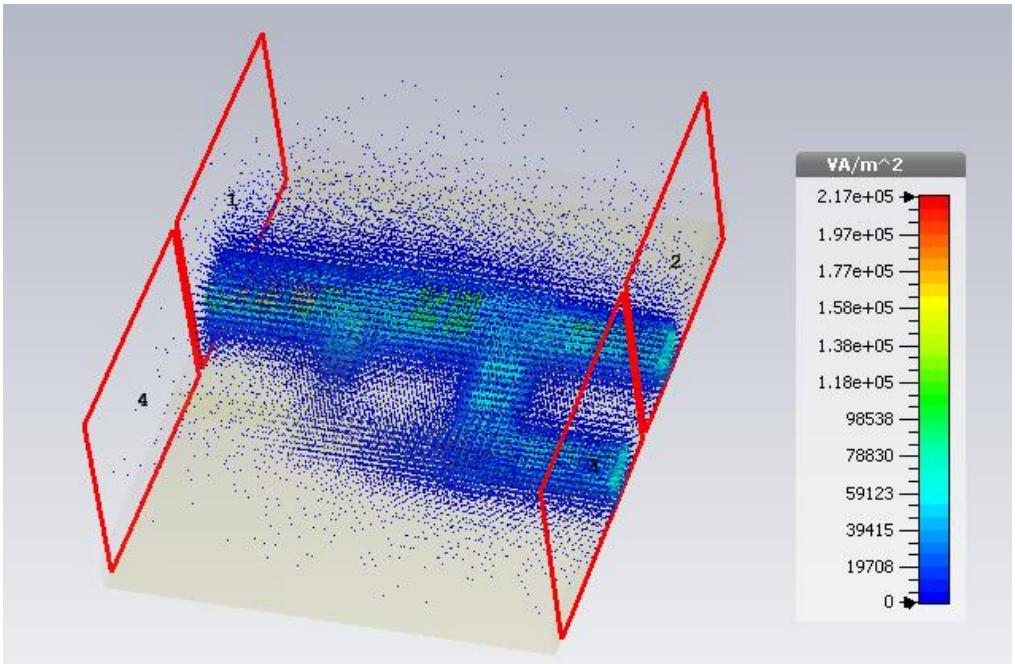


Figure 5. 14 Power flow of hybrid coupler

From these figures above, we can see that port 1 is the input port where signal and power transmitted into the device. And port 2 and port 3 are the output ports with only part of the power. Whereas port 4 is chosen for isolation with no signal obtained.

Although figure 5.12 and 5.13 illustrate that unwanted radiation exists on this coupler which will leads to energy loss in some extent. It is obvious that the electric current flows to port 2 and port 3 from the other figures. Thus almost all the power is delivered to the two output ports with the same percentage and little power goes to isolated port. Therefore this quadrature coupler meets our requirement for power division and isolation.

5.5 Design of the rat race ring in CST

5.5.1 Parameters and structure

Similarly, according to the principle of the rat race ring in 5.3 and the theory of the microstrip line in 3.1 the data of the rat race ring can be obtained as follows. Here a 50 Ω transmission line and FR-4 are also employed in the design.

Parameters	Original Value	Adjusted value
Width of 50 Ω transmission line	3.832 mm	1.675 mm
Width of 75 Ω transmission line	1.789 mm	2.5 mm
Quarter wavelength	6.5mm	6.5 mm
Length of feedline	6.5mm	6.5 mm
Width of substrate	22.85 mm	15.615 mm
Length of substrate	22.85 mm	35.511 mm
Radius of the ring	6.207 mm	8.878 mm

Table 5. 2 Parameters of rat race ring

Here the differences between theory and simulation are due to consideration of the width of the transmission line in the ring design and also the effect of the ground plane. Because the port in CST can only be set aligned with the axis, two feedlines have to be extended to support the port. It will also influence the performance of this ring coupler.

The geometry of it in CST is given in figure 5.15. It consists of the rat race ring which is realized by microstrip line, the substrate and the metal ground plane.

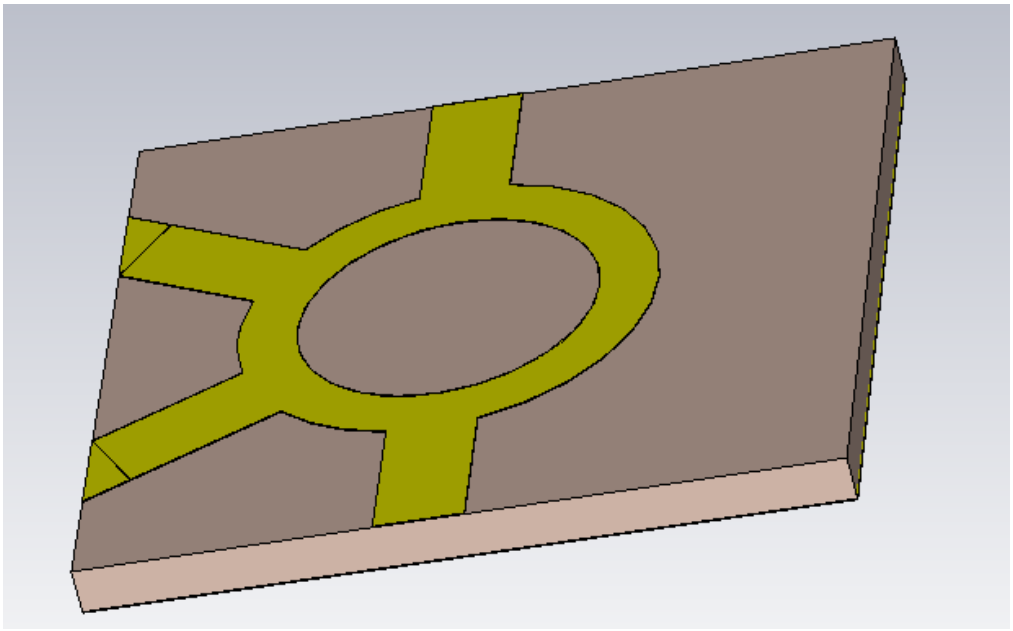
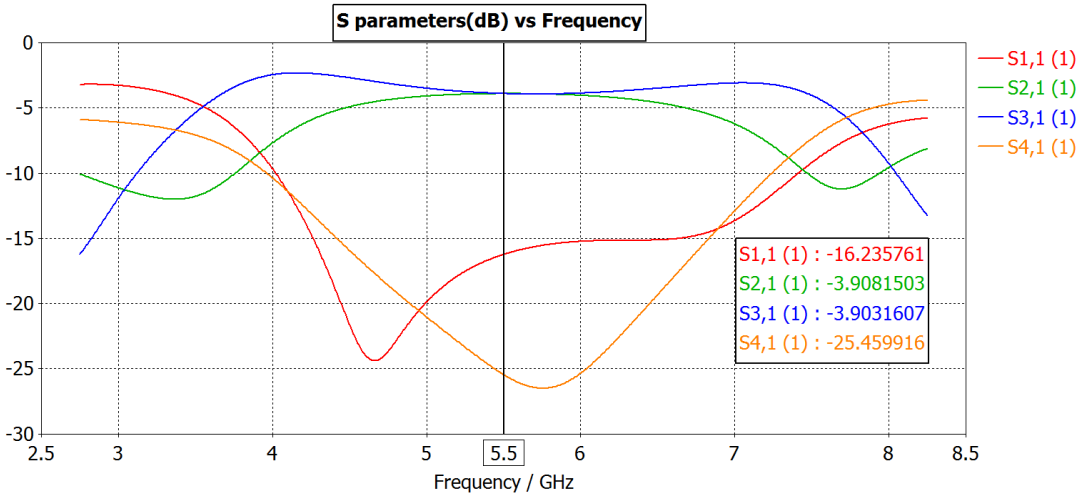


Figure 5. 15 Geometry of rat race ring in CST

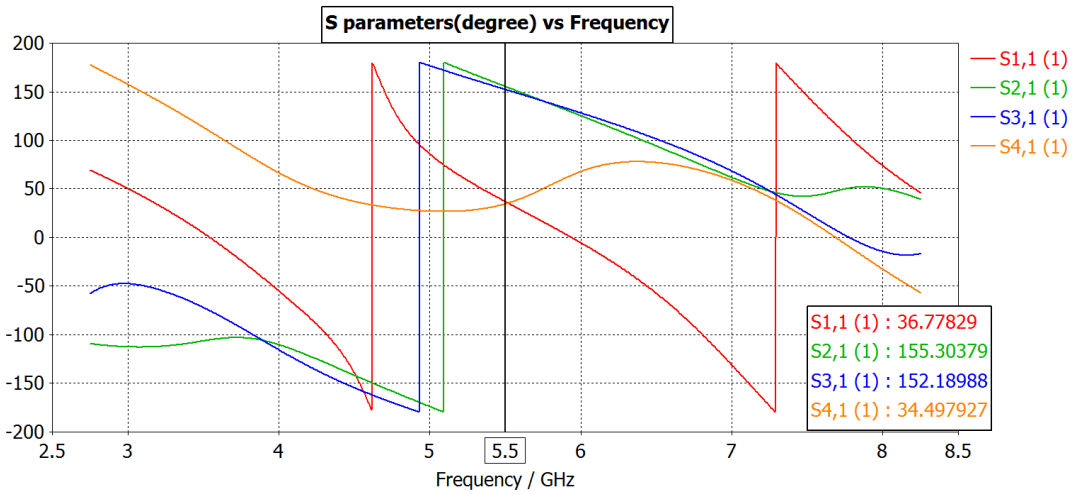
5.5.2 Simulation results

- S parameters

In this case, we have broadened the simulation frequency range, which can be seen from the following figure. That is because the curves under this situation are not as sharp as the former one of the quadrature hybrid coupler. If we use the same frequency range from 4.8 GHz to 6.2 GHz some important details about the coupler will be missed. Therefore a wider frequency range is chosen for better observation of the performance and change tendency of this rat race ring.



(a) Magnitude



(b) Phase

Figure 5. 16 S parameters of rat race ring

It can be seen that the port 2 and port 3 get -3.9082 dB and -3.9032 dB power respectively from the input power source with the phase of 155.3038° and 152.1899°. They are almost the same not only in magnitude but also in phase measurement. And based on equation (5.8), we could also obtain the characteristic of this rat race ring.

$$Coupling = C = -11.8284\ dB$$

$$Directivity = D = -16.2888\ dB$$

$$Isolation = I = -28.1172\ dB$$

$$Insertion\ loss = L = -11.8395\ dB$$

The following figures give a distinct explaination on the working principle of this ring coupler.

- Surface current

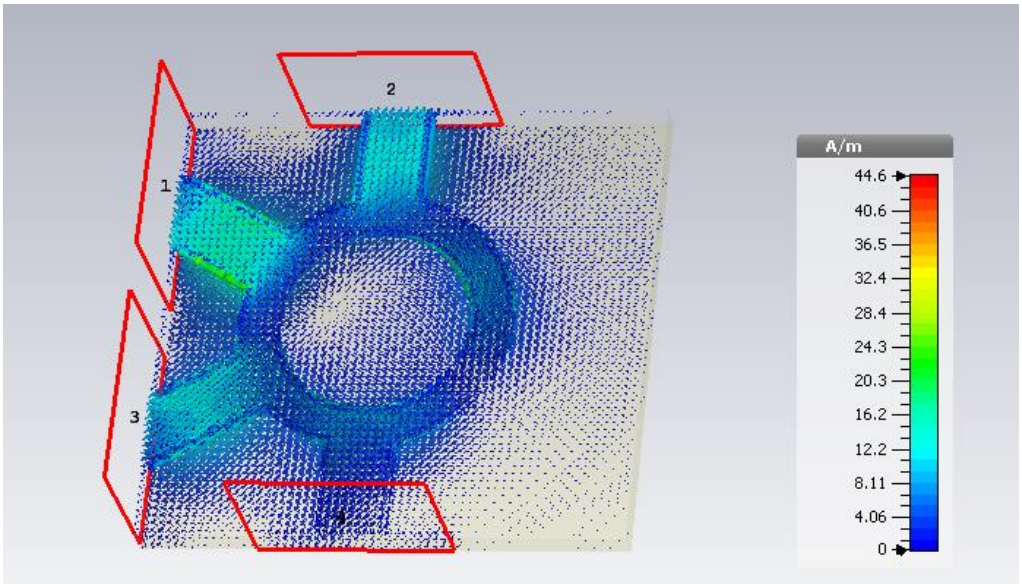


Figure 5. 17 Surface current of rat race ring

- E-field

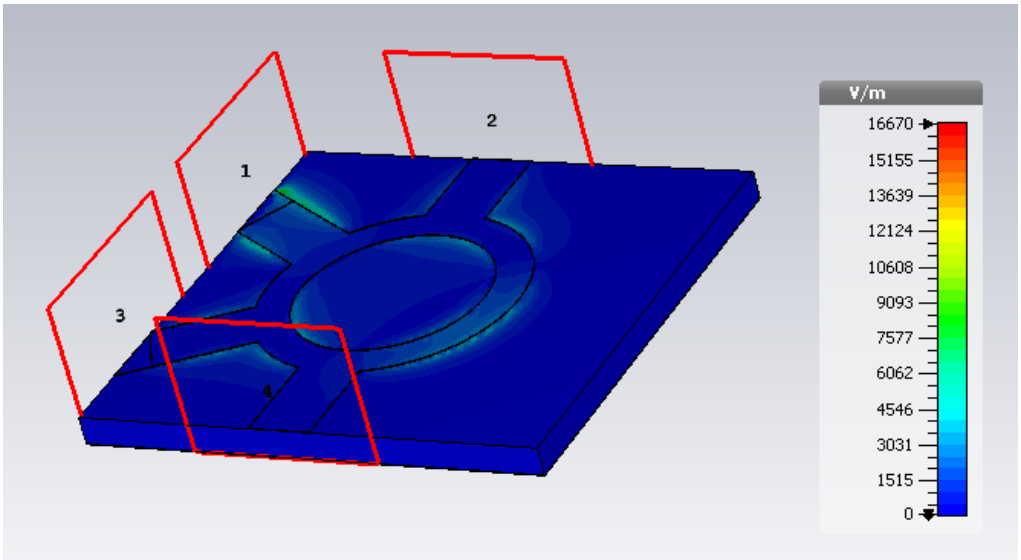


Figure 5. 18 E-field of rat race ring

- H-field

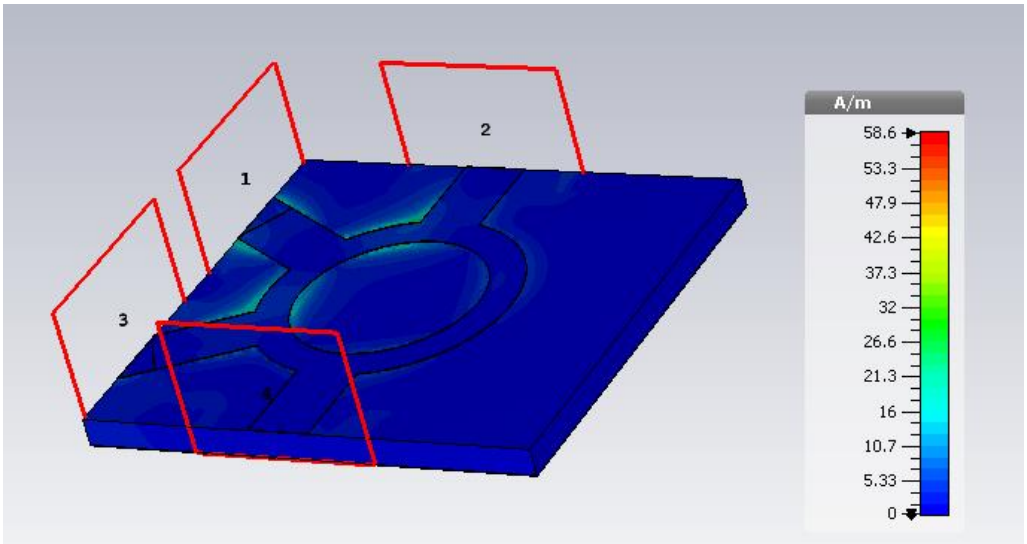


Figure 5. 19 H-field of rat race ring

- Power flow

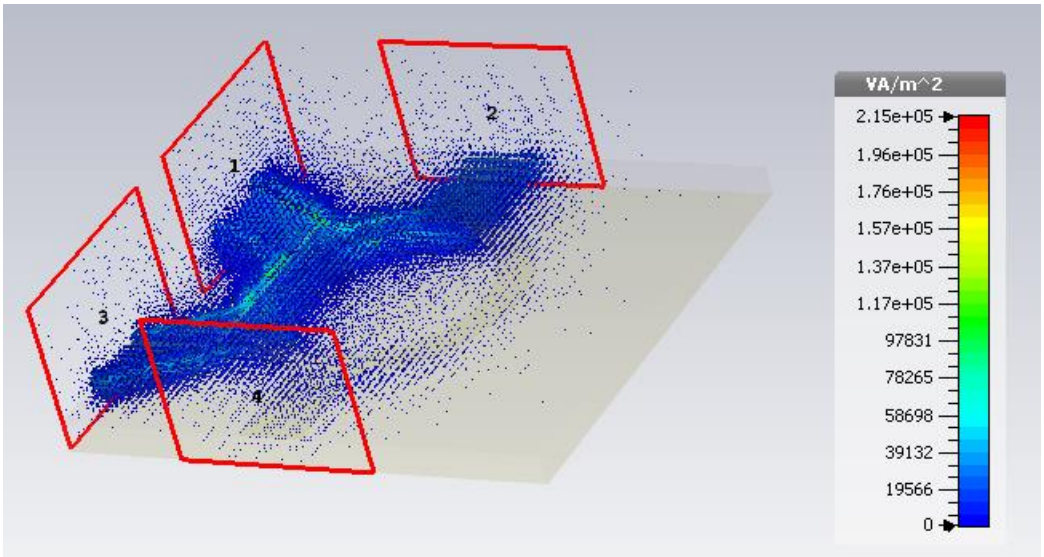


Figure 5. 20 Power flow of rat race ring

From these figures above which can be clearly seen is that the port 1 is the input port. It delivers power to port 2 and port 3 equally and little power transforms to port 4 or reflects back to port 1.

From figure 5.17, it is obvious that the electric current flows to port 2 and port 3, that is the reason why E-field and H-field are located on the two output ports. Figure 5.18 and 5.19 also describe that not too much power is lost to unwanted radiation. Figure 5.20 illustrates that almost all the power has delivered to the two output ports with the same percentage whereas little power goes to the isolated port.

Like the quadrature hybrid coupler in section 5.4, this ring coupler also provides power division and isolation.

5.6 Comparison between two couplers

After design and simulation of these two kinds of coupler, here is a comparison between these two couplers in table 5.3.

Item	Quadrature hybrid coupler	Rat race ring
Coupling(C)	-11.6839	-11.8284
Directivity (D)	-19.4917	-16.2888
Isolation (I)	-31.1756	-28.1172
Insertion loss(L)	-11.5576	-11.8395
Phase shift in output	88.3°	3.2°
Dimensions	30 mm*22.85 mm	35.511 mm*15.615 mm
Energy lost	Unwanted radiation	Less radiation

Table 5. 3 Comparison between hybrid coupler and rat race ring

We can see that both of these two couplers have small physical size. According to the table 5.3, the quadrature hybrid coupler has better performance in coupling, directivity and isolation, although with a nearly 90 degree phase shift and unwanted radiation. Whereas rat race ring has same output in phase but the characteristics like coupling are not good enough.

Therefore the quadrature hybrid coupler is chosen for the following design to connect with a microstrip antenna.

5.7 The microstrip antenna connected to coupler

5.7.1 Structure of MSA with coupler

As we have designed two kinds of devices, the antenna and the coupler, all realized by microstrip line. An investigation of connecting them together has been done in the latter section to see the relevant performance. The main reason is connecting them directly would reduce the connecting loss between two independent element and would increase the integration while manufacture.

Figure 5.21 gives the geometry of the rectangular microstrip antenna connected to a quadrature hybrid coupler. The two elements lie on the same substrate and ground plane providing high integration.

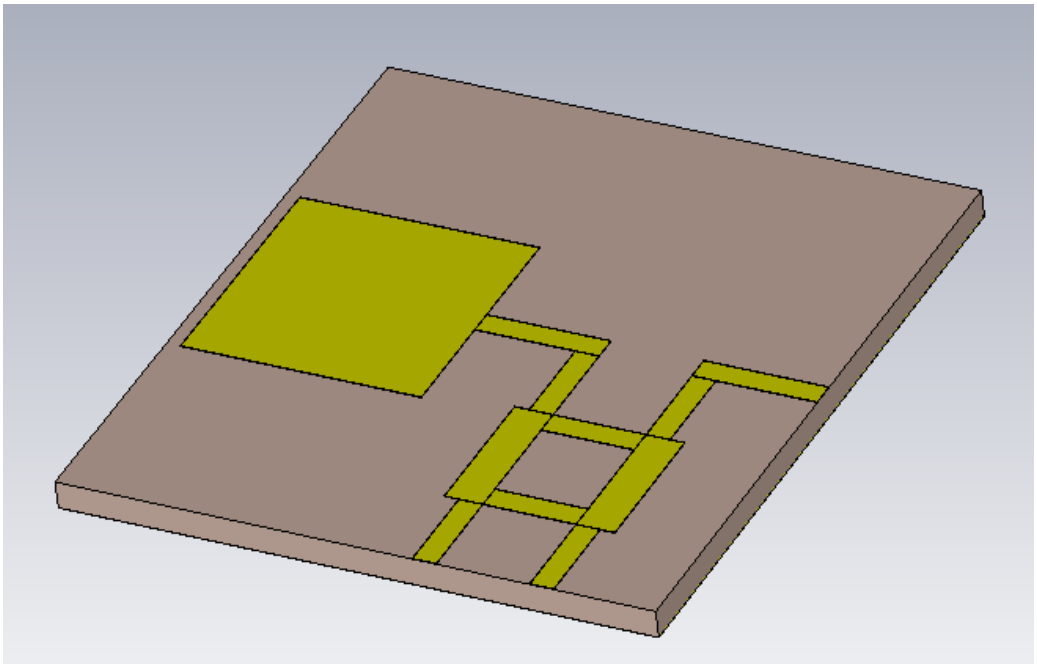


Figure 5. 21 Structure of MSA connected to the coupler

5.7.2 Simulation results

- S_{11} parameter

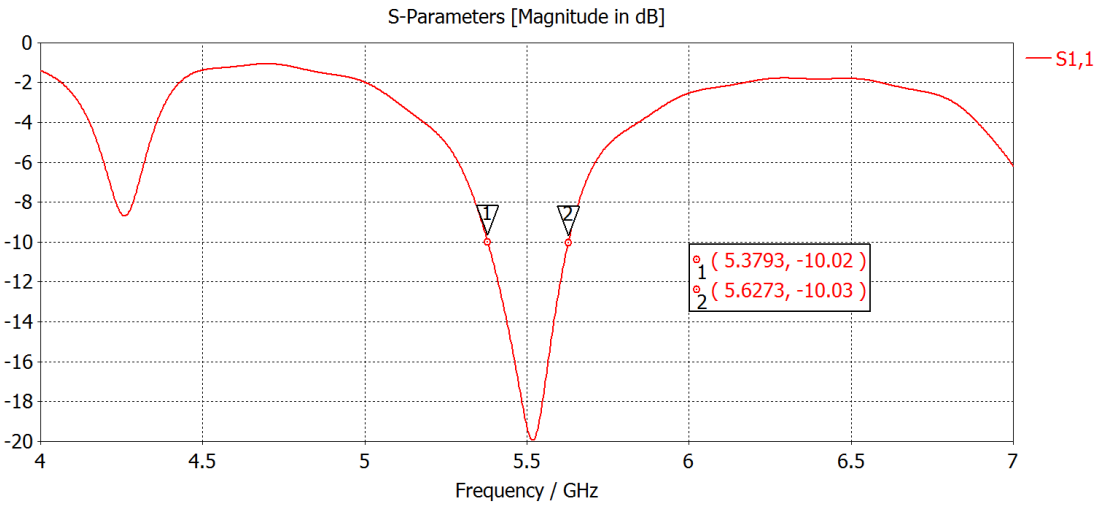


Figure 5. 22 S11 of MSA connected to the coupler

It can be seen that the figure has minimum at around 4.3 GHz but this does not meet the requirement for a resonance (lower than -10dB). After that, the curve experiences a slow fluctuation from 4.5 GHz to 5GHz and also 6 GHz to 7 GHz. However it changes sharply from 5 GHz to 6 GHz and peak at 5.5 GHz with the magnitude of -20 dB, in which the resonant frequency is located. It also illustrates a good match of impedance because the value of the

parameter at 5.5 GHz is pretty low. From section 2.1.2, the frequency bandwidth can also be determined as follow.

$$BW = 5.6273\ GHz - 5.3793\ GHz = 0.248\ GHz = 4.5\%$$

- Efficiency

According to the theory in section 2.1.6, the radiation efficiency and total efficiency can be obtained from figure 5.23.

$$\eta_e = -5.0202\ dB$$

$$\eta_t = -5.3919\ dB$$

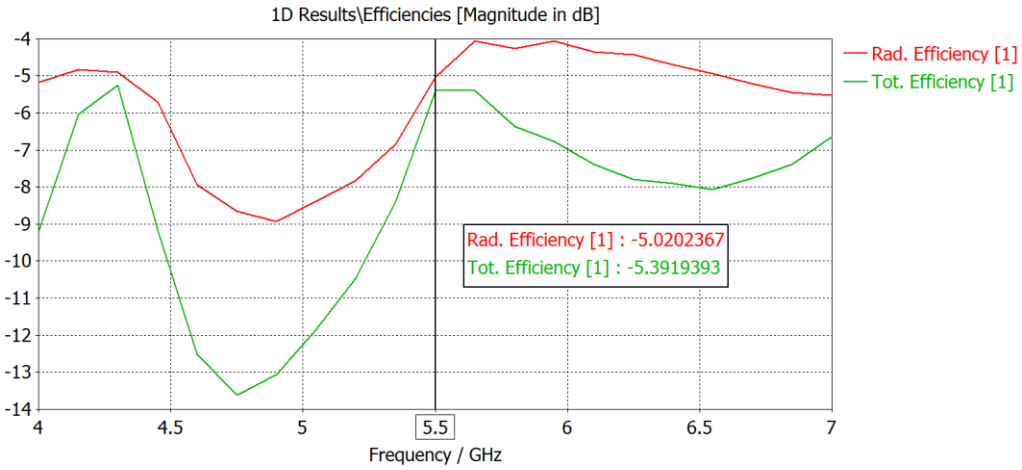


Figure 5. 23 Efficiency of MSA connected to the coupler

In this picture, the red line refers to the radiation efficiency whereas the green line applies to the total efficiency. They have two peaks at the same position where two minimums of S_{11} is located in figure 5.22 at 4.3 GHz and 5.5 GHz separately. Also it can be seen that both of these lines experience a similar trend over the whole frequency band. More specifically, the radiation efficiency changes from -9 dB at about 4.8 GHz to -4 dB at 5.7 GHz. And it reaches -5.02 dB at resonant frequency. As for the total efficiency, it fluctuates severer from -14 dB at 4.75 GHz to -5.5 GHz at central frequency.

- Gain

Based on the knowledge in section 2.1.7, the gain of the antenna at resonant frequency is shown in figure 5.24.

$$G = 1.2292\ dB$$

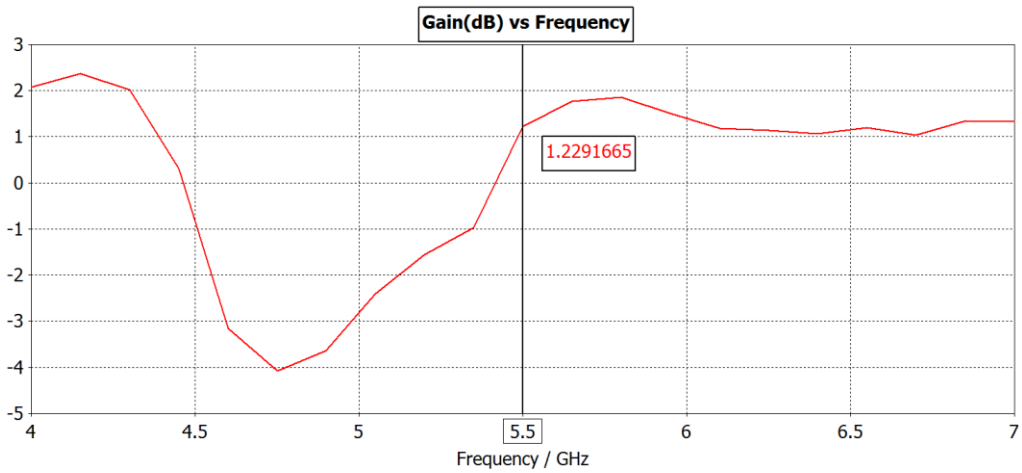


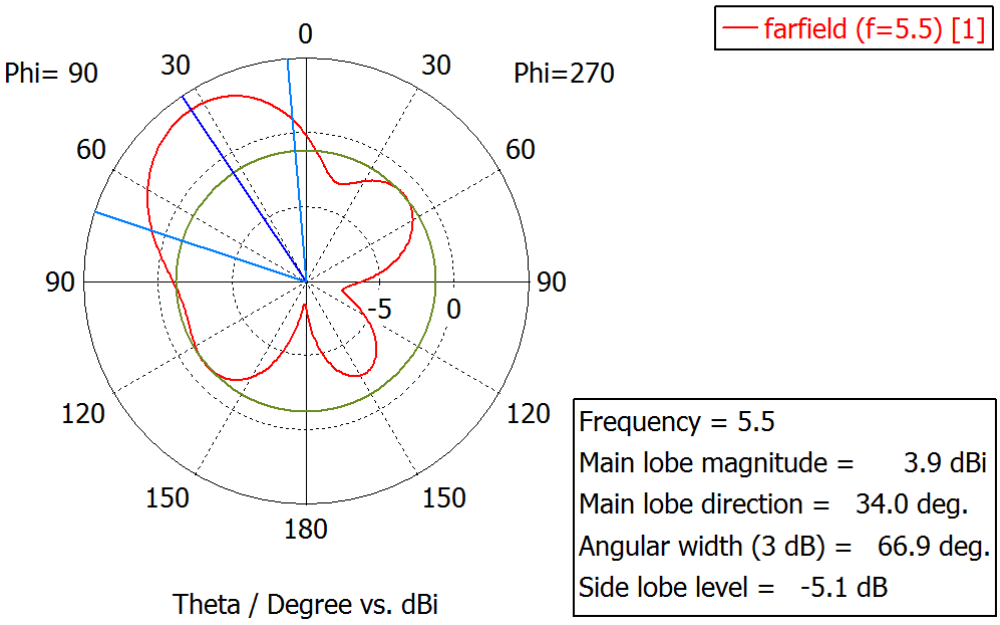
Figure 5. 24 Gain of MSA connected to the coupler

The line in this figure varies through the simulation band from -4 dB to 2.3 dB and reaches 1.2292 dB at resonant frequency, which shows the similar trend of the radiation efficiency in figure 5.23. It is due to the relation between radiation efficiency and gain in (2.9).

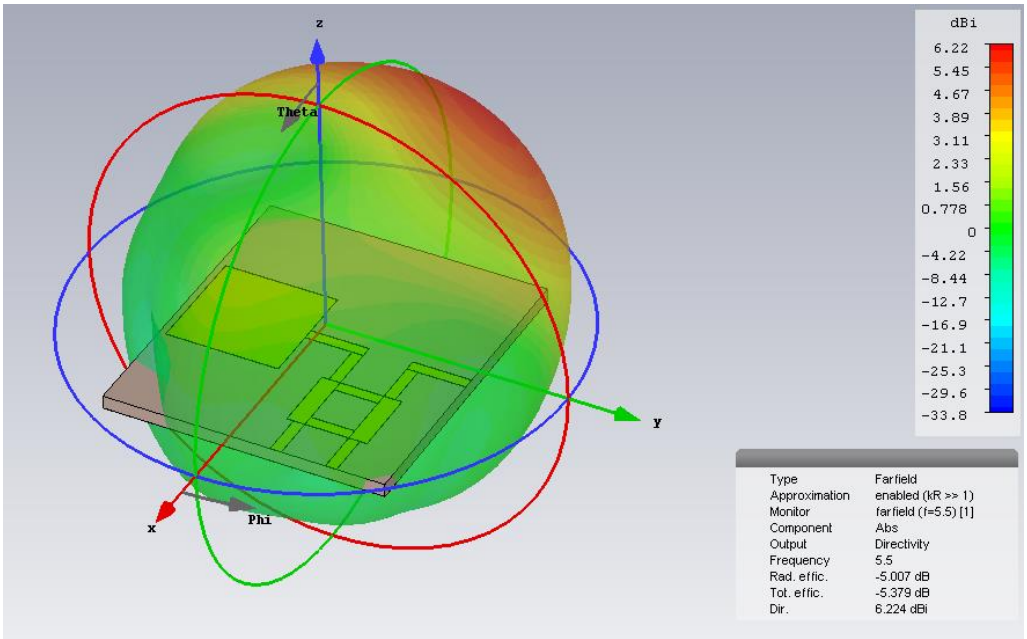
- Radiation pattern

From section 2.1.5, the directivity of the antenna can be obtained from figure 5.25 (a).

$$D = 6.224\ dBi$$



(a) Polar pattern



(b) 3D pattern

Figure 5. 25 Radiation pattern of MSA connected to the coupler

Here it gives the 2D polar and 3D radiation pattern. Compared with the single MSA in 4.2, the shape of the radiation pattern turns sharper and more directional. The directivity of this antenna is 6.224 dB as shown in figure 5.25 (b). Taking (2.9) into consideration, the relation between radiation efficiency (η_e), directivity (D) and gain (G) can be easily verified that

$$G(dB) = D(dB) + \eta_e(dB)$$

In this case, G=1.23 dB, D=6.224 dB, and η_e=-5 dB.

5.8 Comparison with the single MSA without the coupler

The characteristic of single MSA and antenna connected to coupler have been discussed in section 4.3 and 5.7 respectively. And table 5.4 below gives a clearer comparison between these two kinds of device.

Characteristic	Single MSA	MSA with a coupler
S_{11} at 5.5 GHz	-27 dB	-20 dB
BW	0.2855 GHz (5.2%)	0.248 GHz (4.5%)
Radiation efficiency	-2.7797 dB	-5.0202 dB
Total efficiency	-3.1376 dB	-5.3919 dB
Gain	3.5756 dB	1.2292 dB
Directivity	6.357 dBi	6.224 dBi
Radiation pattern	Rounded No side lobe	Sharper Side lobe

Table 5. 4 Comparison between single MSA and MSA with coupler

From the table, it can be seen that single MSA has wider bandwidth of 0.2855 GHz than the antenna connected with coupler of 0.248 GHz. And the S_{11} value at resonant frequency in single MSA is lower than the other, which refers to the impedance match. It can be also seen from the total efficiency which takes the mismatch loss into consideration we have mentioned in section 2.1.6. It is due to the MSA being fed through a coupler instead of the feedline directly to the signal port, which leads to the mismatch loss.

Also since the coupler possesses the property of half power division, the gain of MSA connected with coupler is approximately half of the single MSA as well as the radiation efficiency.

As for the radiation pattern, we can see that side lobe occurs when the antenna is connected with a coupler. Although the directivity is similar with the single MSA, the shape of its radiation pattern is sharper at particular direction.

In conclusion, the antenna connected with a coupler has worse performance than the individual antenna due to the mismatch and half power transmission. But the efficiency and gain is approximately half of the original one which may be useful in some application.

5.9 Summary

This chapter deals with the principle theory of couplers like the network analysis and odd-even excitation mode. Two kinds of couplers, the quadrature hybrid coupler and rat race ring coupler are designed for power division. After comparing the properties of these two kinds of coupler, quadrature hybrid coupler is chosen for the investigation to connect with the microstrip antenna for further discussion. Finally we also compare the performance of single microstrip antenna and the one connected with a coupler.

Chapter 6 Conclusion and future work

6.1 conclusion

During this period of time, an in-depth understanding of antennas and couplers has been developed for designing them, which includes the basic principles and methodology formulas. After comparison of different simulation methods, CST software with FIT method is chosen for simulation. Thus the operation skills of CST software also have been gained and practiced to design and simulate the microstrip antenna and different couplers.

All the devices in this thesis are operated at 5.5 GHz for wireless communication. A rectangular microstrip antenna is chosen due to its small size and the copper coin shape antenna can be seen as a further development for wider bandwidth. Specifically, the copper coin shape antenna gets -42 dB of S_{11} at resonant frequency and pretty wide bandwidth of 25.05% compare to those of -26 dB and 5.2% of the rectangular MSA.

As for the couplers, two of them are discussed and designed for investigation of the power flow in them. After comparison of these two couplers, the quadrature one is chosen due to its better coupling performance.

Finally an investigation of connecting the antenna with coupler has been completed. Since the coupler possesses the property of half power division, the gain of MSA connected with coupler is approximately half of the single MSA as well as the radiation efficiency. But it provides another output which is same as the input signal of the antenna which is useful in some application.

To sum up, regardless of the challenges all the objectives and the previously aims have been achieved successfully.

6.2 Future work

6.2.1 Unsolved problem

Various problems appear during the process of the project. Most of them are solved according to the theory and simulation results. While there are still several problems remain to be solved in the future like the efficiency peak in section 4.3.2 and the radiation pattern of the copper coin shape antenna. More research and reading works on such field are required in the following study.

6.2.2 Manufacture

It can be determined that, the simulation results with little adjusting agree with the methodology in the literature theory. However, the practical results are unknown for further comparison. Therefore the next step is to fabricate the antennas and couplers to test their properties using measurement tools like the vector network analyser. In which way not only the practical performance can be measured but also the accuracy of the CST software can be determined after comparing the result of simulation and measurement.

6.2.3 Application on the antenna with coupler

Although connecting the antenna to a coupler possesses poor performance, the second coupler output provides another same signal as the one used as input for the antenna. This output can be used for another microstrip antenna. Due to the highly integration it may be a new investigation for MIMO [58] (Multi-input Multi-output) system. As MIMO has been adopted for IEEE 802.11n [59], worldwide interoperability for microwave access (WiMAX) and long term evolution (LTE)[29, 60]. It becomes more popular in wireless systems comprised multiple antenna elements as transmitter and receiver as well[58]. The antenna with coupler could provide multiple output with phase control, which is usually required in antenna array. Therefore MIMO is an important research direction of the future work.

Reference

[1] C. Prommak, J. Kabara, D. Tipper, and C. Charnsripinyo, "Next generation wireless LAN system design," in *MILCOM 2002. Proceedings*, 2002, pp. 473-477.

[2] A. Goldsmith, *Wireless communications*: Cambridge university press, 2005.

[3] R. Ludwing, "RF Circuit Design Theory and Applications," 2011.

[4] A. Khidre, J. W. Jervis, and S. Ponnuswamy, "ANTENNA DESIGNS," ed: US Patent 20,160,064,808, 2016.

[5] Y. Huang and K. Boyle, *Antennas: from theory to practice*: John Wiley & Sons, 2008.

[6] w. d. project, "demonstrations. wolfram/dipole antenna radiation pattern."

[7] http://www.cisco.com/c/en/us/products/collateral/wireless/aironet-antennas-accessories/prod_white_paper0900aecd806a1a3e.html, "antenna patterns and their meaning," Aug 07, 2007.

[8] D. M. Pozar, *Microwave engineering*: John Wiley & Sons, 2009.

[9] M. I. Maricar, "Low Profile X-Band Antenna," August, 2010.

[10] L. Sun, G. Ou, S. Tan, and Y. Lu, *Axial Ratio Bandwidth of a Circularly Polarized Microstrip Antenna*: INTECH Open Access Publisher, 2013.

[11] K. F. Leea and K.-F. Tongb, "Microstrip patch antennas," 2015.

[12] P. S. Nakar, "Design of a compact microstrip patch antenna for use in wireless/cellular devices," 2016.

[13] H. Kan, R. Waterhouse, A. Abbosh, and M. Bialkowski, "Simple broadband planar CPW-fed quasi-Yagi antenna," *Antennas and Wireless Propagation Letters, IEEE,* vol. 6, pp. 18-20, 2007.

[14] A. Deshmukh, A. Kadam, S. Agrawal, and K. Ray, "Broadband CPW Fed Hexagonal Shape and Hexagonal Slot Cut Microstrip Antenna," in *Computing Communication Control and Automation (ICCUBEA), 2015 International Conference on*, 2015, pp. 117-121.

[15] A. Kahwaji, H. Arshad, S. Sahran, A. G. Garba, and R. I. Hussain, "Hexagonal microstrip antenna simulation for breast cancer detection," in *2016 International Conference on Industrial Informatics and Computer Systems (CIICS)*, 2016, pp. 1-4.

[16] M. R. Ahsan, M. T. Islam, and M. H. Ullah, "A simple design of planar microstrip antenna on composite material substrate for Ku/K band satellite applications," *International Journal of Communication Systems,* 2015.

[17] L. Anchidin, R. Topor, R. D. Tamas, A. Dumitrascu, A. Danisor, and S. Berescu, "Improvement of antenna decoupling in radar systems," in *Advanced Topics in Optoelectronics, Microelectronics, and Nanotechnologies 2014*, 2015, pp. 925831-925831-6.

[18] R. Waterhouse, *Microstrip Patch Antennas: A Designer's Guide: A Designer's Guide*: Springer Science & Business Media, 2003.

[19] G. A. Deschamps, "Microstrip microwave antennas," in *3rd USAF Symposium on Antennas*, 1953, pp. 22-26.

[20] R. E. Munson, "Conformal microstrip antennas and microstrip phased arrays," *Antennas and Propagation, IEEE Transactions on,* vol. 22, pp. 74-78, 1974.

[21] D. M. Pozar, "Microstrip antenna aperture-coupled to a microstripline," *Electronics letters,* vol. 21, pp. 49-50, 1985.

[22] D. M. Pozar and B. Kaufman, "Increasing the Bandwidth of a Microstrip Antenna by Proximity Coupling," *Electronics Letters,* vol. 23, pp. 369-369, Apr 9 1987.
[23] R. F. J. Broas, D. F. Sievenpiper, and E. Yablonovitch, "A high-impedance ground plane applied to a cellphone handset geometry," *Microwave Theory and Techniques, IEEE Transactions on,* vol. 49, pp. 1262-1265, 2001.
[24] Y. Y. Guo, X.-M. Zhang, G.-L. Ning, D. Zhao, X. W. Dai, and Q. Wu, "Miniaturized modified dipoles antenna for WLAN applications," *Progress In Electromagnetics Research Letters,* vol. 24, pp. 139-147, 2011.
[25] B. Jyothi, B. Madhav, V. Murthy, P. S. Sundar, and V. Pisipati, "Comparative Analysis of Microstrip Coaxial Fed, Inset Fed and Edge Fed Antenna Operating at Fixed Frequency," *International journal of scientific and research publications,* vol. 2, p. 1, 2012.
[26] W.-L. Chen and G.-M. Wang, "Small Size Edge-Fed Sierpinski Carpet Microstrip Patch Antennas. Doc," *Progress In Electromagnetics Research C,* vol. 3, pp. 195-202, 2008.
[27] V. G. Kasabegoudar and K. Vinoy, "Coplanar capacitively coupled probe fed microstrip antennas for wideband applications," *Antennas and Propagation, IEEE Transactions on,* vol. 58, pp. 3131-3138, 2010.
[28] P. Soh, M. K. A. Rahim, A. Asrokin, and M. A. Aziz, "Design, Modeling, and performance comparison of feeding techniques for a microstrip patch antenna," *Jurnal Teknologi,* vol. 47, pp. 103–120, 2012.
[29] H.-W. Liu, C.-H. Ku, and C.-F. Yang, "Novel CPW-fed planar monopole antenna for WiMAX/WLAN applications," *Antennas and Wireless Propagation Letters, IEEE,* vol. 9, pp. 240-243, 2010.
[30] D. B. Davidson, *Computational electromagnetics for RF and microwave engineering*: Cambridge University Press, 2010.
[31] R. F. Harrington and J. L. Harrington, *Field computation by moment methods*: Oxford University Press, 1996.
[32] J. H. Stock, J. H. Wright, and M. Yogo, "A survey of weak instruments and weak identification in generalized method of moments," *Journal of Business & Economic Statistics,* 2012.
[33] G. Strang and G. J. Fix, *An analysis of the finite element method* vol. 212: Prentice-Hall Englewood Cliffs, NJ, 1973.
[34] T. P. Fries and T. Belytschko, "The extended/generalized finite element method: an overview of the method and its applications," *International Journal for Numerical Methods in Engineering,* vol. 84, pp. 253-304, 2010.
[35] K. S. Yee, "Numerical solution of initial boundary value problems involving Maxwell's equations in isotropic media," *IEEE Trans. Antennas Propag,* vol. 14, pp. 302-307, 1966.
[36] A. H. Mohammadian, V. Shankar, and W. F. Hall, "Computation of electromagnetic scattering and radiation using a time-domain finite-volume discretization procedure," *Computer Physics Communications,* vol. 68, pp. 175-196, 1991.
[37] S. D. Gedney, "Introduction to the finite-difference time-domain (FDTD) method for electromagnetics," *Synthesis Lectures on Computational Electromagnetics,* vol. 6, pp. 1-250, 2011.
[38] T. Weiland, "A discretization model for the solution of Maxwell's equations for six-component fields," *Archiv Elektronik und Uebertragungstechnik,* vol. 31, pp. 116-120, 1977.

[39] F. Hirtenfelder, "Effective antenna simulations using CST MICROWAVE STUDIO®," in *Antennas, 2007. INICA'07. 2nd International ITG Conference on*, 2007, pp. 239-239.
[40] T. Banova, W. Ackermann, and T. Weiland, "Systematic Determination of Eigenfields in Time and in Frequency Domain," 2016.
[41] R. Garg, I. Bahl, and M. Bozzi, *Microstrip lines and slotlines*: Artech house, 2013.
[42] F. M. Ali, "Estimate Microstrip Substrate Relative Dielectric Constant," *Microwaves and RF,* 2007.
[43] M. Ramesh and Y. KB, "Design formula for inset fed microstrip patch antenna," *Journal of Microwaves, Optoelectronics and Electromagnetic Applications (JMOe),* vol. 3, pp. 5-10, 2003.
[44] J.-Y. Sze, K.-L. Wong, and C.-C. Huang, "Coplanar waveguide-fed square slot antenna for broadband circularly polarized radiation," *Antennas and Propagation, IEEE Transactions on,* vol. 51, pp. 2141-2144, 2003.
[45] W. C. Tang and Y. L. Chow, "CAD formulas, their inverses and interrelations for microstrip, CPW lines without and with a backing ground plane, by successive synthetic asymptotes," *Journal of electromagnetic waves and applications,* vol. 16, pp. 1-20, 2002.
[46] http://www.microwaves101.com/, *microstrip-patch-antennas*.
[47] www.antenna-theory.com, "Video: The Analysis of the Patch Antenna."
[48] C. A. Balanis, *Antenna theory: analysis and design*: John Wiley & Sons, 2016.
[49] M. Kumar and K. Ray, "Design and Performance of a Compact Broadband Circularly Polarized Rectangular Ring Antenna," *International Journal of Electromagnetics and Applications,* vol. 4, pp. 49-55, 2014.
[50] R. Waterhouse, *Microstrip patch antennas: a designer's guide*: Springer Science & Business Media, 2013.
[51] M. R. Harati, M. Naser-Moghadasi, A. A. Lotfi-Neyestanak, and A. Nikfarjam, "Improving the Efficiency of Transparent Antenna Using Gold Nano Layer Deposition."
[52] D. Kumar, T. Singh, R. Dwivedi, and S. Verma, "A compact monopole CPW-fed dual band notched square-ring antenna for UWB applications," in *Computational Intelligence and Communication Networks (CICN), 2012 Fourth International Conference on*, 2012, pp. 57-60.
[53] S. Lu, "Design of Microwave Hybrid Couplers Using Inter-coupled Resonators," April 2012.
[54] J. Reed and G. Wheeler, "A method of analysis of symmetrical four-port networks," *Microwave Theory and Techniques, IRE Transactions on,* vol. 4, pp. 246-252, 1956.
[55] M. Sisodia, *Microwaves: introduction to circuits, devices and antennas*: New Age International, 2007.
[56] K. Chang and L.-H. Hsieh, *Microwave ring circuits and related structures* vol. 156: John Wiley & Sons, 2004.
[57] E. Problems, "Theoretical Information About Ring Hybrid Junction," http://kilyos.ee.bilkent.edu.tr/~microwave/programs/magnetic/hybrid/rtheory.htm.
[58] Q. H. Spencer, A. L. Swindlehurst, and M. Haardt, "Zero-forcing methods for downlink spatial multiplexing in multiuser MIMO channels," *IEEE Transactions on Signal Processing,* vol. 52, pp. 461-471, 2004.
[59] E. Tanghe, D. Gaillot, W. Joseph, M. Li, W. De Ketelaere, and L. Martens, "Capacity simulation and analysis of an IEEE 802.11 n system in a residential

house," in *2016 10th European Conference on Antennas and Propagation (EuCAP)*, 2016, pp. 1-5.
[60] S. BEVINAKOPPA, B. K. RANABHAT, S. SABOJI, C. AKKI, and A. I. INDIA, "Performance Analysis of WiMAX with MIMO Antenna."